Through-Space Interactions In Charge-Transfer Reactions

Inauguraldissertation

zur Erlangung der Würde eines Doktors der Philosophie

vorgelegt der
Philosophisch-Naturwissenschaftlichen Fakultät
der Universität Basel

von

Hauke Christoph Schmidt

aus Heide (Holstein), Deutschland

Basel, 2018

Genehmigt von der Philosophisch-Naturwissenschaftlichen Fakultät auf Antrag von

Fakultätsverantwortlicher/Dissertationsleiter: Prof. Dr. Oliver S. Wenger
Korreferent: Prof. Dr. Marcel Mayor

Basel, den 14.11.2017

Prof. Dr. Martin Spiess

When the spirits are low, when the day appears dark, when work becomes monotonous, when hope hardly seems worth having, just mount a bicycle and go out for a spin down the road, without thought on anything but the ride you are taking.

Arthur Conan Doyle

Abstract

Considering the importance of electron-transfer reactions in chemistry and nature, especially regarding light-to-energy conversion by (dye-sensitized) solar-cells and the production of solar-fuels, a fundamental understanding of their mechanisms is necessary for the design of efficient systems. This thesis has its focus on the through-space interaction of donor-acceptor pairs, which was investigated in two fundamentally different ways – photoinduced electron-transfer and organic mixed-valency.

A short perspective is outlined in **Chapter I** and brief overviews over the relevant aspects of electron-transfer reactions and mixed-valence systems are presented in **Chapters II** and **IV**, respectively.

In **Chapter III**, the synthesis and spectroscopic measurements of a right-angled and linear series of homologous complexes, bearing a $[Ru(bpy)_3]^{2+}$ photosensitizer and a triarylamine electron-donor connected by fluorene bridges with different lengths, are described. Their behavior upon photoexcitaion, with and without an external quencher, was investigated in terms of intramolecular electron-transfer. Electron-transfer rate constants were determined and an unexpectedly weak distance-dependence was observed for the right-angled series. Molecular mechanics calculations indicate that this is caused by the flexibility of the fluorene bridge leading to small through-space donor-acceptor separations. The very weak distance-dependence suggests a mainly through-space pathway for the electron-transfer. For the linear complexes, electron-transfer was too fast to be detected with the employed method.

In **Chapter V**, the synthesis of compounds with a "triple-decker" geometry, based on phenothiazine and carbazole as redox-active moieties, is presented. Analysis of electrochemical and spectroscopic data, obtained for the compounds in their singly-oxidized mixed-valence state, revealed weak interaction for the phenothiazine-based compounds. The through-space charge-transfer pathway may be explained by an $n-\pi-n$- or $\pi-\pi$-interaction. The carbazole-based mixed-valence compounds suffered from inconclusive data that were obtained from the spectroscopic measurements.

Acknowledgements

At first, I want to thank Prof. Dr. Oliver Wenger for accepting and keeping me in his group for all my theses in my academic life. You granted me a lot of freedom, but you were always there to give advice or revive my motivation, when times were challenging.
I thank Prof. Dr. Marcel Mayor for accepting to be my co-examiner, although being the maybe most busy person in the department.
Prof. Dr. Konrad Tiefenbacher kindly agreed to chair the examination.
Working at the Department of Chemistry in Basel was easy, due to the outstanding organization by the secretaries and the quick and proficient service provided by the workshop team. I'd like to thank Prof. Dr. Markus Meuwly for the private lessons in DFT calculations. In addition, I thank the staff of the chemistry department, who contributed to the characterisation of my compounds, Dr. Heinz Nadig, Sylvie Mittelheisser, Dr. Markus Neuburger, Dr. Alessandro Prescimone, Dr. Mariana Spulber, Pascal Richard and Prof. Dr. Cornelia Palivan.
I want to thank the Wenger group with all its past and present members. I've now been part of the group for almost seven years and I can say, the coffee breaks improved a lot since we started playing cards. I want to thank lab 302, especially Julia for making the first time in Basel much easier and Michael for being the calm anchor of the lab, enduring all the stupid stuff I needed to tell throughout the day. I thank Mirj for being my partner for exchanging insults, that was a lot of fun, and for providing me with chocolate, when I had a bad time. Sabine, I really enjoyed the chats we had, especially about sports and my partially hard time with science, oh, and thanks for having that dialect. And I want to thank Chris; since Laura left, nobody kept me from work so much as you... And sometimes, we even talked about science, which was really helpful. Special thanks go to Chris, Sabine and Mirj for proof-reading this thesis.
I'd like to thank my "Wahlpraktikum"-students David Steinbrunner, Seraina Keller, Jasmine Furter and Amadeus Matthias for their work and for playing lab-rats for new synthetic ideas.
I want to thank Henning, for being the friend I can always count on, the never-ending exchange of new music discoveries, many drinks and long discussions about all technical details of bicycles. I'd like to express my deep gratitude for all the support from my family during undergraduate and graduate studies, you were always there for me and I wouldn't have made it without you. Finally, I'm happy to thank Laura for all the splendid time we could spend together in Basel, Tübingen and all over the world; with hopefully more to come. You brought a lot of happiness into my life and helped me to not lose my way and to reach beyond my personal boarders.

Contents

List of Abbreviations

δ	chemical shift
A	electron acceptor
AcOH	acetic acid
Ar	aryl
B	molecular bridge
bpy	2,2'-bipyridine
Bu	butyl
calcd	calculated
CBZ	3,6-dihexylcarbazole
CR	charge-recombination
CS	charge-separation
CV	cyclic voltammetry
D	electron donor
dmb	1,4-dimethoxybenzene
DMF	dimethylformamide
DMSO	dimethylsulfoxide
ESI	electron spray ionization
Et	ethyl
ET	electron-transfer
Fl	9,9'-diethylfluorene
GS	ground state
HOMO	highest occupied molecular orbital
HRMS	high resolution mass spectrometry
HT	hole-transfer
MV	methylviologen
NIR	near-infrared
IVCT	intervalence charge-transfer
LUMO	lowest unoccupied molecular orbital
Me	methyl
MLCT	metal-to-ligand charge transfer
MO	molecular orbital
NMR	nuclear magnetic resonance
Ph	phenyl
ppm	parts per million

PTZ	phenothiazine
SCE	saturated calomel electrode
TAA	triarylamine
TD	triple-decker
Tf	triflyl
TBA	tetra(*n*-butyl)ammonium
THF	tetrahydrofuran
tmb	tetramethoxybenzene
UV	ultraviolet
Vis	visible

I Perspective

Electron transfer can be considered as one of the most important reactions in chemistry and nature.[1] All three traditional branches of chemistry (organic, inorganic and physical chemistry) are equally interested in electron-transfer, due to its ubiquitous nature. The possibility of using visible light to trigger electron-transfer processes keeps this research field highly topical.[2,3] Efficient light-to-chemical-energy conversion is a major goal in photochemistry. This is either targeted in a direct manner by generating a photo-current with dye-sensitized solar cells, or in an indirect manner through the production of solar fuels.[3,4] The reverse phenomenon to a photo-current is called electroluminescence. The production of light from electric energy with light-emitting diodes (LEDs) or their organic counterpart (OLEDs) has already made it into our everyday life in the form of mobile phones and TV screens.[2] In solar fuel production, the creation of an artificial photosynthetic system is the primary objective. The two primary reactions of interest are photochemical water splitting and CO_2 reduction. In recent years, photoinduced electron-transfer reactions have further attracted a lot of attention in organic synthesis, especially the field of photoredox catalysis.[5] The major advantage of photoredox catalysts is that they act as powerful single electron oxidizing/reducing agents in their excited states.[6] In their ground states, the photocatalysts have only limited oxidizing/reducing capabilities, making them relatively stable.
Exploring the electron-transfer properties of molecular bridges has set the stage for the field of molecular electronics. Using single-molecule devices in electronics would be the next step, considering the current top-down approach for metal- and silicon-based components.[7]
A profound understanding of the factors governing electron-transfer processes, and their respective influences, is mandatory for a purpose-tailored system. These factors can be roughly divided into two groups; factors inherent in the system, and factors determined by the environment. Examples for the latter would be the temperature or the medium, which surrounds the electron-transfer system. The system itself bears a variety of possibilities to influence the electron-transfer, mainly based on the choice of the donor-acceptor couple and their connection. One further distinguishes between a through-bond interaction of donor and acceptor, determined by the bridge connecting them, and a through-space interaction, whereby the latter is far less understood.
The aim of this thesis is to give new insights in the role of through-space interactions in intramolecular electron-transfer reactions. Two fundamentally different approaches were applied in this matter: a) photoinduced electron-transfer; b) organic mixed-valency.

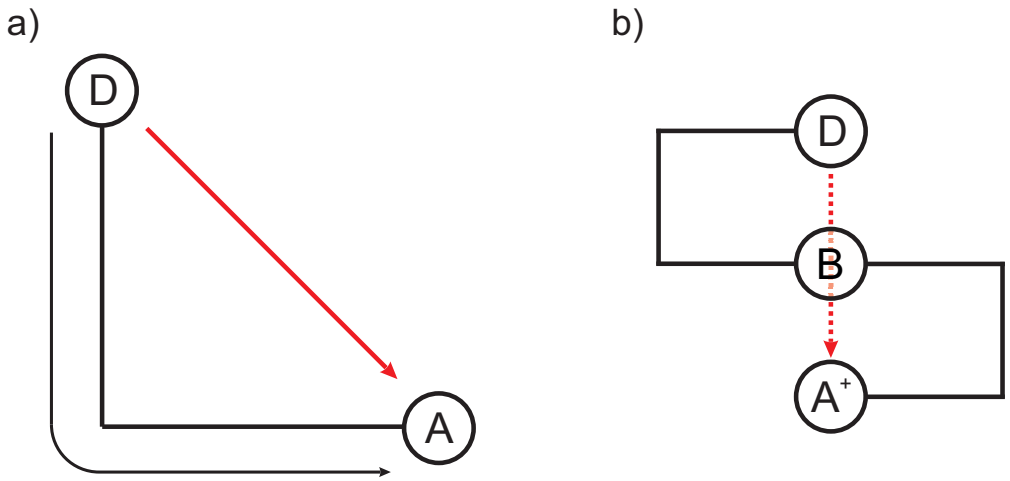

Figure I.1. Schematic depiction of the two systems employed to target through-space interaction (red arrows) in electron-transfer reactions; a) a right-angled system for photoinduced electron-transfer; b) an organic mixed-valent system with a "triple-decker" geometry.

The first approach has its focus on the distance-dependence of the through-space pathway in photoinduced electron-transfer. A right-angled series of homologous complexes with varied bridge lengths is compared to its linear counterpart. The second approach deals with the extension of through-space orbital interactions, beyond the widely studied $\pi-\pi$-interactions. In organic mixed-valent systems with a "triple-decker" geometry, the possibility of a $n-\pi-n$-interaction between two amines and a central aryl-unit is investigated.

II Electron-Transfer Theory

II.1 Outer-Sphere vs Inner-Sphere Electron-Transfer

Electron-transfer (ET) is fundamentally the most basic chemical reaction possible – an electron is transferred from a donor, D, to an acceptor, A, creating a charge-separated state.

Initially, the theory of ET rates was based on studies of intermolecular self-exchange reactions of metal complexes.[8] Within this framework, one can distinguish between two fundamentally different mechanisms. In the "outer-sphere" ET mechanism, charge is transferred, without breaking or forming any chemical bonds, between two redox-centers with weak interaction between the relevant electronic orbitals.[9] If the two reactants share a common ligand or atom after approaching each other, the resulting ET is called "inner-sphere".

II.1.1 Adiabatic vs Non-Adiabatic Electron-Transfer

The energy profiles of a donor-bridge-acceptor system are presented in Figure II.1. For the intersection of these potential energy surfaces, two different possibilities exist, depending on the electronic coupling between donor and acceptor (H_{DA}).[10] In the strong-coupling regime, a large splitting of the potential energy surfaces is present. ET occurs only on the potential energy surface connecting the reactant and product state and is called "adiabatic", requiring no external energy. The electron-transfer rate, k_{ET}, for adiabatic ET is independent of H_{DA}.[11] In the weak-coupling regime the ET process requires external energy and is labelled "non-adiabatic". This is reflected by a temperature-dependence of k_{ET} for non-adiabatic ET.

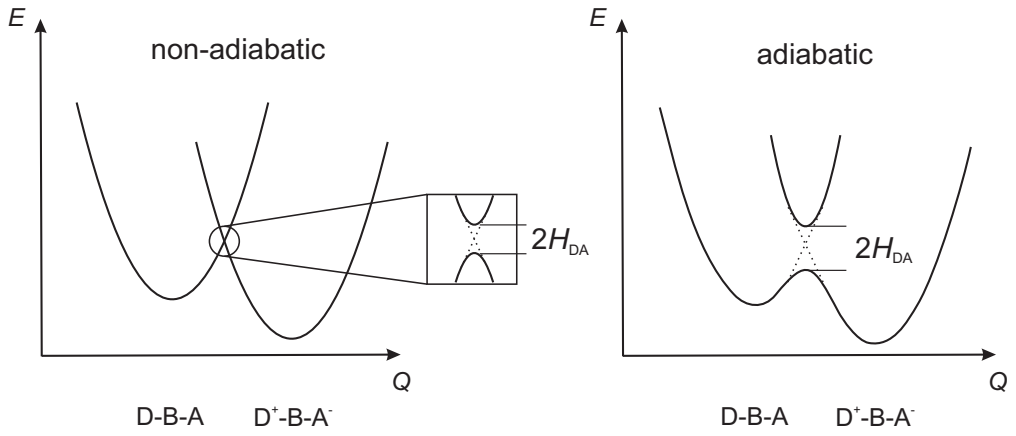

Figure II.1. Potential energy surfaces for adiabatic and non-adiabatic ET.

The systems discussed in this work are usually in the weak-coupling regime, therefore

the focus will be on non-adiabatic ET. k_{ET} can now be described by the Fermi Golden Rule (eq. II.1), with the reduced Planck constant, $\hbar$, and the Franck-Condon-weighted density of states, FCWD.

$$k_{ET} = \frac{2\pi}{\hbar}|H_{DA}|^2(\text{FCWD}) \tag{II.1}$$

The FCWD describes the thermally averaged overlap between the reactant and product vibrational wave functions.[12] The most prominent way to calculate FCWD is by the Marcus semi-classical treatment (eq. II.2), including the Boltzmann-constant, k_B, and temperature, T.

$$\text{FCWD} = (4\pi\lambda k_B T)^{-\frac{1}{2}} \exp\left(-\frac{\left(\Delta G^0 + \lambda\right)^2}{4\lambda k_B T}\right) \tag{II.2}$$

The main parameters are the reorganization energy, λ, and the reaction free energy, ΔG^0. These parameters are also reflected in the potential energy surface picture (Figure II.2). In addition, the energy difference from the potential well of the reactant to the crossing point of the reactant and product potentials is the activation barrier, $\Delta G^{\ddagger}$.

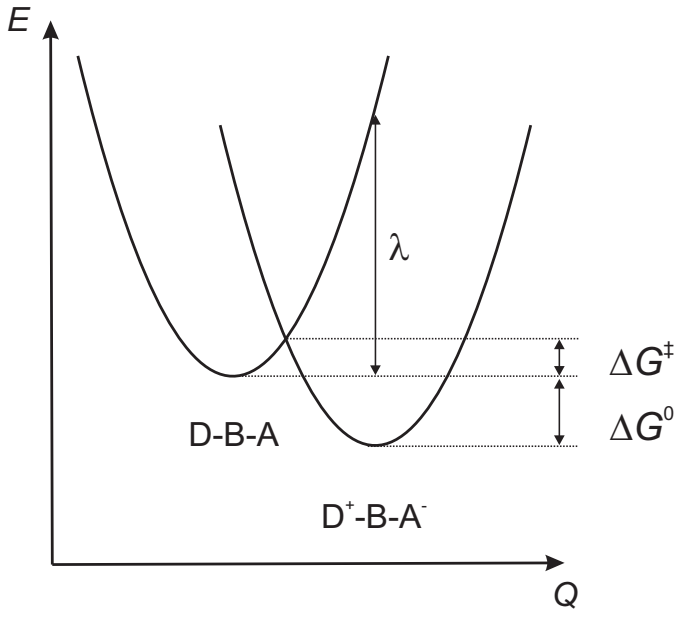

Figure II.2. Potential energy surfaces for non-adiabatic ET.

λ represents the required energy for the D-B-A potential well to adopt to the D^+-B-A^- equilibrium geometry, and pays tribute to the fact that an electron-transfer process involves an adjustment of bond-lengths and -angles in the compound (λ_i) and that the solvent shell has to adapt to the new environment (λ_o) (eq. II.3).[9]

$$\lambda = \lambda_i + \lambda_o \tag{II.3}$$

ΔG^0 is determined by the relative energy-difference between the reactant and product potential energy surface minima. Three different regions, regarding $\Delta G^{\ddagger}$, exist by varying ΔG^0 (Figure II.3): (1) the Marcus-normal region, where increasing ΔG^0 leads to a lower $\Delta G^{\ddagger}$; (2) the activation-less point ($\Delta G^{\ddagger} = 0$), where the intersection of the potential energy surface is located at the reactant potential well minimum; (3) the Marcus-inverted region, where increasing ΔG^0 leads to a higher $\Delta G^{\ddagger}$.

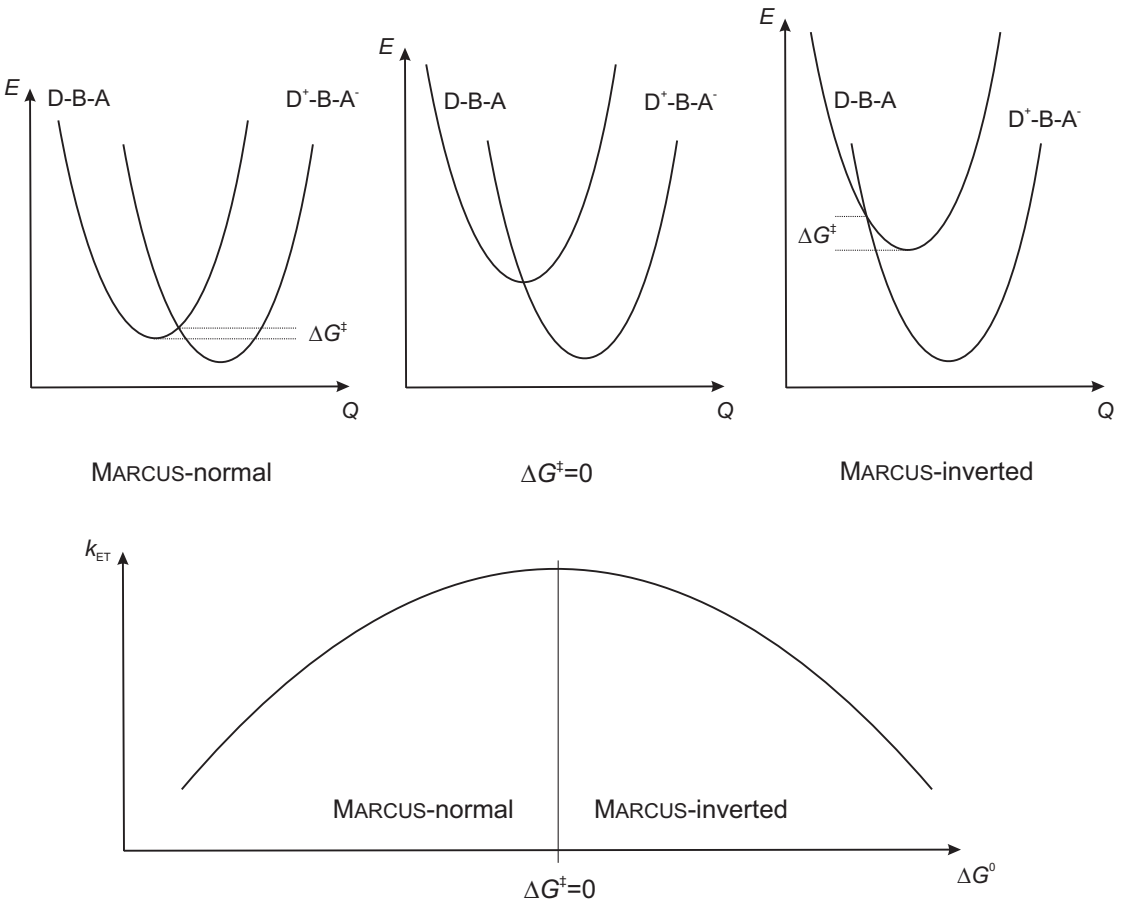

Figure II.3. Potential energy surfaces for non-adiabatic ET in the Marcus regimes and k_{ET} as a function of ΔG^0.

H_{DA} can be divided into two terms, a term taking account of the direct coupling of donor and acceptor orbitals (V_{DA}) and a so-called superexchange term (V_S). V_S describes the perturbation of donor and acceptor orbitals, resulting from mixing with orbitals from the bridge. V_{DA} is the relevant term for the through-space pathway and is very small for long-range through-bond ET.[13] Having a closer look at the mechanism for the coherent superexchange, one can write (eq. II.4):

$$H_{DA} = V_{DA} + V_S \simeq V_S \tag{II.4}$$

In the following, H_{DA} will be used equivalently to V_S.
McConnell's relation is another way to describe H_{DA}, if the donor, D, and the acceptor, A, are connected by a bridge, B, consisting of n repeating units. H_{DA} is written as a relation of the coupling strengths h_{ij} of each donor and acceptor with the bridge states and the adjacent bridge states among each other, and the energy gap ($\Delta\epsilon$) between the virtual ionic states of the bridge and the initial/final states of the ET process (eq. II.5).[12,14]

$$H_{DA} = \frac{h_{DB}}{\Delta\epsilon}\left(\frac{h_{BB}}{\Delta\epsilon}\right)^{n-1} h_{BA} \tag{II.5}$$

This relationship can be written as an exponential dependence-dependence of H_{DA} on n with the decay constant β_n (eq. II.6).[10]

$$\beta_n = 2\ln\left(\frac{h_{BB}}{\Delta\epsilon}\right) \tag{II.6}$$

From equations II.1 and II.5, an exponential dependence-dependence of k_{ET} can be formulated as eq. II.7 with the distance between donor and acceptor, r.

$$k_{ET} \propto \exp(-\beta r) \tag{II.7}$$

Therefore, β can be expressed as a function of $\Delta\epsilon$, the length of a single bridge unit r_B and the inter-bridge interaction (h_{BB}) (eq. II.8).[14]

$$\beta = \frac{2}{r_B}\ln\left(\frac{h_{BB}}{\Delta\epsilon}\right) \tag{II.8}$$

Hence, a low LUMO or a high HOMO energy of the bridge will increase k_{ET}. A β-value determined for a bridge with a certain donor-acceptor pair can not necessarily be transferred to different donors or acceptors, as $\Delta\epsilon$ depends on their respective potential energies. β-values generally range between nearly 0 $Å^{-1}$, for conducting materials like metals, and 3.5 $Å^{-1}$, for vacuum.[15]

II.1.2 Electron-Transfer vs Hole-Transfer

One further distinguishes between an electron- and a hole-transfer mechanism. A schematic depiction of charge-separation is presented in Scheme II.1.[14] The nature of charge-transfer is decided by the lowest $\Delta\epsilon$.

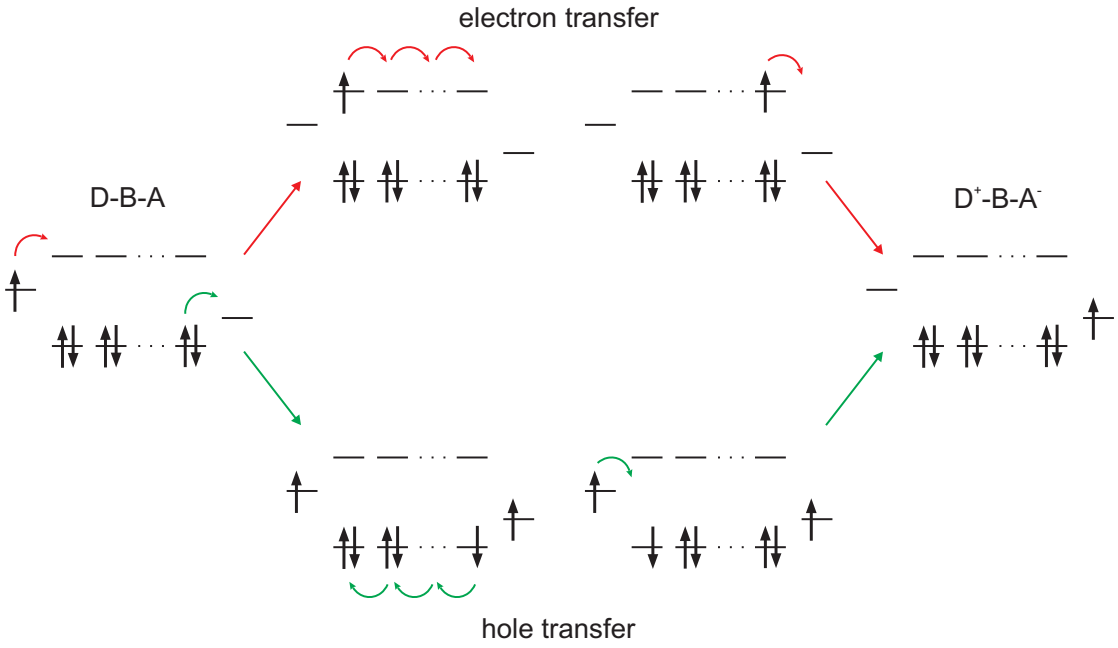

Scheme II.1. Schematic depiction of (red) the electron- and (green) hole-transfer pathways.

II.1.3 Superexchange vs Hopping

A key requirement for McConnell's theory is that the expression $\frac{|h_{BB}|}{\Delta\epsilon}$ is significantly smaller than unity. This assumption fails if the relevant bridge states are close to the donor/acceptor energy levels. If for example, the bridge LUMO becomes lower in energy than the initial excited state, the previously virtual ionic bridge states become real intermediate states in the ET process. The mechanism changes from the coherent superexchange to an incoherent charge-transport called hopping.[12]

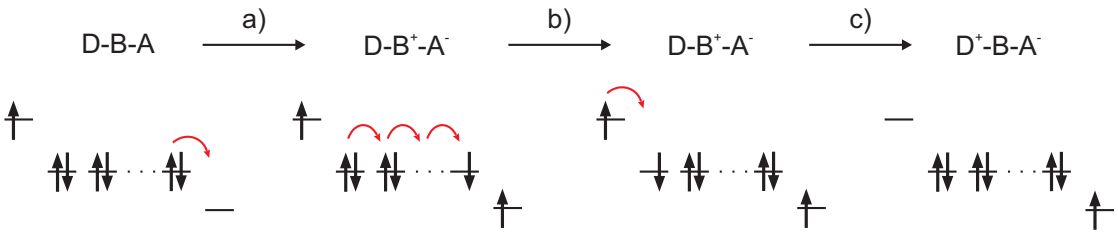

Scheme II.2. Schematic depiction of the hopping mechanism.

The hopping mechanism can be divided into three steps (Scheme II.2): a) charge injection into the bridge; b) random reversible charge migration through the bridge; c)

charge trapping. The ET rates are faster compared to those for the superexchange mechanism at the same distance. The distance dependence of the hopping mechanism is related to the number of repeating bridge units, n, with the coefficient η (eq. II.9).[12]

$$k_{ET} \propto n^{-\eta} \quad \text{with} \quad 1 \leq \eta \leq 2 \tag{II.9}$$

II.2 Photoinduced Electron-Transfer

After excitation of a chromophore, there are four possible pathways to the ground-state (Scheme II.3).[16]

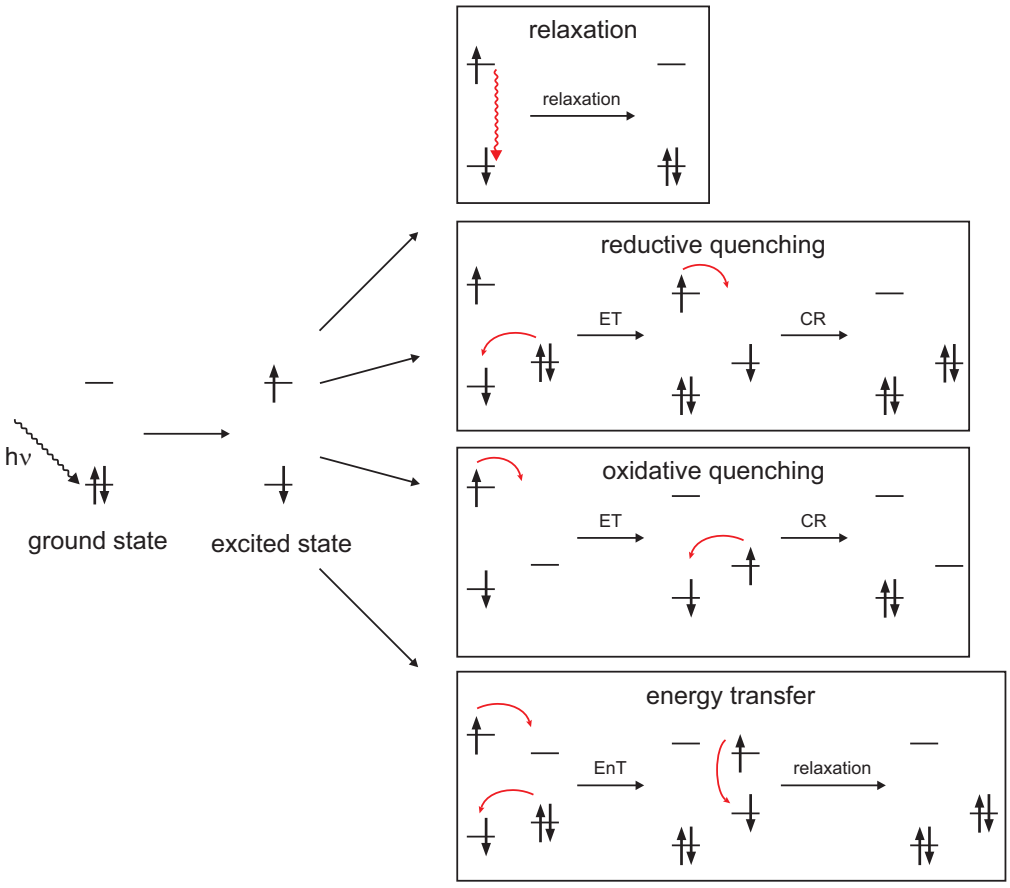

Scheme II.3. Reaction pathways of an excited chromophore back to its ground-state; all examples are depicted within a singlet manifold.

The simplest one is the unproductive relaxation of the excited state to ground state, that can occur either non-radiatively or via emission of a photon (radiatively). Electron-transfer can occur either in an oxidative or reductive fashion with respect to the excited chromophore, dependent on suitable orbitals of the quencher. After charge-recombination, both chromophore and quencher reach their ground-states again. If

not only the HOMO or LUMO of the quencher is accessible but both, energy-transfer is possible as competing reaction. The intermediate state is the excited quencher, which finally relaxes back to its ground-state.

II.3 Through-Space/Solvent Electron-Transfer Studies

Through-space and through-solvent ET are both basically electron-tunneling processes, in which the electronic coupling is not provided by covalently-bound direct neighboring groups. If the void between the groups participating in ET is large enough to allow solvent molecules to fill in the void, one speaks of through-solvent ET. The tunneling-barrier height will be affected by the solvent.[17] Different approaches to investigate the non-bridge mediated ET will be presented in the following.

II.3.1 C- and U-Shaped Molecular Systems

An obvious approach to decrease the through-space donor-acceptor distance with respect to a through-bond pathway is to create systems with a bent C- or U-shaped structure (Figure II.4). The research groups of Paddon-Row, Zimmt and Waldeck have dominated this strategy.[17–25]
In general, the studied systems consist of an organic donor/acceptor-pair connected by a rigid saturated hydrocarbon spacer. ET occurs from the excited state of the aromatic donor moiety. The spacer should hold the donor-acceptor pair at a relatively fixed distance, while preferably allowing only weak through-bond electronic coupling.

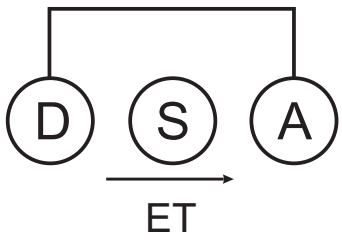

Figure II.4. Schematic depiction of a U-shaped system with a solvent molecule, S, between donor and acceptor.

One of the first examples of this kind was presented by Zimmt and Waldeck (Figure II.5).[18] In the nearly linear compound **A1**, the donor-acceptor (D-A) separation is identical for the through-space and through-bond pathway at approximately 12 Å, while for the C-shaped compound **A2** the through-space distance is significantly smaller at 7 Å. H_{DA} only showed a distinct solvent dependence for C-shaped **A2** (15–64 cm^{-1}), whilst being constant and generally weaker for **A1** ($\sim$ 14 cm^{-1}). The solvent-dependence of H_{DA} was accounted for by the presence of solvent molecules in the gap between

donor and acceptor. Direct through-space coupling was ruled out by molecular mechanics calculations, revealing that only a negligible fraction of molecules can access conformations with D-A-distances allowing through-space H_{DA}. Benzonitrile, as the only aromatic solvent tested, was found to show the strongest H_{DA}.

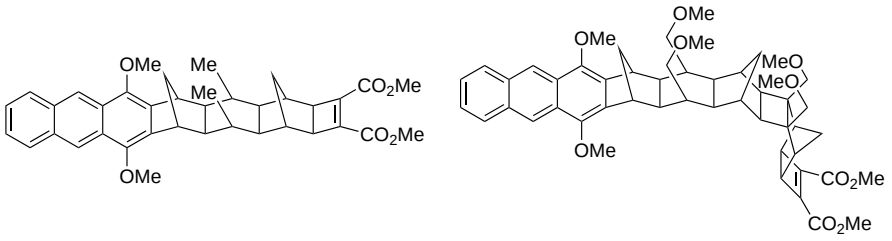

A1 **A2**

Figure II.5. D-A-compounds **A1** and **A2**, for the determination of H_{DA} in solvent-mediated ET.

The solvent-dependence of **A2** was further studied in more detail.[26] Alkyl-substituted aromatic solvents with varying steric bulk were tested for their effect on H_{DA}. For benzene, toluene and cumene, H_{DA} was approximately constant, but it decreased strongly for more sterically demanding solvents. Molecular mechanics energy optimizations revealed that within the tested series, solvents bulkier than cumene cannot diffuse far enough into the cleft to enable sufficient orbital overlap with the donor and acceptor π-orbitals.

The distance-dependence of through-solvent ET was investigated by C-shaped compounds **B1**–**B3**, with decreasing respective bite-sizes (Figure II.6).[17] Every compound has D-A-separation of 10 σ-bonds, but their through-space distance decreases with the stronger curvature from 13.4 for **B1**, to 9.5 for **B2**, to 7.5 Å for **B3**. For **B1**, the solvent dependence is low, indicating only little through-solvent contribution to the ET. The through-bond coupling is caused by an all-*trans* configuration of the σ-bonds. By disrupting this configuration in **B2** and **B3**, the through-bond interaction is weakened and the curvature increased at the same time. For **B2**, the D-A-distance is still too great to enable significant through-solvent H_{DA}, evidenced by much slower ET compared to **B1**. This changes for **B3**, where ET rate constants are highly solvent dependent, and their values outweigh those of **B1** by factors of up to 10.

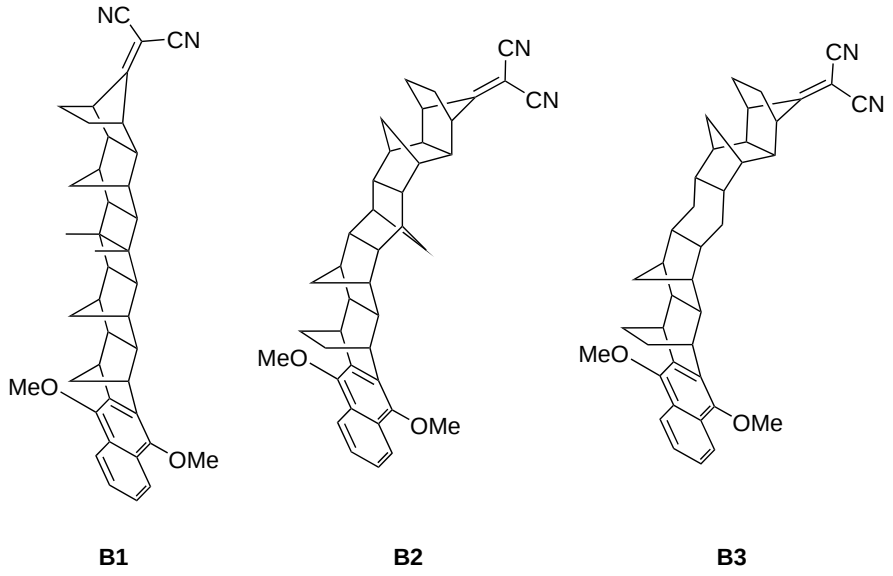

Figure II.6. C-shaped D-A-compounds with different bite-sizes.

In order to further study the effect of different residues within the gap between donor and acceptor in U-shaped compounds, Paddon-Row and Waldeck developed a system in which different residues for this purpose can be covalently bound to the bridge as a quasi-solvent (Figure II.7).[20,21,25] The residues are decoupled from the through-bond pathway, but are directly positioned in the through-space pathway. With this strategy, all compounds could be studied in the same solvent, minimizing changes in λ_i and ΔG^0 that could result from the use of a different solvent. Effects from the different residues can therefore be directly associated with a change in through-solvent H_{DA}.

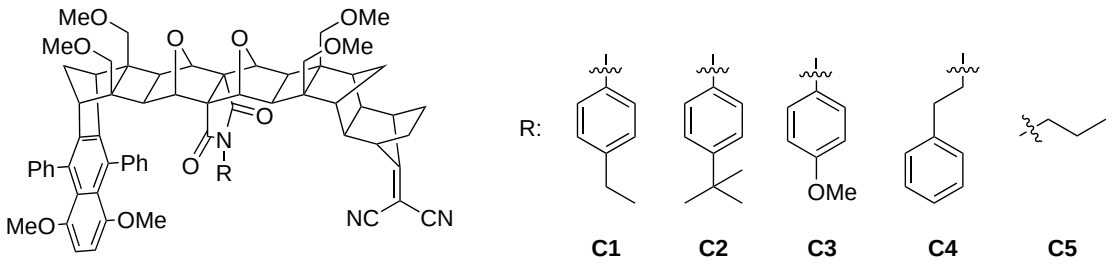

Figure II.7. U-shaped D-A-system with a variable residue in the cleft.

The aromatic residues exhibited stronger H_{DA} compared to the aliphatic one, due to the overlap of the respective π-systems.
At room temperature, the ET behavior of **C1** and **C5** could be explained by the non-adiabatic superexchange mechanism. However, this approach failed for low-temperature

measurements in high polarity solvents – a transition to solvent-controlled ET was observed.[24,27] Where, at high temperatures, electron-tunneling is the rate-limiting step, this changes for low temperatures. Nuclear motion through the region of the crossing point of the reactant and product potentials (Figure II.2), the transition state region, is slowed down by frictional coupling to the solvent, thereby making it rate-limiting.[27]

II.3.2 π-π-Interactions

π-π-Interactions between the donor and acceptor moieties are an effective way to facilitate through-space H_{DA}.[28] Therien and co-workers observed an unusual distance-dependence of photo-induced ET for a series of D-A-compounds (**D1**–**D3**), where the π-systems of porphyrin-donors, quinone-acceptors and bridge aryl-units are cofacially orientated (Figure II.8). The determined β-values for charge-separation (CS) and charge-recombination (CR) are both around 0.4 $Å^{-1}$ and therefore in the region of through-bond systems with conjugated bridges. This behavior was accounted for by the sub-van der Waals distance between the aromatic planes of 2.98 Å.

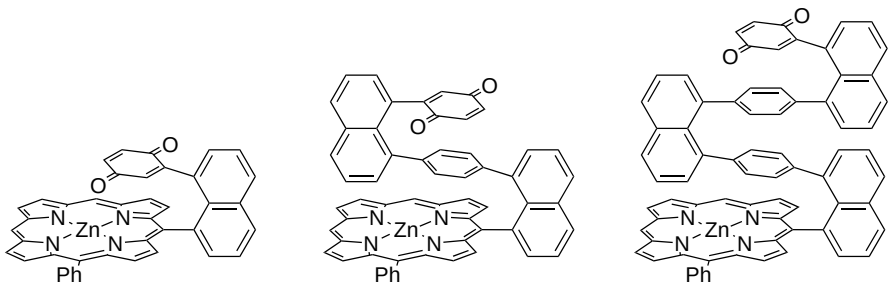

Figure II.8. Series of D-A-compounds with a stacked arrangement of donor, acceptor and bridge π-systems.

Porphyrins and fullerenes are known to display strong van der Waals attractions. Generally, small D-A-distances in flexible dyads containing a porphyrin-C_{60} pair are attributed to this attraction.[29] The importance of this π-π-interaction in ET was demonstrated by Hirsch and Guldi by a comparison of two porphyrin-C_{60} dyads with different orientations of the porphyrin-moiety (Figure II.9). Only the face-to-face orientation of **E1** allows close contact, resulting in rate constants for photoinduced ET after excitation of the porphyrin that are greater by an order of magnitude for **E1** compared to the face-to-edge oriented **E2**. The effect is even more pronounced for CR, enhancing it by four orders of magnitude.

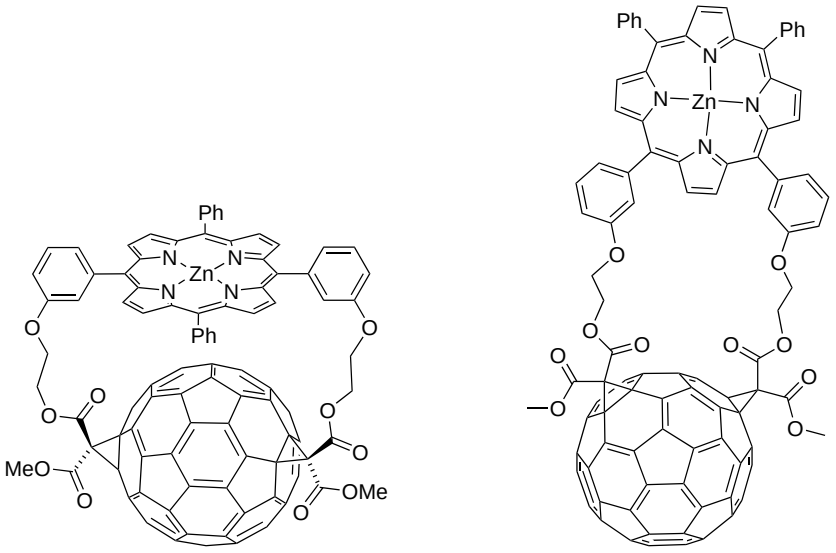

E1 **E2**

Figure II.9. Porphyrin-C_{60} dyads with face-to-face (**E1**) and face-to-edge (**E2**) orientation.

Strong π-π-interactions between phorphyrins and C_{60} are also demonstrated in the parachute-shaped dyad **F** (Figure II.10).[29] In the lowest energy conformation, the porphyrin is strongly bent towards the fullerene, resulting in an edge-to-edge D-A-distance of 4.2 Å. In this configuration, through-space interactions of the π-systems play a significant role in the ET process.

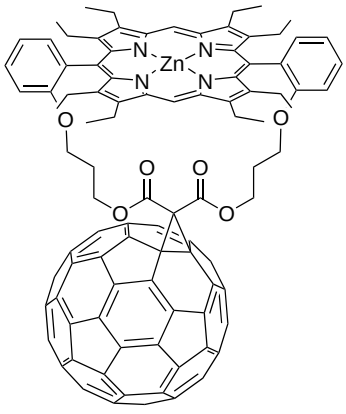

F

Figure II.10. Porphyrin-C_{60} dyad **F** with a parachute-shaped geometry.

II.3.3 Supramolecular Systems

An elegant way to enable efficient through-space ET is the use of supramolecular systems for intermolecular ET. The lack of covalent connection between the D-A-pair prevents through-bond H_{DA}.

By comparing rotaxane-based D-A-compounds to a related covalently bound dyad (Figure II.11), it was found that the energy of the charge-separated state was decreased for the rotaxanes.[30] As a consequence, CS in **G1** and **G2** occurs via the triplet excited state of the C_{60}-acceptor, whereas in the dyad **G3**, CS takes place via the singlet state. The resulting charge-separated state was only long-living for the rotaxane compounds ($\tau \approx 300$ ns for both compounds). CS and CR in the dyad **G3** took place within the laser pulse of 6 ns. The center-to-center D-A-distances were estimated by MM2 force-field calculations. The charged compound **G1** showed a longer D-A-distance compared to **G2** (21 vs 17 Å). This calculated difference had no effect on the measured k_{ET}-values though.

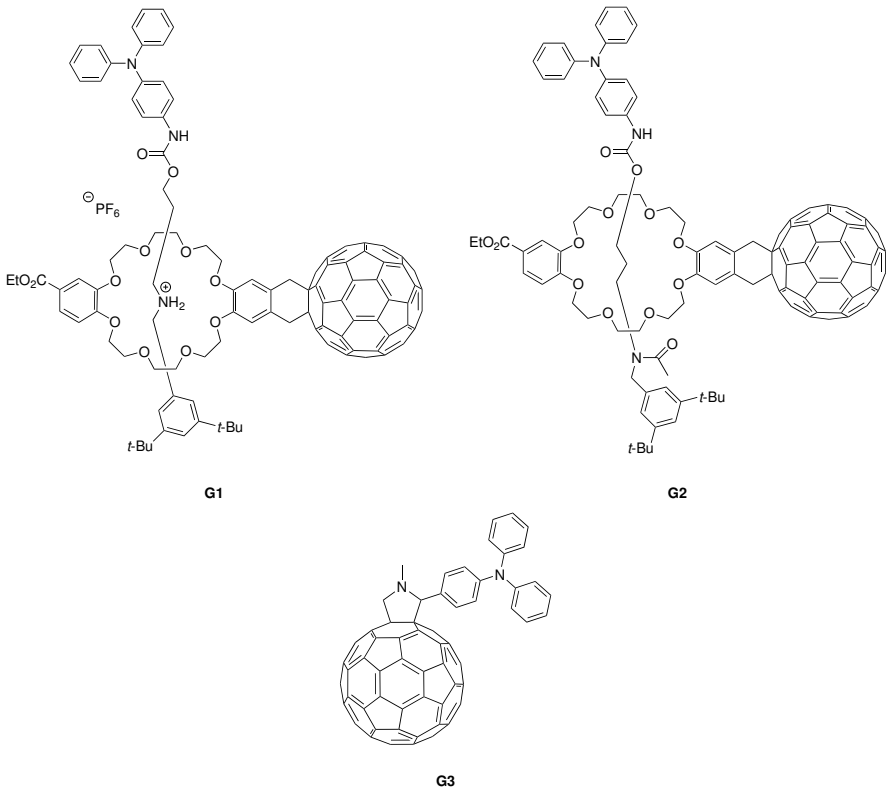

Figure II.11. Rotaxane D-A-compounds **G1** and **G2**, and a related covalently connected D-A-dyad **G3**.

Ultrafast photoinduced ET was observed in a supramolecular assembly of C_{70} encap-

sulated in **H** after excitation of the porphyrin cage (Figure II.12).[31] The rigidity of the cage results in a relatively fixed edge-to-edge D-A-distance of 2.8 Å and, as a consequence, an unusually strong H_{DA} for supramolecular porphyrine-fullerene compounds. CS occurs on the sub-picosecond time-scale and the rate could not be determined. The lifetime for CR could be determined to be approximately 650 ps in toluene. Minimizing the structural flexibility was found to be the key factor for the observed high τ_{CR}/τ_{CS} ratio.[31]

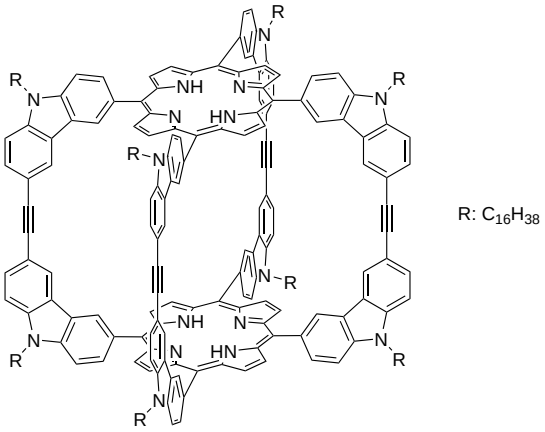

H

Figure II.12. Molecular structure of the porphyrine-based cage **H**.

The so-called $Exbox^{4+}$ (**I**; Figure II.13) is a boxlike cyclophane, consistent of two viologens liked by *p*-phenylene linkers. Stoddart and Wasielewski presented a system where a perylene is incorporated into $Exbox^{4+}$, which undergoes ultrafast ET and CR after excitation of the perylene chromophore.[32] CS occurs within the instrument response of approximately 200 fs; the lifetime of the charge-separated state was determined to be 42 ps. The observed short lifetimes were accounted for by a small D-A-separation, strong electronic coupling and a high ΔG^0 .

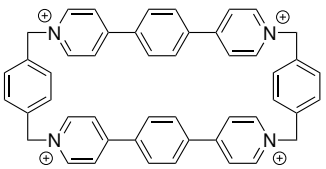

I

Figure II.13. Molecular structure of $Exbox^{4+}$ **I**.

III Probing Through-Solvent Electron-Transfer With A Molecular Corner

Electron-transfer through conjugated or aliphatic bridges has been widely studied.[12,33] Comparably less is known about the through-solvent pathway, especially with respect to its distance dependence. This is mainly due to the fact that deconvoluting different possible intramolecular electron-transfer pathways is a challenging task. Variation of the donor-acceptor distance is achieved by modification of the bridge. However, changing the bridging unit always has an influence on the through-bond pathway,[18] making it difficult to identify the isolated contribution for an increase of the through-solvent distance.
The spirobifluorene geometry allows two doubly substituted isomers, linear and right-angled. By attaching a donor and an acceptor side-arm with different bridge lengths, one obtains two homologous series of donor-acceptor compounds (Figure III.1).

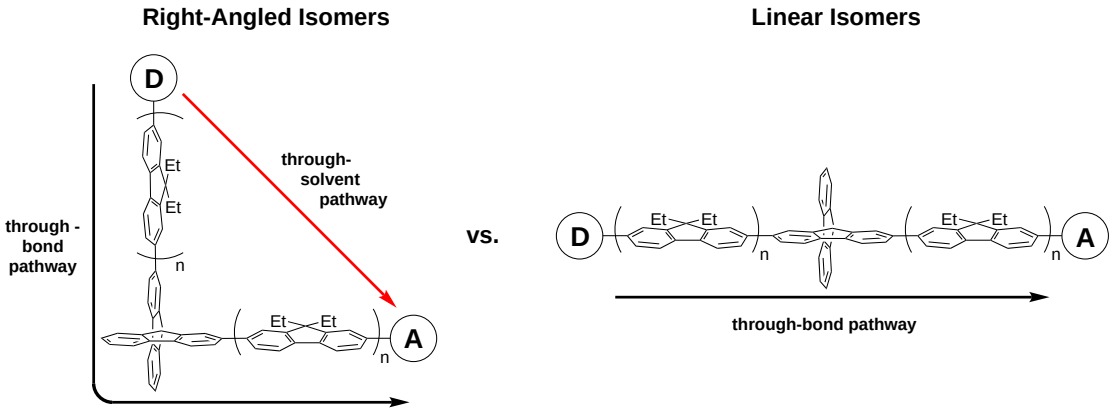

Figure III.1. Right-angled and linear series of donor-acceptor compounds (n = 1-3) and their possible electron-transfer pathways.

In the linear reference series, electron-transfer can only occur via the through-bond pathway. The right-angled structure enables the through-solvent pathway as a second possibility. Through-bond electron-transfer can still occur through the π-system of the fluorene bridge.

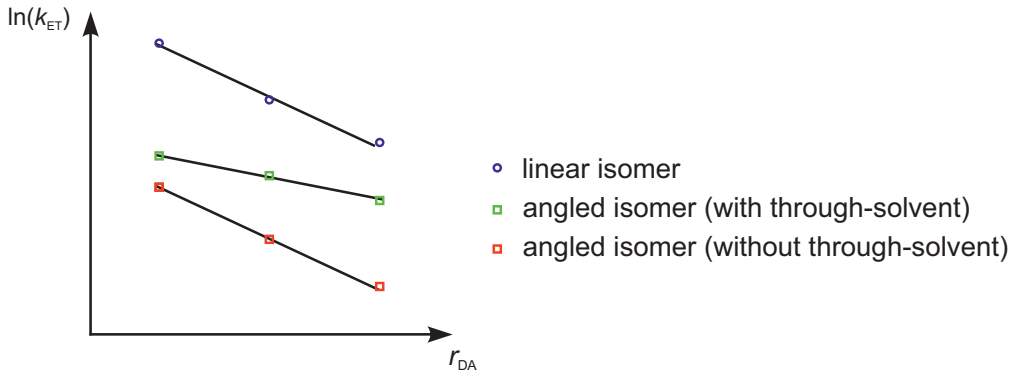

Figure III.2. Hypothesized distance-dependence of k_{ET} for the linear and angled series of complexes.

A comparison of the distance-dependence of electron-transfer rate constants for the two series can either result in the same or a different value (Figure III.2). The same value would point towards a negligible contribution of the through-solvent pathway. The overall values of the electron-transfer rate constants will be lower for the right-angled series, as the orthogonal orientation of the donor and acceptor side-arm π-systems leads to a significant decrease in electronic coupling. The disruption of the π-conjugation by the central carbon atom in the spirobifluorene should emphasize this effect. But this effect would be a constant factor, and hence not be an influence on the overall distance dependence. Any effect of the through-solvent pathway would lead to different β-values for the two series. This difference can then be accounted as the through-solvent distance dependence.

Dianisylphenylamine was chosen as a donor moiety, due to its characteristic radical cation absorption. The combination of triarylamine donors with a $[Ru(bpy)_3]^{2+}$ photosensitizer is well established in our group.[34–36] The redox-properties of $[Ru(bpy)_3]^{2+}$ in the ground- and ^{3}MLCT excited state are presented in Figure III.3, illustrating the more pronounced capabilities of ^{3}MLCT excited $[Ru(bpy)_3]^{2+}$ to act as electron donor or acceptor.[37]

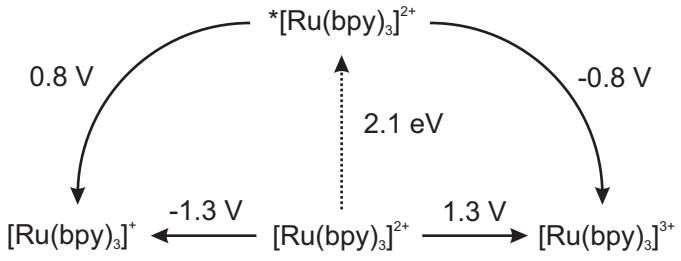

Figure III.3. LATIMER diagram of $[Ru(bpy)_3]^{2+}$; redox-potentials are reported as V vs SCE in acetonitrile.

III.1 Synthesis

The synthesis of the ligand is based on a building block strategy. Two isomeric twofold bromo-substituted spirobifluorenes, **Br-spiro(A)-Br** (Scheme III.2 and III.3) for the angled series, and **Br-spiro(L)-Br** (Scheme III.1) for the linear series, are the central building blocks. The synthesis of dibromo-substituted spirobifluorenes from 9*H*-fluorene has been previously reported in the literature.[38,39]

Br-spiro(L)-Br was synthesized according to literature procedures (Scheme III.1).[38] The reaction sequence starts with the bromination of 9*H*-fluorene, followed by oxidation to the corresponding fluorenone, **Br-FlO-Br**, and the nuclephilic addition of a Grignard-reagent prepared from the bromo-substituted biphenyl **biph-Br**. An acid-catalyzed cyclisation of the non-isolated intermediate formed **Br-spiro(L)-Br**.

Following a similar sequence to Scheme III.1, the unsubstituted spirobifluorene **spiro-Fl** was obtained (Scheme III.2). As the purification of its bromination product, **Br-spiro(A)-Br**, was time-consuming, a second synthetic route, also previously reported in the literature, was explored.[39] An adaptation of this synthetic route was achieved by splitting up the synthesis of **TMS-biph-CO** from **TMS-biph-Br** in two separate reactions, to provide reasonable yields (Scheme III.3).

TMS-Fl-BA (Scheme III.4) was the building block used to build up the triarylamine and bipyridine side-arms. The amine side-arms containing one fluorene unit (**TAA-Fl-BA** and **TAA-Fl-BE**) were synthesized over five steps with overall yields of 11% and 47%, respectively (Scheme III.5). As the reaction forming the boronic acid (**TAA-Fl-BA**) only afforded 19% yield, the boronic ester (**TAA-Fl-BE**), prepared by a Miyaura-coupling, was chosen as an alternative. The bipyridine side-arm **bpy-Fl-BE** was synthesized using a similar route (Scheme III.6). The bromo-substituted bipyridine was coupled with **TMS-Fl-BA** in a Suzuki-Miyaura coupling, followed by iodo-desilylation with iodine monochloride, and a Miyaura-coupling with $B(pin)_2$ to form **bpy-Fl-BE** with an overall yield of 48% over four steps (Scheme III.6).

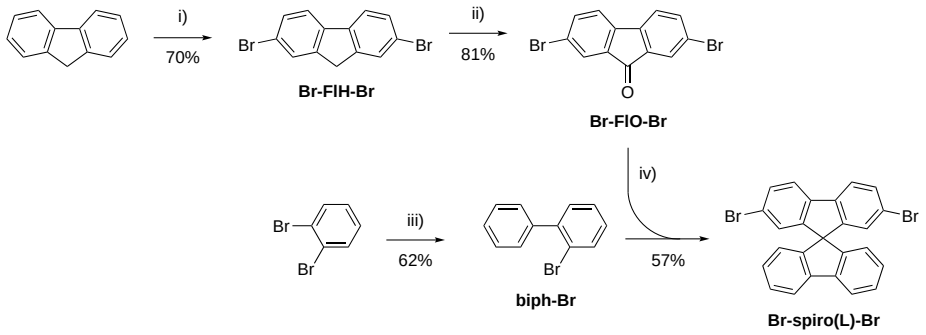

Scheme III.1. Synthesis of **Br-spiro(L)-Br**: i) Br_2, CH_2Cl_2, 0 °C; ii) *t*-BuOOH, KI, CH_2Cl_2/MeCN, r.t.; iii) phenylboronic acid, Na_2CO_3, $[Pd(PPh_3)_4]$, THF/H_2O, 80 °C; iv) a) Mg, Et_2O/THF, reflux b) acetic acid/hydrochloric acid, 125 °C.

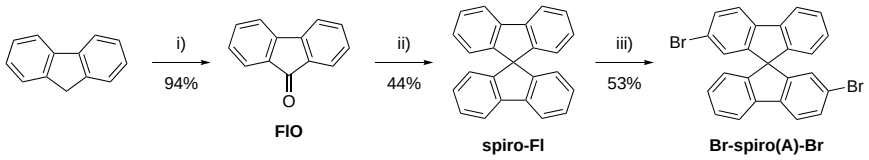

Scheme III.2. Synthesis of **Br-spiro(a)-Br** route 1: i) *t*-BuOOH, KI, MeCN, r.t.; ii) a) **biph-Br**, Mg, Et_2O/THF, reflux b) acetic acid/hydrochloric acid, 125 °C; iii) Br_2, $FeCl_3$, $CHCl_3$, 0 °C.

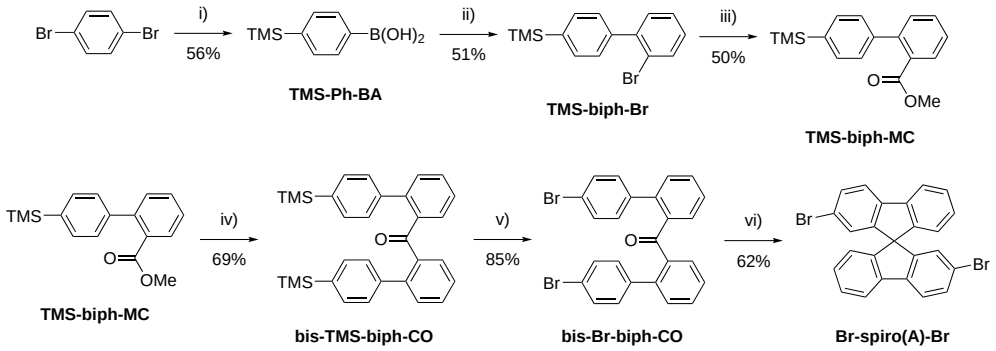

Scheme III.3. Synthesis of **Br-spiro(a)-Br** route 2: i) *n*-BuLi, Me_3SiCl, $B(i\text{-}PrO)_3$, THF, -78 °C; ii) 1,2-dibromobenzene, Na_2CO_3, $[Pd(PPh_3)_4]$, THF/H_2O, 80 °C; iii) *n*-BuLi, dimethylcarbonate, THF, -78 °C; iv) **TMS-biph-Br**, *n*-BuLi, THF, -78 °C; v) Br_2, NaOAc, THF, 0 °C; vi) methanesulfonic acid, 120 °C.

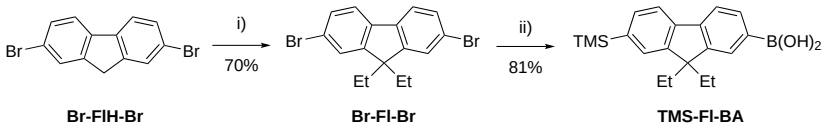

Scheme III.4. Synthesis of **TMS-Fl-BA**: i) ethylbromide, KOH, KI, DMSO, r.t.; ii) *n*-BuLi, Me_3SiCl, $B(i\text{-}PrO)_3$, THF, -78 °C.

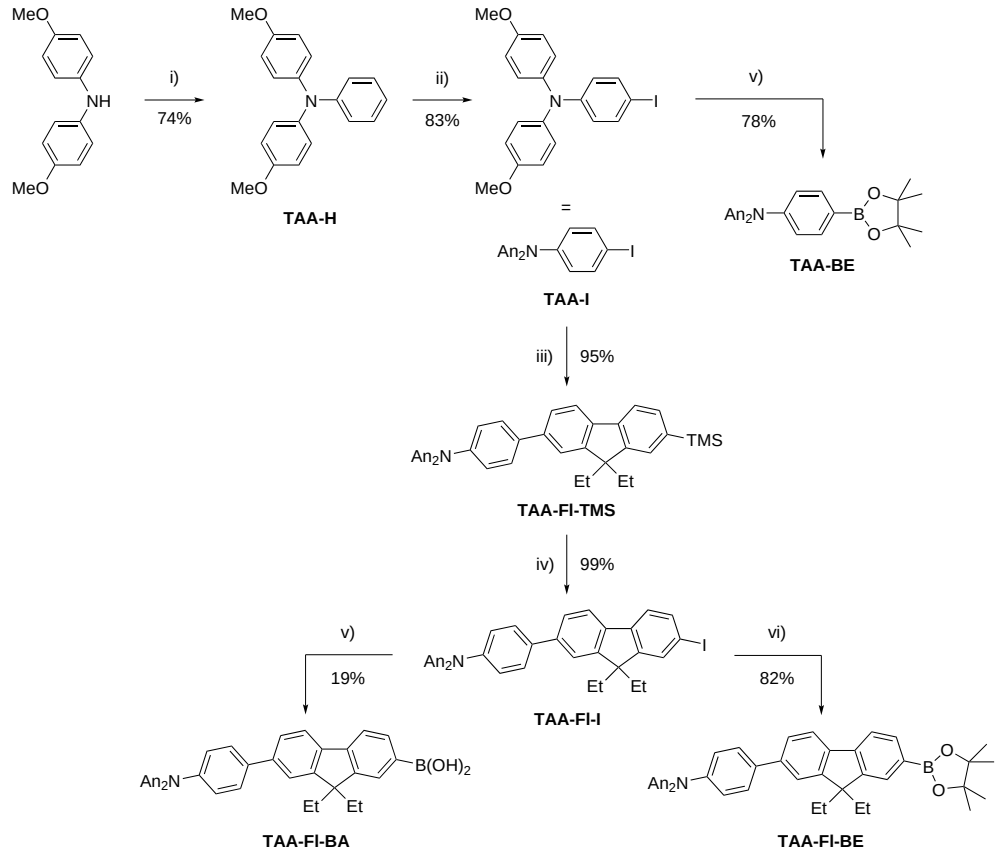

Scheme III.5. Synthesis of **TAA-BA**, **TAA-Fl-BA** and **TAA-BE**: i) bromobenzene, $[Pd(dba)_2]$, NaO*t*Bu, $[HP(t\text{-}Bu)_3]BF_4$, toluene, 80 °C; ii) I_2, bis(trifluoroacetoxy)iodobenzene, CH_2Cl_2, 45 °C; iii) **TMS-Fl-BA**, Na_2CO_3, $[Pd(PPh_3)_4]$, THF/H_2O, 80 °C; iv) ICl, CH_2Cl_2, -78 °C; v) *n*-BuLi, $B(i\text{-}PrO)_3$, THF, -78 °C; vi) $B(pin)_2$, KOAc, $[Pd(PPh_3)_2Cl_2]$, DMSO, 80 °C.

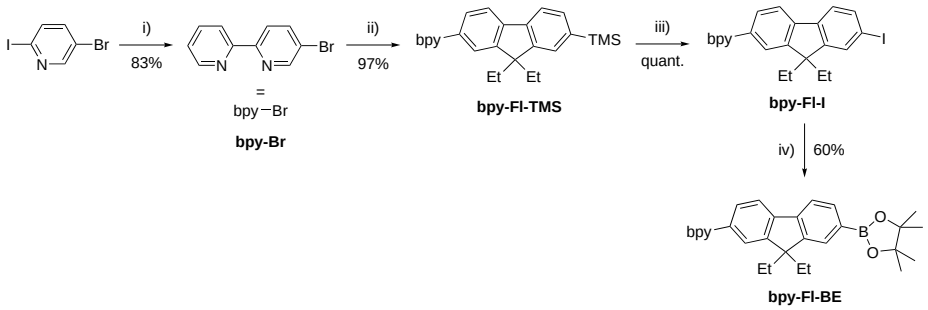

Scheme III.6. Synthesis of **bpy-Fl-BE**: i) 2-pyridylzinc, $[Pd(PPh_3)_4]$, THF, r.t.; ii) **TMS-Fl-BA**, Na_2CO_3, $[Pd(PPh_3)_4]$, THF/H_2O, 80 °C; iii) ICl, CH_2Cl_2, -78 °C; iv) $B(pin)_2$, KOAc, $[Pd(PPh_3)_2Cl_2]$, DMSO, 80 °C.

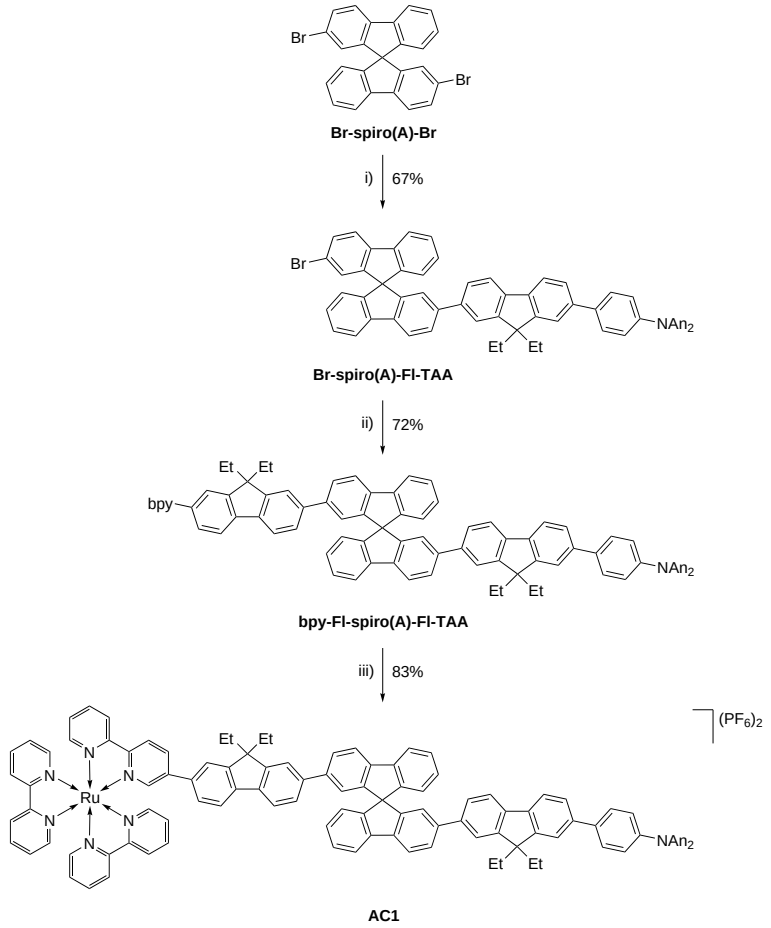

Scheme III.7. Synthesis of **AC1**: i) **TAA-Fl-BA**, Na_2CO_3, $[Pd(PPh_3)_4]$, THF/H_2O, 80 °C; ii) **bpy-Fl-BE**, Na_2CO_3, $[Pd(PPh_3)_4]$, THF/H_2O, 80 °C; iii) $[Ru(bpy)_2Cl_2]\cdot 2H_2O$, KPF_6, ethylene glycol/acetone/CH_2Cl_2, 65 °C.

Successive Suzuki-Miyaura-couplings of **TAA-Fl-BA** and **bpy-Fl-BE** with the brominated spirobifluorenes yielded the right-angled (Scheme III.7) and linear (Scheme III.8) ligands with single fluorene bridging units. The yields for the first coupling were low due to the statistical nature of this reaction. Although the amine side-arm has a longer reaction sequence, it was chosen for the first coupling as the bipyridine route was more time-consuming in total. The complexes **AC1** (Scheme III.7) and **LC1** (Scheme III.8) were obtained by complexation with $[Ru(bpy)_2Cl_2]$. The solvent mixtures were adapted to the solubilities of ligand and precursor.

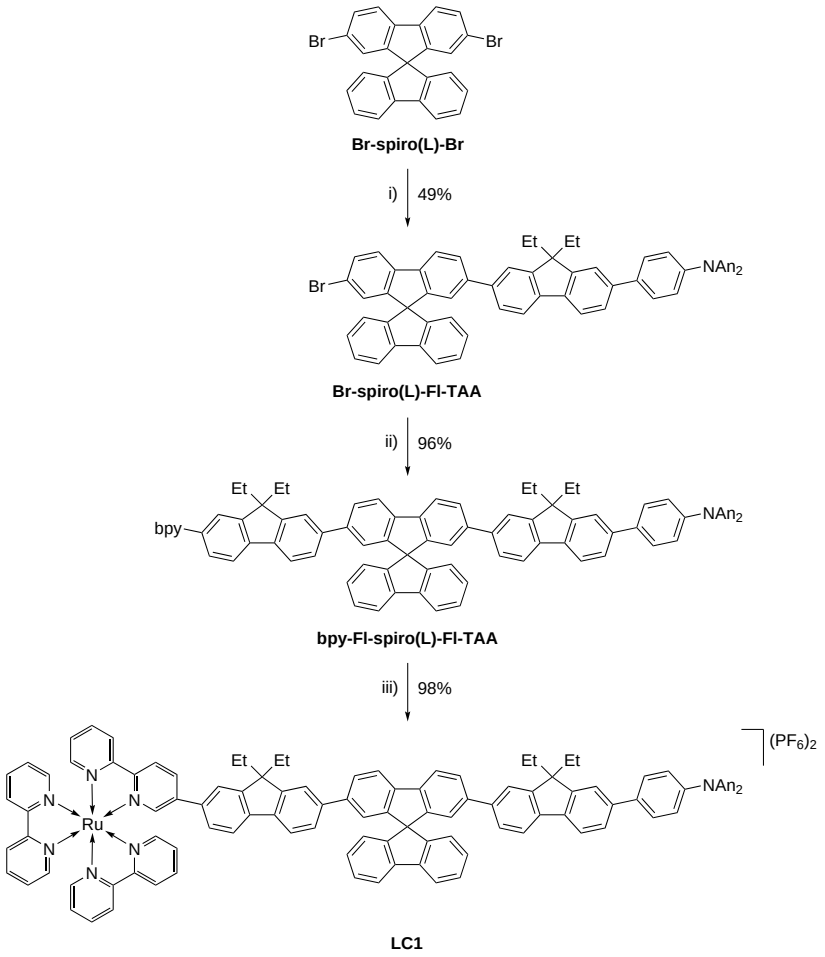

Scheme III.8. Synthesis of **LC1**: i) **TAA-Fl-BA**, Na_2CO_3, $[Pd(PPh_3)_4]$, THF/H_2O, 80 °C; ii) **bpy-Fl-BE**, Na_2CO_3, $[Pd(PPh_3)_4]$, THF/H_2O, 80 °C; iii) $[Ru(bpy)_2Cl_2]\cdot 2H_2O$, KPF_6, ethylene glycol/acetone/CH_2Cl_2, 65 °C.

For the synthesis of the ligands bearing two fluorene bridging units, the central spiro-

bifuorenes were coupled with **TMS-Fl-BA** (Scheme III.9 and III.10), instead of the side-arms, in order to reduce the overall number of reactions. A main point of concern in the extension of the spirobifluorenes was the iodo-desilylation, due to possible unwanted halogenation of the spiro-center. A concentrated solution of the substrate and a reduction of added equivalents of iodine monochloride, compared to the general iodo-desilylation method, were found to yield suitable reaction conditions.
Stability issues of the product were revealed when the amine side-arm was coupled first to the extended spirobifluorene in test-reactions. Therefore, the coupling-order of the side-arms was switched in comparison to the the smallest ligands. The increasing size of the ligands had a negative effect on their solubility. The linear complex **LC2** could still be obtained by using the $[Ru(bpy)_2Cl_2]$ precursor in moderate yields (Scheme III.9), but no complex could be isolated with the angled ligand. Therefore, the precursor was changed to $[Ru(bpy)_2(MeCN)_2](OTf)_2$, which has enhanced solubility in low polarity solvents. CH_2Cl_2 was replaced by the higher-boiling 1,2-dichloroethane in the solvent mixture, to increase the reaction temperature for the complexation (Scheme III.10).

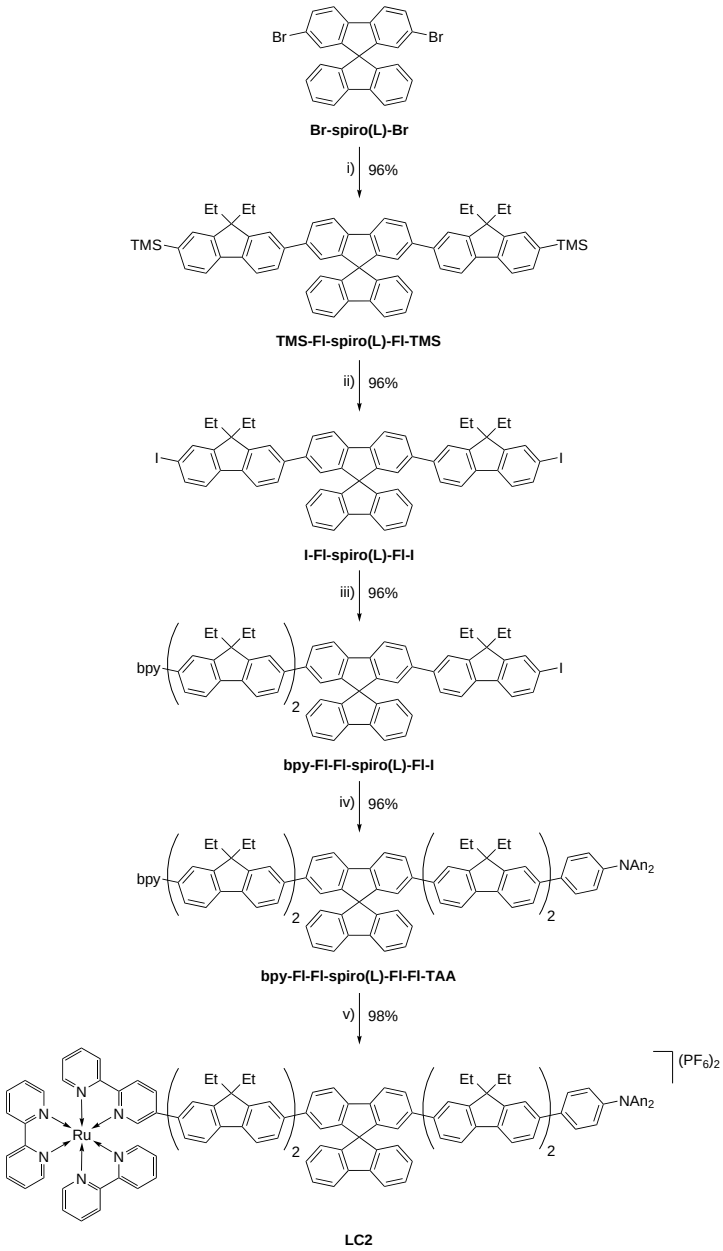

Scheme III.9. Synthesis of **LC2**: i) **TMS-Fl-BA**, Na_2CO_3, $[Pd(PPh_3)_4]$, THF/H_2O, 80 °C; ii) ICl, CH_2Cl_2, -78 °C; iii) **bpy-Fl-BE**, Na_2CO_3, $[Pd(PPh_3)_4]$, THF/H_2O, 80 °C; iv) **TAA-Fl-BE**, Na_2CO_3, $[Pd(PPh_3)_4]$, THF/H_2O, 80 °C; v) $[Ru(bpy)_2Cl_2] \cdot 2H_2O$, KPF_6, ethylene glycol/acetone/CH_2Cl_2, 65 °C.

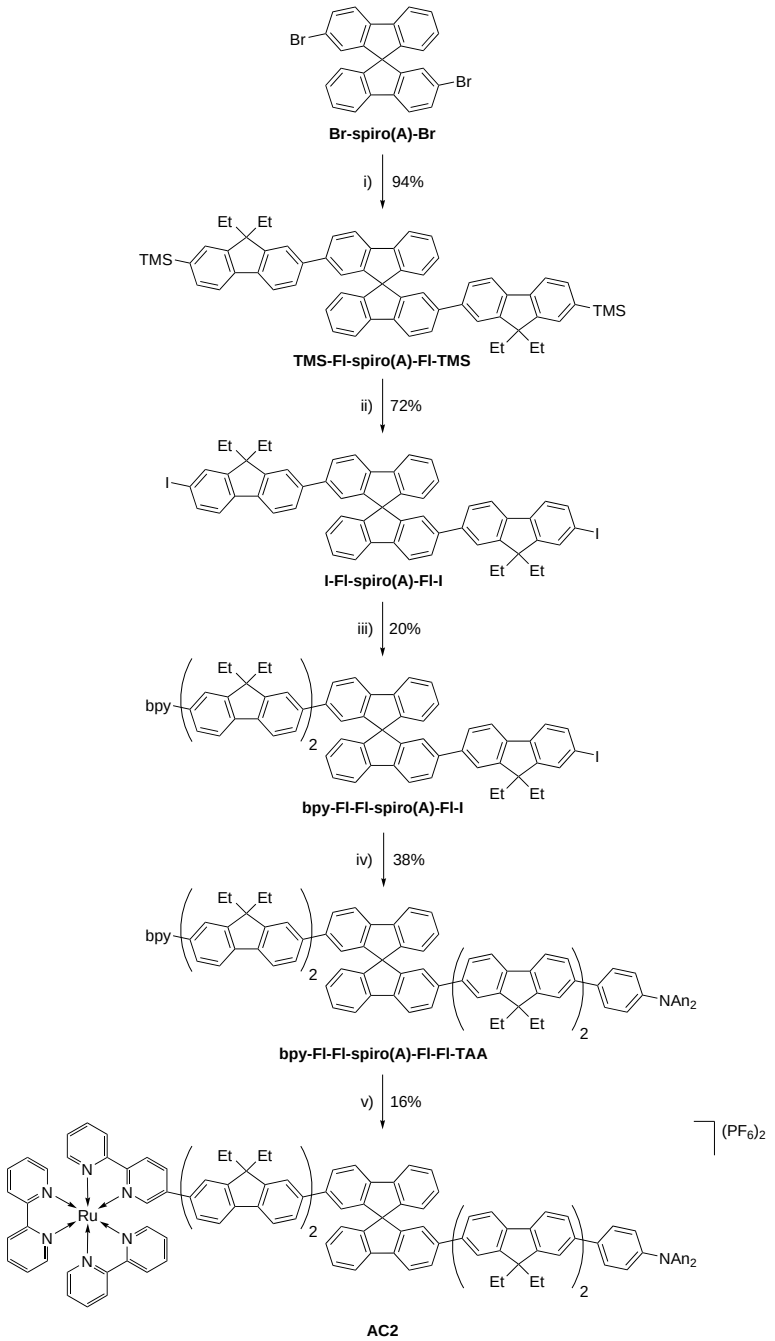

Scheme III.10. Synthesis of **AC2**: i) **TMS-Fl-BA**, Na_2CO_3, $[Pd(PPh_3)_4]$, THF/H_2O, 80 °C; ii) ICl, CH_2Cl_2, -78 °C; iii) **bpy-Fl-BE**, Na_2CO_3, $[Pd(PPh_3)_4]$, THF/H_2O, 80 °C; iv) **TAA-Fl-BE**, Na_2CO_3, $[Pd(PPh_3)_4]$, THF/H_2O, 80 °C; v) $[Ru(bpy)_2(MeCN)_2](OTf)_2$, KPF_6, ethylene glycol/acetone/1,2-dichloroethane, 85 °C.

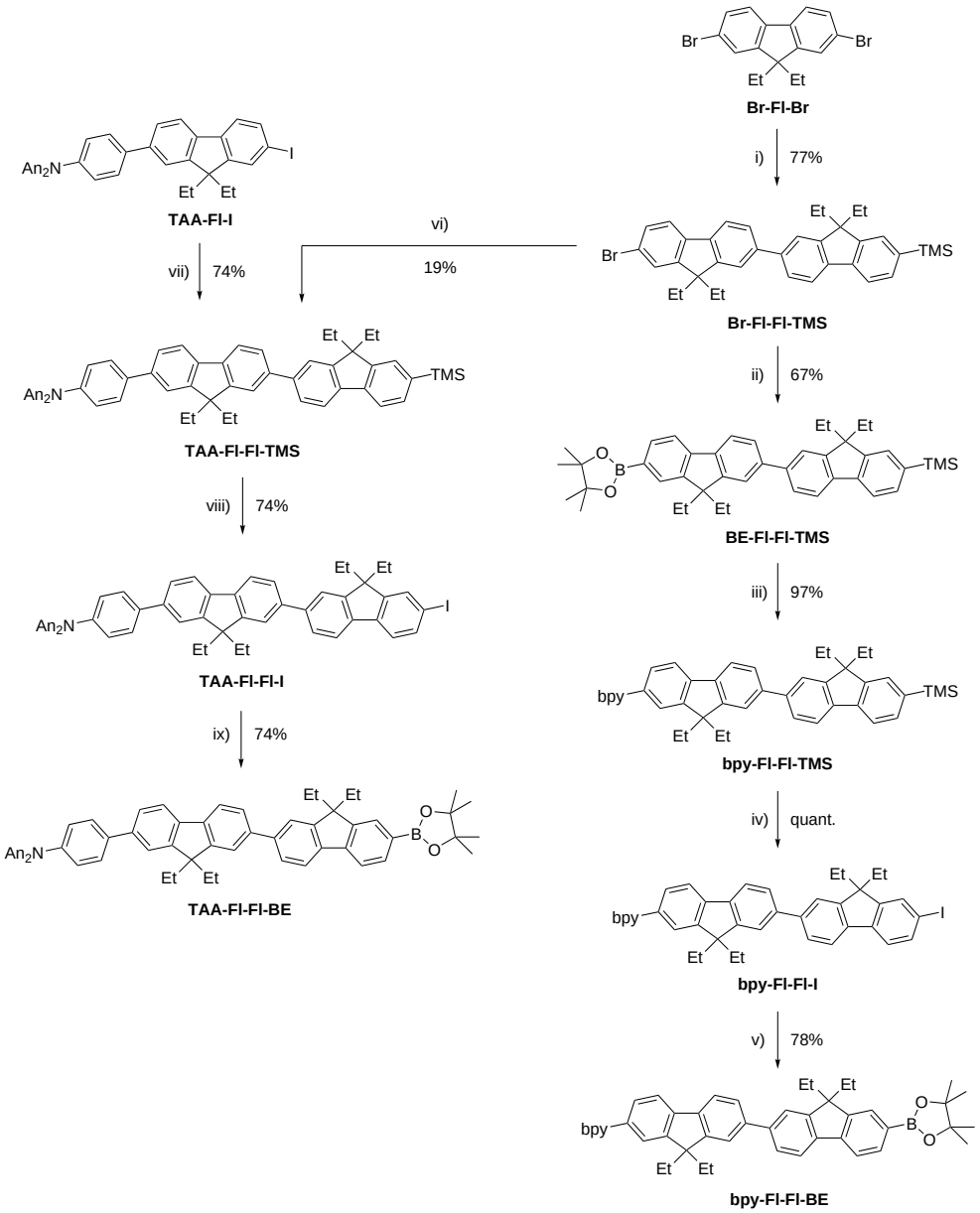

Scheme III.11. Synthesis of **bpy-Fl-Fl-BE** and **TAA-Fl-Fl-BE**: i) **TMS-Fl-BA**, Na_2CO_3, $[Pd(PPh_3)_4]$, THF/H_2O, 80 °C; ii) $B(pin)_2$, KOAc, $[Pd(PPh_3)_2Cl_2]$, DMSO, 80 °C; iii) **bpy-Br**, Na_2CO_3, $[Pd(PPh_3)_4]$, THF/H_2O, 80 °C; iv) ICl, CH_2Cl_2, -78 °C; v) $B(pin)_2$, KOAc, $[Pd(PPh_3)_2Cl_2]$, DMSO, 80 °C; vi) **TAA-BE**, Na_2CO_3, $[Pd(PPh_3)_4]$, THF/H_2O, 80 °C; vii) **TMS-Fl-BA**, Na_2CO_3, $[Pd(PPh_3)_4]$, THF/H_2O, 80 °C; viii) ICl, CH_2Cl_2, -78 °C; ix) $B(pin)_2$, KOAc, $[Pd(PPh_3)_2Cl_2]$, DMSO, 80 °C.

Instead of coupling to the central spirobifluorene, the side-arms were extended by one additional fluorene unit (Scheme III.11) for the syntheses of the ligand bearing three fluorene bridging units. This approach was hypothesized to lead to a better separability of the coupling reaction products. In the first step, **TMS-Fl-BA** was coupled once with **Br-Fl-Br**, using a large excess of the latter. The resulting **Br-Fl-Fl-TMS** could be converted to the corresponding boronic ester and subsequently be coupled with **bpy-Br**. **TAA-Fl-Fl-TMS** was synthesized in two different ways. Direct coupling of **TAA-BE** with **Br-Fl-Fl-TMS** gave only a low yield of 19% (Scheme III.11 (vi)). Using **TAA-Fl-I**, available from the previous routes, as the substrate improved the overall yield of **TAA-Fl-Fl-TMS** (Scheme III.11). The side-arms were sequentially coupled, starting with the bipyridine and followed by the triarylamine unit (Scheme III.12 and III.13). Only the complex **AC3** was stable enough for characterisation and measurements.

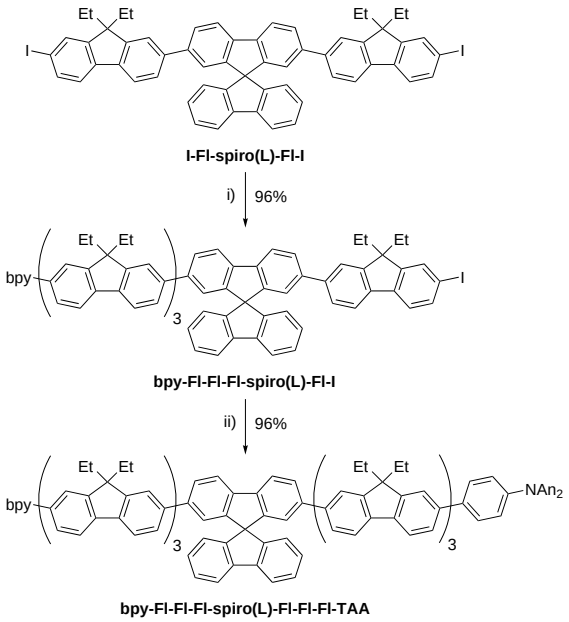

Scheme III.12. Synthesis of **bpy-Fl-Fl-Fl-spiro(L)-Fl-Fl-Fl-TAA**: i) **bpy-Fl-Fl-BE**, Na_2CO_3, $[Pd(PPh_3)_4]$, THF/H_2O, 80 °C; ii) **TAA-Fl-Fl-BE**, Na_2CO_3, $[Pd(PPh_3)_4]$, THF/H_2O, 80 °C.

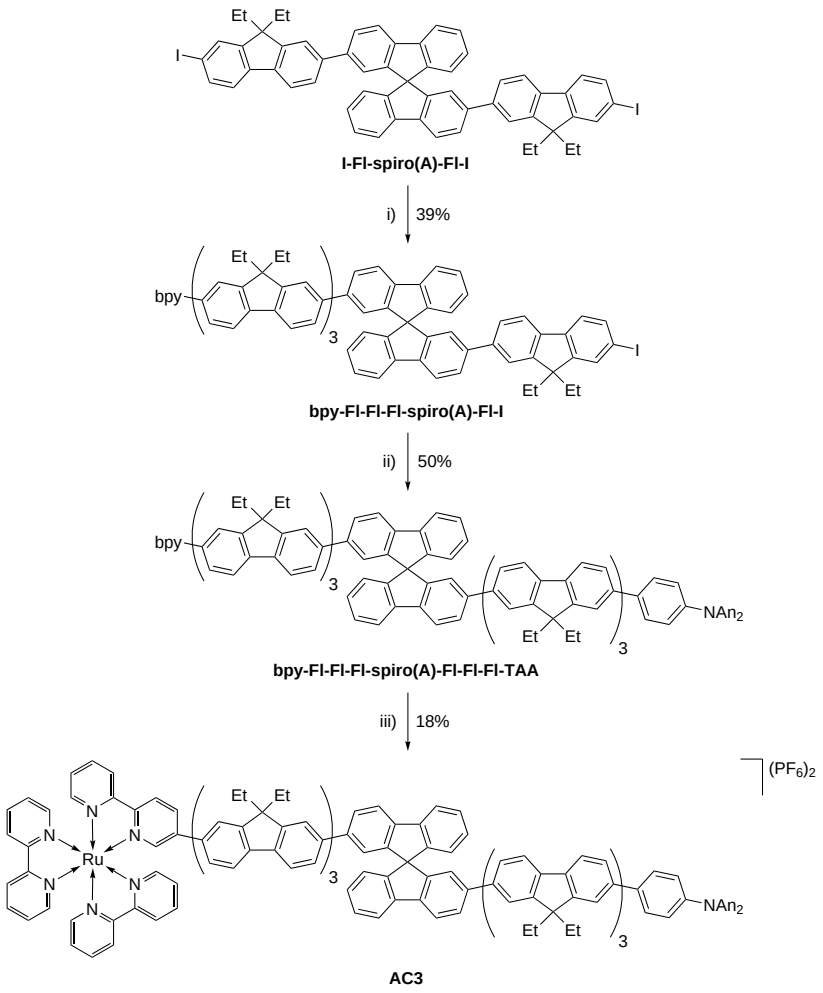

Scheme III.13. Synthesis of **AC3**: i) **bpy-Fl-Fl-BE**, Na_2CO_3, $[Pd(PPh_3)_4]$, THF/H_2O, 80 °C; ii) **TAA-Fl-Fl-BE**, Na_2CO_3, $[Pd(PPh_3)_4]$, THF/H_2O, 80 °C; iii) $[Ru(bpy)_2(MeCN)_2](OTf)_2$, KPF_6, ethylene glycol/acetone/1,2-dichloroethane, 85 °C.

III.2 Measurements

III.2.1 Electrochemistry

Electrochemical measurements were performed on all complexes, so as to estimate the driving forces for electron-transfer. Cyclic voltamograms are presented in Figure III.4, and the relevant half-wave potentials are listed in Table III.1. The first oxidation wave of all complexes, at approximately 0.65 V, is associated with the TAA oxidation and is consistent with the unsubstituted TAA unit.[40] The extension of the bridge π-system has no effect on its oxidation potential. The second oxidation at a constant value of 1.30 V, is assigned to the Ru^{III}/Ru^{II} oxidation.[37]

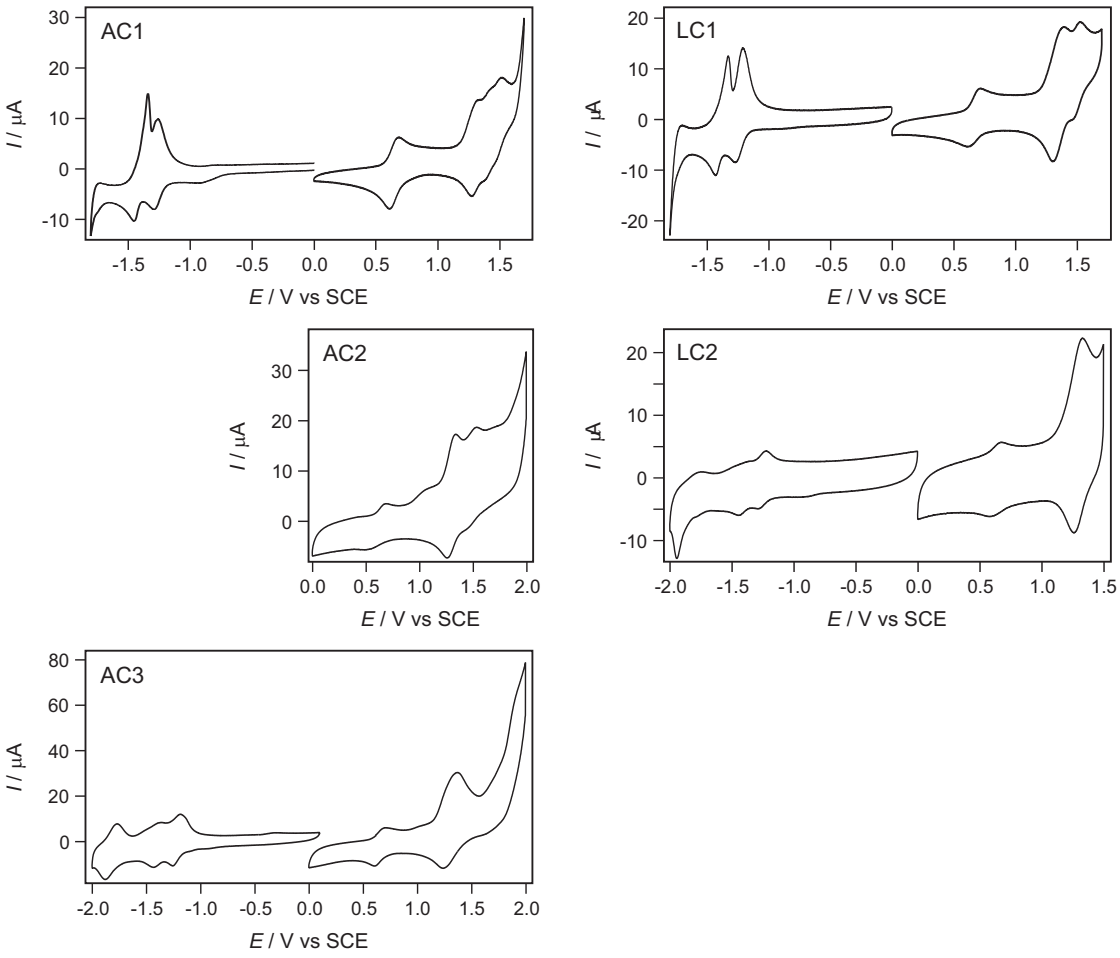

Figure III.4. Cyclic voltammograms of the right-angled and linear series of complexes, measured in deaerated MeCN with 0.1 M $TBAPF_6$ as electrolyte; potential sweep rate of 0.2 V/s.

At higher potentials, further non-reversible oxidation waves were visible for most complexes. A clear assignment to either bridge oxidation or the second TAA oxidation is not

possible, as the oligofluorene oxidation occurs at a similar potential as the TAA^{2+}/TAA^{+} oxidation.[41]

Table III.1: Electrochemical reduction and oxidation potentials of the angled and linear series of complexes, measured in deaerated MeCN with 0.1 M $TBAPF_6$ as electrolyte; potential sweep rate of 0.2 V/s.

Compound	$E_{1/2}^{(bpy/bpy^-)}$/V*	$E_{1/2}^{(TAA^+/TAA)}$/V	$E_{1/2}^{(Ru^{III}/Ru^{II})}$/V*
AC1	−1.27	0.65	1.30
AC2	-	0.63	1.30
AC3	−1.22	0.65	1.30
LC1	−1.24	0.66	1.34
LC2	−1.25	0.62	1.30
TAA[40]	-	0.63	-
$[Ru(bpy)_3]^{2+}$[37]	−1.33	-	1.29

* measured vs SCE.

Data quality for the reductive scans was highly dependent on the bridge length. Whilst for **AC1** and **LC1**, two quasi-reversible bipyridine reduction waves were clearly visible, reduction waves were less pronounced for the complexes with greater bridge lengths. No reproducible reduction could be measured for **AC2**. The first reduction of all measurable complexes was between −1.2 and −1.3 V vs SCE, hence negligible deviation from unsubstituted $[Ru(bpy)_3]^{2+}$.

Assuming the reduction potential of **AC2** does not fall out of alignment with the other complexes, the driving force for photoinduced electron-transfer is constant over both series of complexes at approximately 0.20 eV (Table III.2). A constant driving force is also present for electron-transfer after oxidative quenching of the excited $[Ru(bpy)_3]^{2+}$ unit, as the reduction potential of the $[Ru(bpy)_3]^{3+}$ unit is constant at about 1.30 V for all complexes.

Table III.2: Calculated ΔG^0 values for the intramolecular electron-transfer (1) without and (2) with an oxidative quenching agent.

Compound	ΔG_1^0/eV	ΔG_2^0/eV
AC1	-0.18	-0.65
AC2	-	-0.67
AC3	-0.23	-0.65
LC1	-0.20	-0.68
LC2	-0.23	-0.68

III.2.2 Spectroscopy

UVvis Spectroscopy

Optical absorption spectra of all complexes were recorded as MeCN solutions (Figure III.5). All spectra are dominated by an intense band between 350 and 410 nm, which is assigned to the bridge π,π^*-absorption.

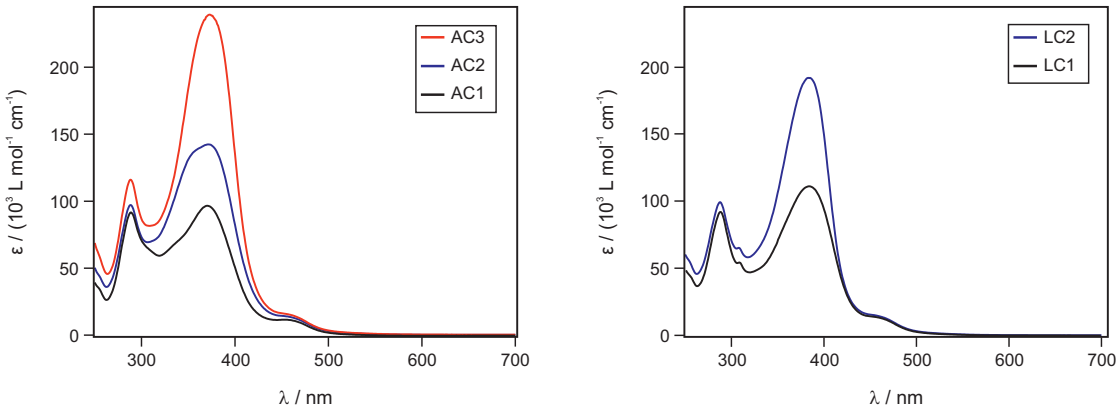

Figure III.5. Optical absorption spectra of (left) the angled and (right) linear series of complexes, measured in MeCN.

The extinction coefficient (ϵ) of this band increases with the number of bridging fluorene units. For the linear complex **LC2**, the band undergoes a minor red-shift compared to **LC1**. A direct comparison of the spectra of **AC1** and **LC1** (Figure III.6) shows that the π,π^*-absorption band of the linear complexes is slightly red-shifted due to the higher level of π-conjugation of the linear ligand. The band at 290 nm can be assigned to either a bipyridine or a TAA absorption[40,42], as the extinction coefficient is approx-

imately independent of the bridge length, and of a similar magnitude for both series of complexes. Overlap of the low-energy part of the MLCT band with ligand based absorptions, as a result of the red-shift, was not visible. In addition, the position of the MLCT absorption does not change over the series and exhibits negligible deviations to unsubstituted $[Ru(bpy)_3]^{2+}$.[42] UV-Vis spectra show that excitation at 532 nm in a pump-probe experiment should result in an exclusive excitation of the $[Ru(bpy)_3]^{2+}$ chromophore, and not of potentially interfering ligand-based transitions. Band positions and extinction coefficients are listed in Table III.3.

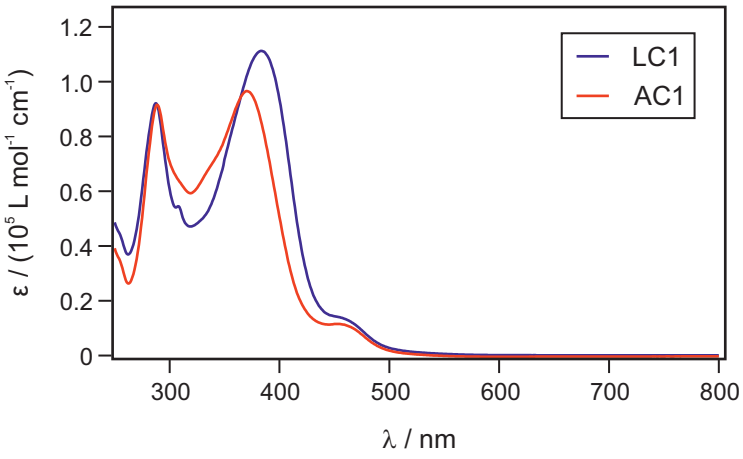

Figure III.6. Superimposed absorption spectra of **AC1** (black trace) and **LC1** (blue trace) measured in MeCN.

Table III.3: Summary of the optical absorption spectral properties of the right-angled and linear series of complexes measured in MeCN.

Compound	π,π_1^*/nm (ϵ^*)	π,π_2^*/nm (ϵ^*)	MLCT/nm (ϵ^*)
AC1	289 (91.6)	370 (96.6)	463 (10.8)
AC2	288 (97.2)	372 (142)	460 (13.4)
AC3	289 (116)	373 (239)	465 (13.9)
LC1	287 (92.1)	383 (111)	462 (13.0)
LC2	288 (99.2)	384 (192)	461 (14.1)

* Extinction coefficient reported in 10^3 L mol^{-1} cm^{-1}.

Spectroelectrochemistry

UV-Vis-NIR-spectroelectrochemical measurements were performed to identify the position of the absorption bands associated with the oxidized TAA-moiety. Spectra of **AC1** and **LC1** show the growth of a band in the red spectral range (Figure III.7), typical for oxidized triarylamines.[40] No difference in the position of the band (725 nm) was observed. The TAA^+ band position seams to be independent on the size of the conjugated π-system, and was therefore be assumed as virtually constant for the remaining complexes.

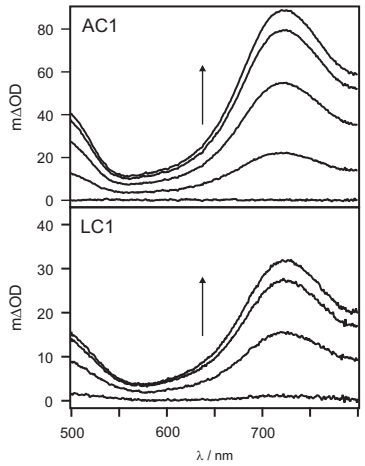

Figure III.7. Spectroelectrochemical oxidation of **AC1** and **LC1** measured in MeCN, with 0.1 M Bu_4NPF_6 as electrolyte and an applied potential of 1.0 V vs SCE.

Pump-Probe Spectroscopy

Subsequent to excitation of the $[Ru(bpy)_3^{2+}]$ chromophore, the resulting ^{3}MLCT state is expected to be reductively quenched by the triarylamine, as suggested by the thermodynamical properties of the excited complexes (Table III.2). This photoinduced electron-transfer should result in a transient absorption spectrum that exhibits a broad ground-state bleach of the MLCT band around 450 nm and a positive signal of oxidized TAA at around 730 nm (see previous section). The growth and decay of the $TAA^{\cdot+}$ band reflects the kinetics for charge-separation and -recombination, respectively.

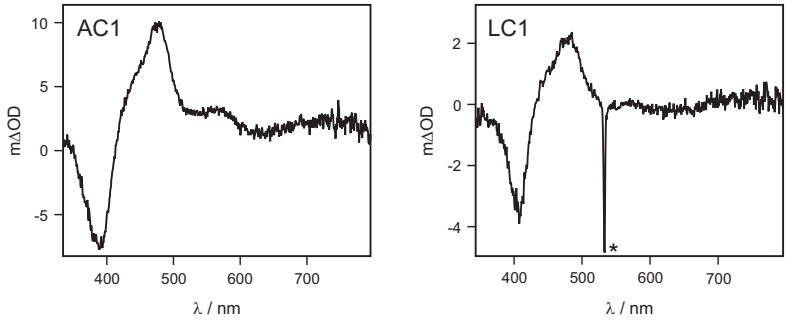

Figure III.8. Transient absorption spectra of a MeCN solution of 15 µM **AC1** (left) or **LC1** (right), respectively, after excitation at 532 nm; asterisk: scattered laser light.

The transient absorption spectrum of a solution of **AC1** in MeCN shows no signals associated with oxidized TAA (Figure III.8). All lifetimes obtained for the present signals were approximately 1.1 µs (Figure III.9), and therefore in the order of unsubstituted $[Ru(bpy)_3]^{2+}$, suggesting a lack of electron-transfer.[43]

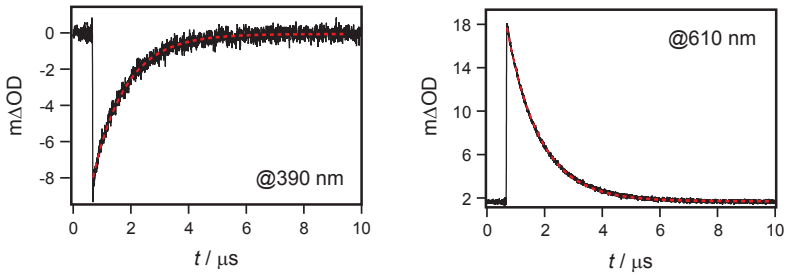

Figure III.9. Bleach recovery (left) at 390 nm and emission decay (right) at 610 nm measured for **AC1**; red dashed lines: exponential fits.

The experiment conducted with **LC1** resulted in a nearly identical transient absorption spectrum (Figure III.8), but with less intensity and a strongly reduced lifetime of 72 ns. This could be explained by quenching through electron-transfer, followed by charge-recombination with $k_{CR} \gg k_{ET}$. A Jablonski diagram can illustrate the relevant electronic transitions within the complexes upon photoexcitation (Figure III.10).

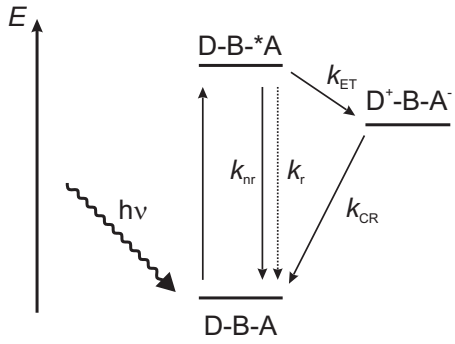

Figure III.10. JABLONSKI diagram of the relevant electronic transitions within the complexes upon photoexcitation.

As the relaxation from the charge-separated state is faster than its formation, the charge-separated state cannot accumulate and is therefore undetectable. k_{ET} was estimated by using the lifetimes of the ^{3}MLCT state of unsubstituted $[Ru(bpy)_3]^{2+}$ [44] and **LC1**. The sum of the rate constants for radiative, k_r, and non-radiative decay from the excited state to the ground state, k_{nr}, was calculated for $[Ru(bpy)_3]^{2+}$:

$$\tau = \frac{1}{k_r + k_{nr}} = 920 \text{ ns} \quad \text{(III.1)}$$

$$k_r + k_{nr} = 1.1 \cdot 10^6 \text{ s}^{-1} \quad \text{(III.2)}$$

In **LC1**, depopulation of the excited state includes electron-transfer, adding k_{ET} to the equation of τ. Under the assumption that k_r and k_{nr} do not differ between $[Ru(bpy)_3]^{2+}$ and **LC1**, one can calculate k_{ET}:

$$\tau_{LC1} = \frac{1}{k_r + k_{nr} + k_{ET}} = 72 \text{ ns} \quad \text{(III.3)}$$

$$k_{ET} = 1.28 \cdot 10^7 \text{ s}^{-1} \quad \text{(III.4)}$$

With a reasonable degree of certainty, one can consider k_{CR} to be greater than $1.28 \cdot 10^7$ s^{-1}. While the fully conjugated π-system of the fluorene units in **LC1** enable fast through-bond electron-tunneling, this pathway is likely prohibited in **AC1**, due to a break of conjugation in the spirobifluorene center. The tunneling barrier of the remaining through-bond or through-solvent pathway is much greater, therefore the relatively small driving force of -0.20 eV is apparently too low for a detectable electron-transfer in **AC1**.

Flash-Quench Experiments

Using an oxidative quencher, the oxidative strength of the Ruthenium complex is increased (see Figure III.3). As a direct consequence, the driving force for the electron-transfer increases by a factor of three to approximately -0.65 eV (Table III.2). Furthermore, the involved bimolecular process slows down the charge-recombination. The PF_6^- salt of methylviologen (MV^{2+}) was chosen as a quencher. To maximize the rate of the bimolecular quenching process, a nearly saturated solution of MV^{2+} (80 mM) was used in all measurements. The reduced methylviologen (MV^+) displays two spectral features, a set sharp bands at around 400 nm and a broad band at 608 nm.[45] As the extinction coefficient of all ligands is very high in the spectral range from 250 to 420 nm, the high energy absorptions of MV^+ were not detected in any measurement.
Transient absorption spectra of the right-angled series of complexes with the related kinetic traces of the $TAA^{\cdot+}$-band are presented in Figure III.11. The determined values for the electron-transfer rate constants (Table III.4) show only very weak dependence on the bridge length.

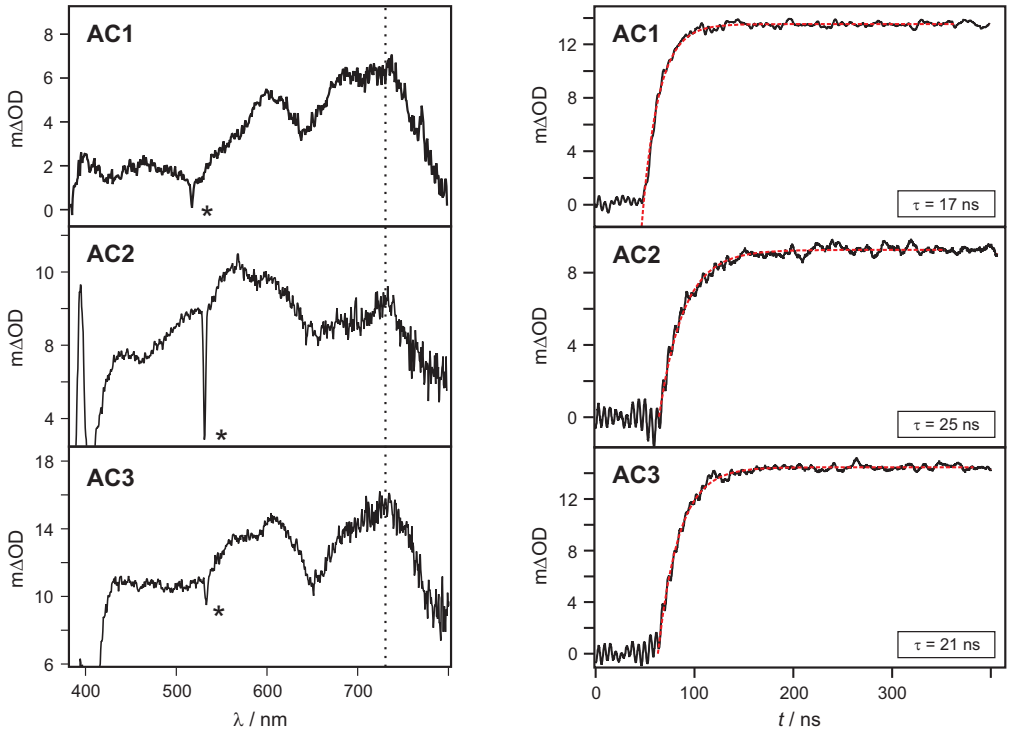

Figure III.11. Transient absorption spectra of a MeCN solution of 80 µM $MV(PF_6)_2$ and 15 µM **AC1**, **AC2** or **AC3**, respectively, after excitation at 532 nm (left), and the related growth of the transient absorption signal (right) at 730 nm (black trances) including their exponential fits (red dashed lines); asterisks: scattered laser light.

Table III.4: Calculated electron-transfer rate constants from fits of the growth of the $TAA^{\cdot+}$ transient absorption signals.

Compound	**AC1**	**AC2**	**AC3**
$k_{ET}/10^7 s^{-1}$	5.9	4.1	4.7

The results from the flash-quench experiments were surprising, as a distinct distance-dependence of the rate constants was expected.[46] The through-solvent tunneling pathway in MeCN should have an especially high tunneling barrier – resulting in a large β-value.
Several reasons for this behaviour are possible. One possibility is that the obtained k_{ET} values are not trustworthy, as they are all close to the limitation of the instrument (≈10 ns). In order to confirm that limiting value, the instrument response function was determined by measuring the decay of the scattered laser light after excitation of a sample of colloidal silica (Figure III.12). The obtained lifetime (≈8 ns) could prove the ten nanosecond limit as valid, and therefore the electron transfer rate constants as reliable.

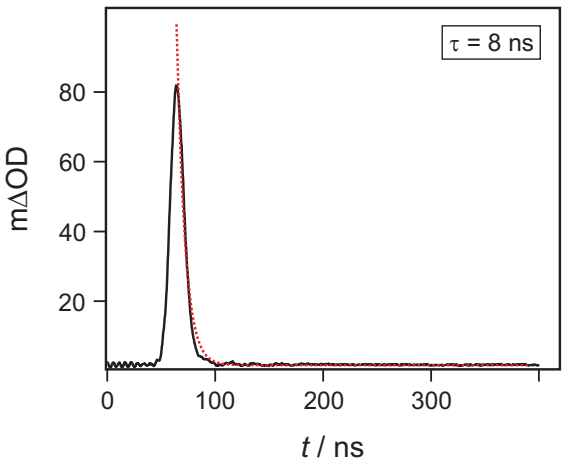

Figure III.12. Growth and decay of scattered laser light after excitation at 532 nm of an aqueous solution of colloidal silica.

Repeating the flash-quench measurements with $[Ru(bpy)_3](PF_6)_2$ gave information about the time-constant for intermolecular quenching. The transient absorption spectrum (Figure III.13) of the $[Ru(bpy)_3]^{2+}$ experiment shows two positive bands, a sharp band at 394 and a broad band 605 nm, associated with the generated reduced methylviologen (MV^+).[45] The negative feature at 450 nm is the bleach of the $[Ru(bpy)_3]^{2+}$ MLCT band.[47]

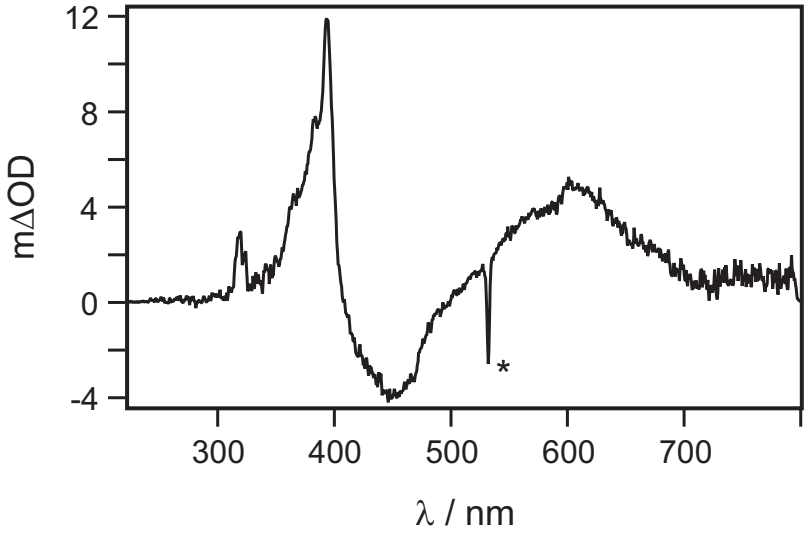

Figure III.13. Transient absorption spectrum of a MeCN solution of 80 mM $MV(PF_6)_2$ and 15 µM $[Ru(bpy)_3](PF_6)_2$ after excitation at 532 nm; asterisk: scattered laser light.

For both MV^+ bands, the growth of the transient absorption signal was measured (Figure III.14). The negative signal visible for the measurement at 605 nm due to stimulated emission during excitation.

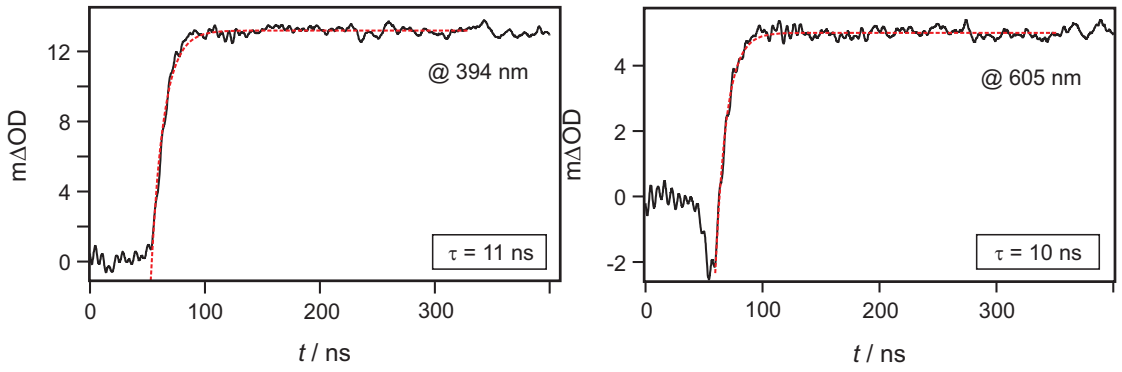

Figure III.14. Growth of the transient absorption signal (black traces); exponential fits (red dotted lines).

Lifetimes obtained from the exponential fits are approximately ten nanoseconds, and therefore laser-limited. Lifetimes obtained for the electron-transfer in **AC1**-**AC3** are around a factor of two larger and can be considered as reliable values. Additionally, the superimposed transient absorption spectra show that the absorption of oxidized TAA does not interfere with the low energy band of MV^+. The determined electron-transfer kinetics are therefore not disturbed by kinetics related to the quenching process.

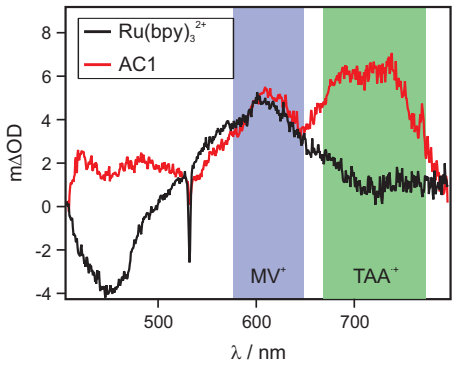

Figure III.15. Superimposed transient absorption spectra of **AC1** and $[Ru(bpy)_3]^{2+}$.

The linear complexes **LC1** and **LC2** exhibit nearly identical transient absorption spectra to their angled counterparts (Figure III.16 and Figure III.17). The time constants for the TAA oxidation are laser-limited and therefore cannot be determined with the used setup. As the electron-transfer pathway through a highly π-conjugated fluorene bridge is expected to be faster compared to the pathway through the spirobifluorene with its saturated center, this result is not surprising.

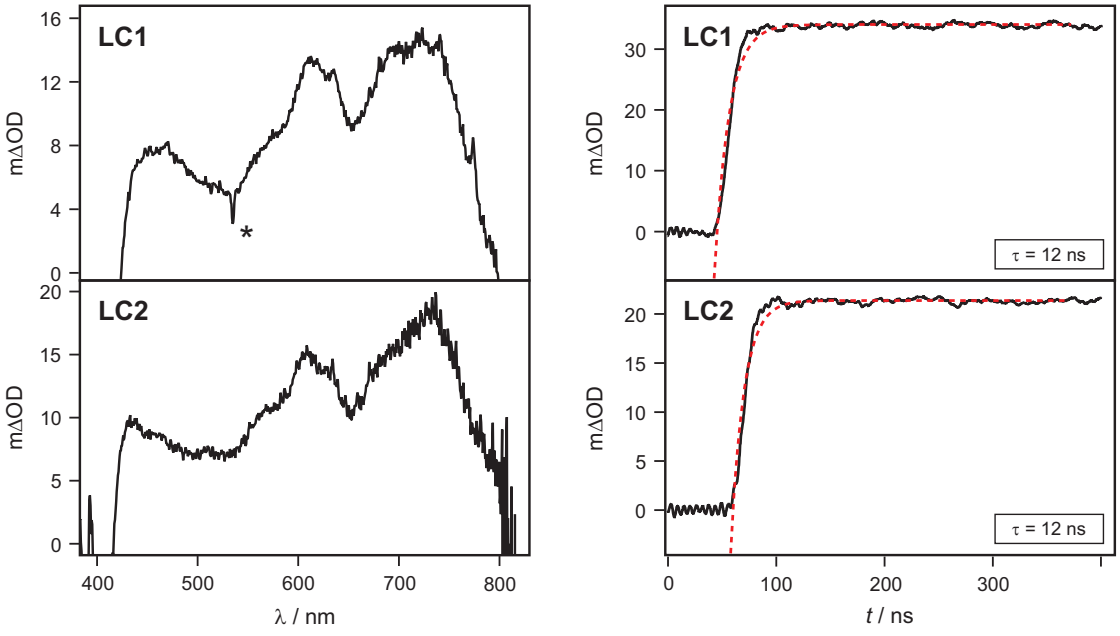

Figure III.16. Transient absorption spectra of a MeCN solution of 80 μM $MV(PF_6)_2$ and 15 μM **LC1** or **LC3**, respectively, after excitation at 532 nm (left) and the related growth of the transient absorption signal (right) at 720 nm (black trances), including their exponential fits (red dashed lines); asterisk: scattered laser light.

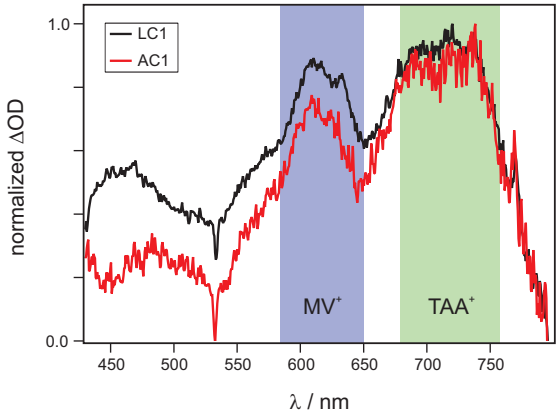

Figure III.17. Superimposed transient absorption spectra of **AC1** and **LC1**.

A comparison of the transient absorption spectra of **AC1** and **LC1** shows that for both complexes, a charge-separated state with the same spectral features is reached. Breaking the conjugation of the bridge by going from the linear to angled isomer had the effect of slowing down the electron transfer from $k_{ET} \geq 10^8 s^{-1}$ to $k_{ET} \leq 5.9 \cdot 10^7 s^{-1}$. For the linear isomers, a distance-dependence could not be determined for experimental reasons. For the missing distance-dependence of the angled series, no experimental explanation was found.

III.3 Molecular Mechanics Calculations

A possible factor that, until now, was not taken into account is the flexibility of aromatic oligomers. Whilst the use of a fluorene bridging unit should decrease the flexibility in a direct comparison to a non-linked biphenyl unit, a certain flexibility will be present, given the number of repeating units. In addition, the bonds in the *para*-positions of the fluorene do not lie on a straight line. This way, conformers with different donor-acceptor distances are possible. In order to estimate the minimal distance between the TAA and the $[Ru(bpy)_3]^{2+}$ moieties, calculations using the MMFF level of theory were performed. The distance between the ruthenium center and the nitrogen atom of the TAA was taken to compare the trend of through-space donor-acceptor distance within the series. The results of the calculations are listed in Table III.5, and the optimized structures are presented in Figure III.18.

Table III.5: Calculated *Ru-N* distances from geometry-optimized structures of the angled series of complexes.

Compound	*Ru-N* distance/Å
AC1	13.8
AC2	8.8
AC3	8.7

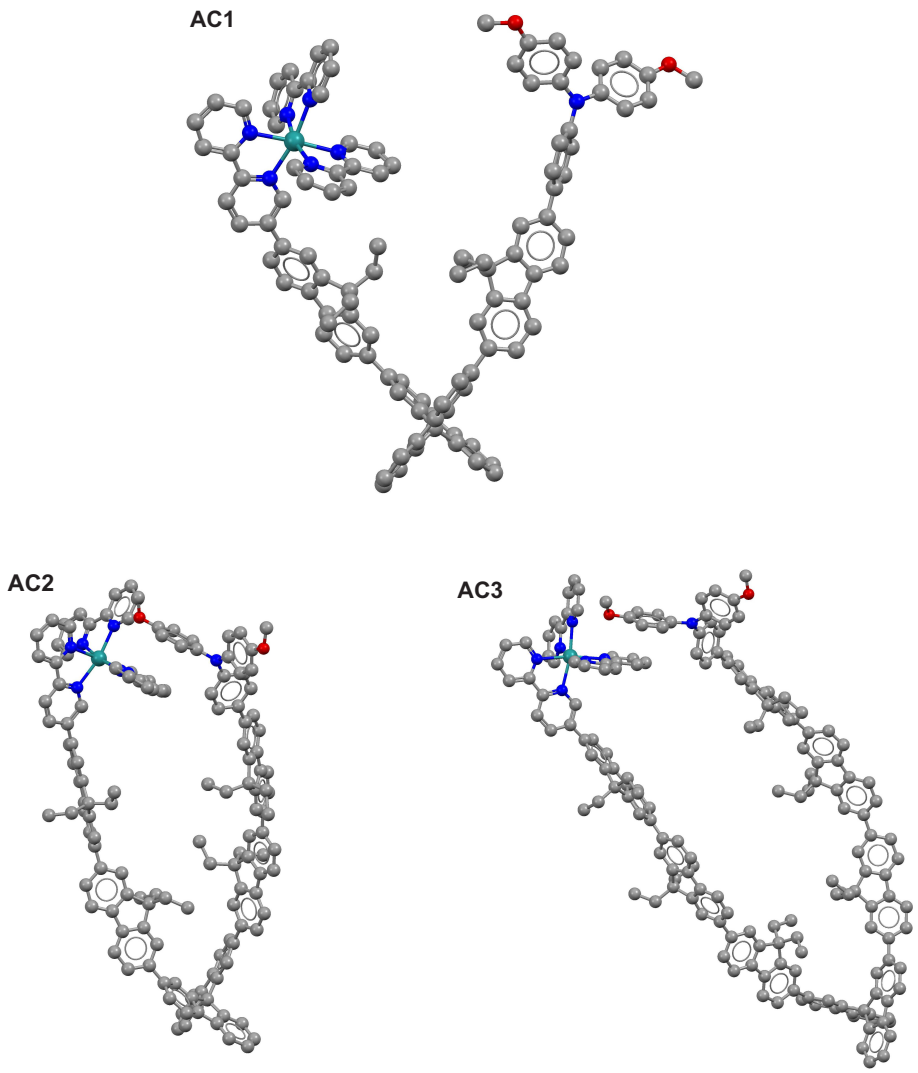

Figure III.18. Geometry optimized molecular structures of **AC1**-**AC3** for the lowest energy close-contact conformation of donor and acceptor.

The oligo-fluorene bridge displays a remarkable flexibility, allowing relatively close contact of donor and acceptor. For the longer bridges in **AC2** and **AC3**, the optimized structures suggest a possible π-stacking of one bipyridine-ligand with one of the aryl-rings of the TAA. Using this low level of theory, results have to be treated with care, but a general trend that the through-space distance does not increase accordingly with the bridge length can be recognized. The underestimated spatial separation of donor and acceptor is a potential explanation for the measured electron-transfer rate constants.

III.4 Conclusion

A right-angled and a linear series of homologous compounds, each bearing $[Ru(bpy)_3]^{2+}$- and TAA endgroups, with different numbers of bridging fluorene units were prepared. A comparison of the distance-dependence of photoinduced electron-transfer rates should have given insight into the through-space distance-dependence of electron-transfer. The increasing bridging length, and therefore extension of the conjugated π-system, had no significant effect on the driving force of 0.2 eV for electron-transfer. Photoinduced electron-transfer from the $[Ru(bpy)_3]^{2+}$ ^{3}MLCT excited state did not occur for the angled series of molecules. For the linear complexes no signal for the oxidized TAA-moiety could be detected either. In combination with a reduced ^{3}MLCT lifetime compared to $[Ru(bpy)_3]^{2+}$, this points towards electron-transfer with subsequent faster charge-recombination. The flash-quench experiment, with methylviologen as an oxidative quenching agent, increased the driving-force for electron-transfer to about 0.65 eV. The driving force was high enough to allow intramolecular electron-transfer for all compounds. The electron-transfer rate constants for the angled series showed only very weak dependence on the bridge length, while their values were close to the limit of resolution. The data was validated by control experiments with $[Ru(bpy)_3]^{2+}$. Electron-transfer for the linear series was on a time-scale faster than the instrument resolution, but by addition of methylviologen, transient absorption spectra proving the presence of the charge-separated state could be obtained. For the right-angled series of complexes, molecular mechanics calculations showed that the longer fluorene-bridges are more flexible than originally expected, allowing close-contact of donor and acceptor. The calculated center-to-center distance between donor and acceptor seem independent of the bridging length for **AC2** and **AC3**. Although the angled series did not exhibit the behavior that it was originally designed for, the very weak distance-dependence suggests a predominant through-space contribution for the observed electron-transfer.

IV Theory

IV.1 Mixed-Valence

Mixed-valency is where a single compound contains two chemically equivalent redox-active moieties (M_1, M_2) in different oxidation states. In the early years of investigating mixed-valency, three different Classes were defined (Figure IV.1).[48] Class I describes a system with no electronic coupling (H_{AB}). Both states are well separated and can be depicted as $M_1^{(n+1)+}/M_2^{n+}$. The lack of electronic coupling results in behaviour of the molecule as the sum of both $M_1^{(n+1)+}$ and M_2^{n+}. Class II describes systems in which the charge is still localized, but the redox-active moieties display weak H_{AB}. This leads to mixing of the diabatic surfaces of $[M_1^{(n+1)+}/M_2^{n+}]$ and $[M_1^{n+}/M_2^{(n+1)+}]$, forming new adiabatic surfaces. The ground state exhibits two minima representing the charge localization with the thermal electron-transfer barrier E_{th}. The energy difference between the adiabtic states at the diabatic crossing point represents the electronic coupling. If the coupling increases, the minima move closer together until they fuse. This full delocalization represents Class III mixed-valence compounds $[M_1^{(n+1/2)+}/M_2^{(n+1/2)+}]$. In reality, the electronic coupling can vary over a broad range – resulting in borderline cases that display characteristic features of both Class II and Class III mixed-valency.

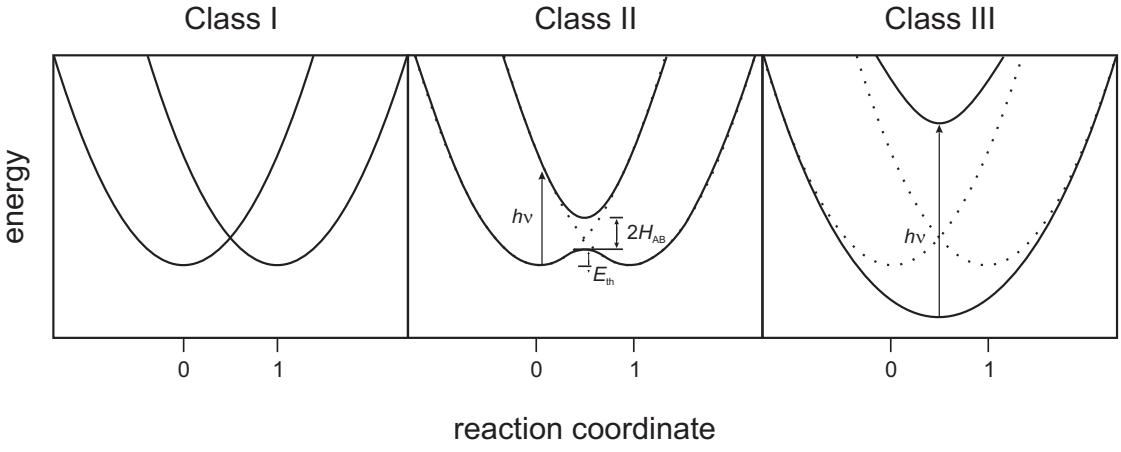

Figure IV.1. Potential energy surfaces of Class I–III mixed-valence systems.

The mixing of states gives rise to new properties that are not present in Class I systems, one of which is a new characteristic absorption feature, the so-called intervalence charge-transfer (IVCT) band. It is the result of an excitation from the adiabatic ground to the excited state. The energy of the absorption maximum of the IVCT band (ν_{max}) is roughly equal to the reorganization energy (λ). An increase in electronic coupling also causes an increase of ν_{max}, meaning that the IVCT band undergoes typically a blue-

shift from Class II ($\lambda = h\nu \gg 2H_{AB}$) to Class III systems ($\lambda = h\nu = 2H_{AB}$). In addition to ν_{max}, the band shape is also dependent on H_{AB}. The greater the delocalization, the more asymmetrical the IVCT band becomes. The low-energy side of band is cut off, as $2H_{AB}$ becomes the lowest possible excitation energy. In the Class III case, the IVCT band should in principal only consist of the high-energy half of the Gaussian-shaped absorption band. The absence of a real cut-off is caused by quantum effects and solvent broadening.[49] Another feature of the IVCT band of Class III compounds is a weaker dependence on solvent polarity as the excitation does not involve a charge-transfer process. Analysis of the IVCT band can therefore give information about the classification and the electronic coupling. The general equation for H_{AB} includes the adiabatic transition dipole moment ($|\mu_{12}|$), the electron-transfer distance (r_{AB}) and the unit electronic charge e.

$$H_{AB} = \frac{|\mu_{12}|}{e r_{AB}} \nu_{max} \tag{IV.1}$$

$$H_{AB} = \frac{2.06 \cdot 10^{-2} (\nu_{max} \epsilon_{max} \Delta\nu_{1/2})^{1/2}}{r_{AB}} \tag{IV.2}$$

Equation IV.1 does not make any assumption about the band shape, as it contains the integral over the whole band; it can therefore be applied for the analysis of any IVCT band. If the present band is of Gaussian shape, and therefore belongs to a Class II compound, the formula can be reduced to equation IV.2. Hereby, ν_{max} is the energy of the IVCT band maximum, ϵ_{max} its extinction coefficient at the band maximum and $\Delta\nu_{1/2}$ the full width at half maximum. Whereas most values can be obtained by Gaussian fitting of the IVCT band, r_{AB} is a significant factor of uncertainty.[50] In inorganic mixed-valence systems, the distance between the metal centers is a relatively reliable value. In organic systems, only rough approximations are possible, as often no defined redox-centers exist, and the charge, to some extent, is delocalized on the bridge.[51] For Class III mixed-valence systems, this deviation of r_{AB} can be determined, as H_{AB} can be directly calculated from the energy of the absorption maximum of the IVCT band.
The barrier for thermal electron-transfer (E_{th}; Figure IV.1) can be estimated by using parameters obtained from fit of the IVCT band (eq. IV.3).[49]

$$E_{th} = \frac{\lambda}{4} - H_{AB} + \frac{H_{AB}^2}{\lambda} \tag{IV.3}$$

E_{th} can also be determined by measuring temperature-dependent EPR spectra.[52] Decreasing the temperature lowers the delocalization of the charge, causing a change in the EPR spectrum. Rate constants for thermal electron-transfer can be extracted from

the fitting of the experimental EPR spectra.

$$k = \frac{k_B T}{h} \exp\left(-\frac{\Delta G^{\ddagger}}{k_B T}\right) = \frac{k_B T}{h} \exp\left(-\frac{\Delta S^{\ddagger}}{k_B}\right) \exp\left(-\frac{\Delta H^{\ddagger}}{k_B T}\right) \tag{IV.4}$$

The Eyring-equation (IV.4) is based on transition-state theory and provides a good general description. Here the preexponential factor consists of the Boltzmann-constant k_B, the temperature T and the Planck-constant h. The entropy $\Delta S^{\ddagger}$ can be considered as a factor consisting of deviations of the preexponential factor and the linear temperature dependence of the reorganization energies, and $\Delta H^{\ddagger}$ as the thermal electron-transfer barrier.[52]

$\Delta H^{\ddagger}$ is usually determined by a plot of $\ln(k/T)$ vs T^{-1}. In order to observe a change in radical delocalization, the electronic coupling has to be rather small.[53] Even most Class II compounds still show too strong coupling. The thermal electron-transfer barrier is too low to measure a transition to the localized state. One of the few examples is the spiro-fused bis(triarylamine) **I** (Figure IV.2), which shows no IVCT band in the NIR region, but spin delocalisation in room temperature EPR.[54]

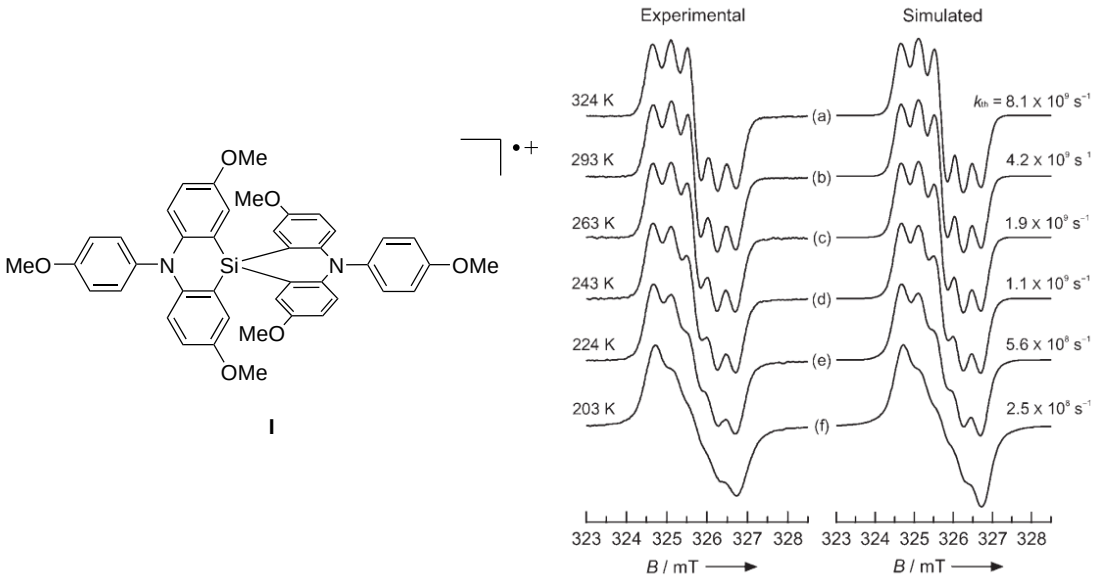

Figure IV.2. Example of a bis(triarylamine)-system to study the spin-delocalization by temperature-dependent EPR measurements.[54]

The thermodynamic stabilisation of the mixed-valent state is expressed by the comproportionation constant K_C.[55]

$$K_C = \frac{[M^+]^2}{[M^{2+}][M]} \tag{IV.5}$$

K_C can be related to the electrochemical properties of a system, M, with the Faraday constant, F, and the ideal gas constant, R, (equation IV.6). The so called half-wave splitting ($\Delta E_{1/2}$) is the difference between the half-wave potentials related to the two one-electron oxidations from M to M^+ and from M^+ M^{2+}.

$$K_C = \exp\left(\frac{F\Delta E_{1/2}}{RT}\right) \tag{IV.6}$$

A larger half-wave splitting is therefore directly correlated with a larger thermodynamic stability of the mixed-valent species M^+. A high stability is often associated with a strong H_{AB}. Electronic coupling is one factor affecting K_C, but its contribution is small compared to electrostatic effects for example. It is therefore hard to predict when there is a correlation between the half-wave splitting and the electronic coupling. The assumption that a low half-wave splitting correlates with weak H_{AB}, tends to fail in two cases: (1) the bridge is actively involved in the redox process; (2) the bridge brings the redox-active moieties into close proximity, whilst exhibiting only little orbital overlap with them.[56]

IV.2 Triarylamines in Mixed-Valence Compounds

Studies on mixed-valence compounds originated from inorganic materials.[57] An intense colour was found to be one of their common features. From this attribute results an application of mixed-valent complexes as pigments. Well known examples are ultramarine blue ($Na_8[Al_6Si_6O_{24}]S_n$, with S_3^- as key chromophore) and Prussian blue ($Fe(III)_4[Fe(II)(CN)_6]_3$). Whilst first interests for mixed-valence systems were based on their pigmentation, recent studies dealt with applications of them in fields like molecular magnetism.[58]

Pure organic molecules in their mixed-valent state have received great interest as model systems to explore electron-transfer properties of conjugated organic or saturated bridges.[59] The usually neutral organic molecule is converted to its mixed-valent radical ion form by single oxidation/reduction.

Among the used redox-active centers in organic mixed-valent systems, triarylamines (TAA) are probably the widest applied.[50,60] The interest in TAAs as well as mixed-valence systems based on them is connected to their application in OLEDs as hole transport and/or emitting material.[50,61,62] They display relatively stable radicals with distinct spectral characteristics, and their oxidation potentials can be tuned by introducing various substituents.[63]

The importance of the electronic properties of the bridge was demonstrated in a study by Lambert and coworkers.[64] A series of compounds with two triarylamines were connected by a fully conjugated bridge, bearing a central aryl unit with different sub-

stituents (Figure IV.3).

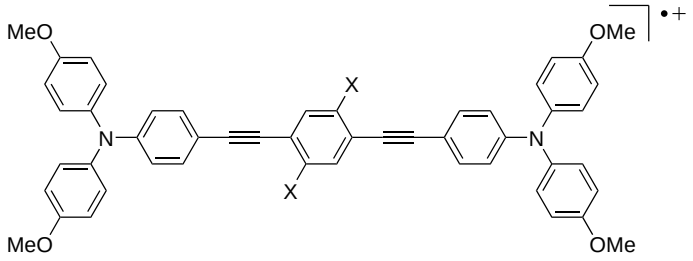

J1-3: X = H, Me, OMe

Figure IV.3. Example of a bis(triarylamine)-system to study the effect of electronic properties of the bridge on H_{AB}.

Increasing the electron density at the bridge through incorporation of electron-donating substituents lead to enhanced electronic coupling of the TAA-groups in the mixed-valent species.[65,66]
A close-related redox-active moiety, which is obtained by fusing the two terminal aryl rings of the TAA unit, is carbazole. By comparing a fused (**K1**) with its related open (**K2**) mixed-valent system it was found that the electronic coupling drops by a factor of roughly two from **K2** to **K1**.[67,68]

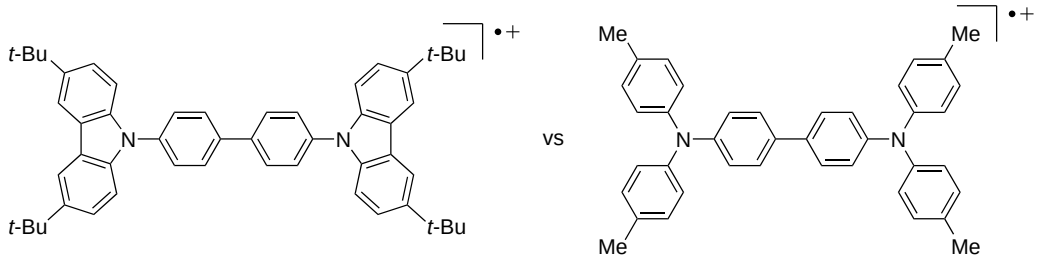

K1 **K2**

Figure IV.4. Examples of two related bis(triarylamines) mixed-valent systems with fused (**K1**) and non-fused (**K2**) terminally aryl rings.

The carbazole moiety reduces the orbital overlap of the nitrogen p-orbital with the π-system of the bridging aryl rings.[68] This reduction is caused by a twist of the carbazole unit against the bridge, which is induced by the greater steric demand of the carbazole. The same carbazole study can serve as an example where it was shown, that upon enhancement of the π-conjugation of the bridge the electronic coupling increases.[68] This was ensured by linking the two bridging aryl rings with additional aliphatic linkers, hence hinder their rotation and lower the torsion angle (Figure IV.5).

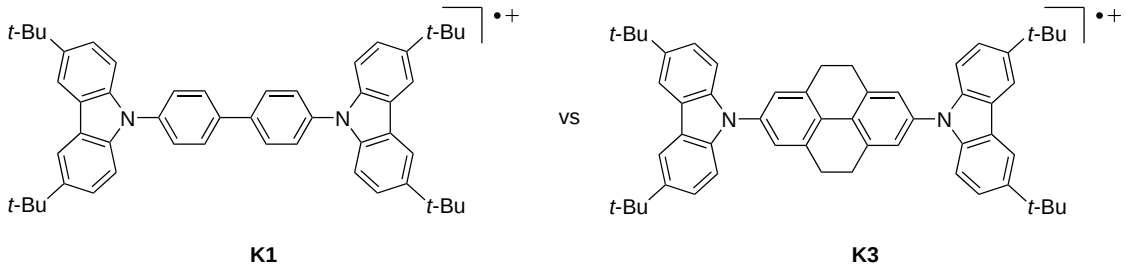

K1 **K3**

Class II Class III

Figure IV.5. Examples of two related carbazole-based mixed-valent systems demonstrating stronger H_{AB} with higher π-conjugation of the bridge.

IV.3 Through-Space Interactions in Mixed-Valence Compounds

Two major approaches to realise through-space interactions dominate this research field: (1) enabling $\pi - \pi$-interaction within the bridge; (2) bringing the redox-active moieties into close spatial proximity with a C- or U-shaped molecular geometry.
The most prominent examples with a relatively fixed π-stacking distance are paracyclophanes (Figure IV.6).

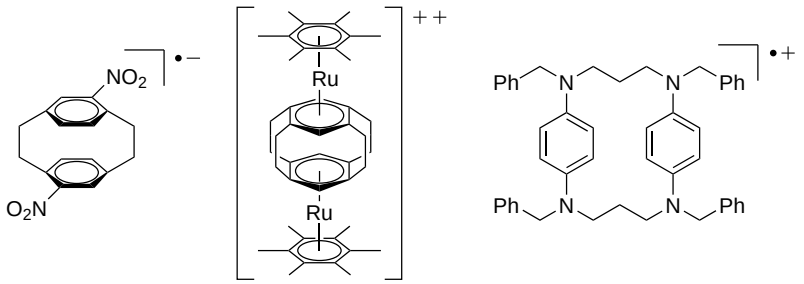

L1 **L2** **L3**

Figure IV.6. Examples of the use of the paracyclophane geometry for the investigation of through-space charge-transfer in mixed-valence compounds.

Although the two phenylene units of a paracyclophane do not belong to a single conjugated system, their small spatial distance results in a substantial orbital overlap. It was shown that this geometry gives rise to a strong through-space interaction, while some through-bond interaction is still present. One of the first mixed-valence compounds with the paracyclophane motif was published by Nelsen.[69] The monocations of the pseudo-para (**L1**; Figure IV.6) and -otho nitro substituted [2.2]paracyclophane were studied by UV-Vis absorption spectroscopy. Through solvent variation, the pseudo-para substituted compound could be shifted from Class II to Class III – demonstrating

the charge-transfer capabilities of paracyclophanes. The optical absorption spectrum of the pseudo-ortho substituted isomer showed less influence on solvent polarity. The change of the substitution pattern results in a lower cross-ring interaction clearly visible in calculated orbital densities. A diruthenium complex (**L2**; Figure IV.6) with a paracyclophane as a double η^6-coordinating ligand was synthesized.[70] The mixed-valent species is formed by a net two-electron reduction of one of Ru^{2+} to Ru^0. Reference compounds strongly suggest that the corresponding ligand π-system changes its coordination from η^6 to η^4. This is a rare example of a mixed-valent compound where the oxidation states differ of a number greater one.
The paracyclophane unit is not limited to a pure hydrocarbon backbone. By introducing nitrogen into the bridging alkane (**L3**; Figure IV.6), it was possible to create a mixed-valence species mimicking a dimeric *p*-phenylenediamine radical cation.[71] This leads to a borderline Class II/III state in dichloromethane, where the charge is almost completely delocalized over the two π-systems, including the four nitrogen atoms.

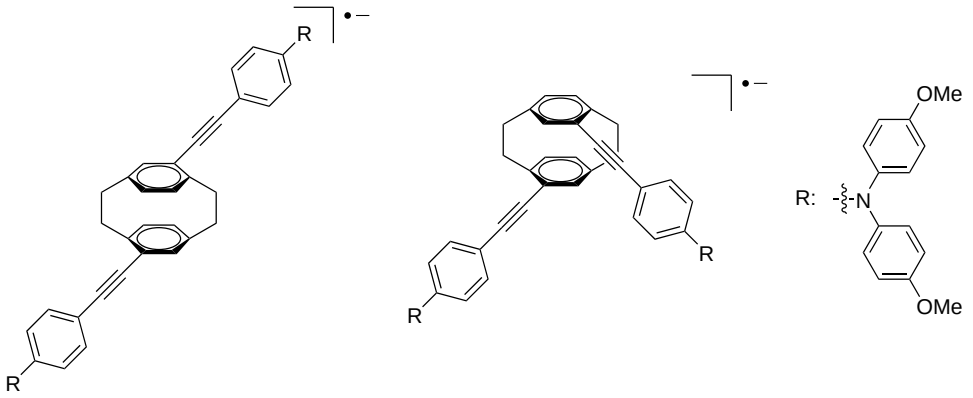

M1 **M2**

Figure IV.7. Examples of triarylamine substituted mixed-valent compounds for the investigation of the contribution of the through-space charge-transfer pathway in paracyclophanes.

Using triarylamine substituted paracyclophanes, Lambert and co-workers obtained similar electronic couplings for the two isomers **M1** and **M2** (Figure IV.7).[72] In addition, they could determine that the electronic coupling through paracyclophane bridges is only little less than through a fully conjugated xylene bridge. Quantum chemical calculations, performed by Kaupp *et al.* on that particular set of mixed-valence compounds, dealt with the question to what extent the through-bond pathway is involved in the electronic coupling.[73] Calculated electronic couplings changed only to a small extent when the dimethylene linkers in the paracyclophane were replaced with hydro-

gen atoms while keeping the rest of the calculated geometry unchanged. This indicates that the linker has a predominantly structural role, keeping the two π-systems well aligned, and only a small electronic role.

Bringing two redox-active moieties into close proximity can lead, at least partially, to through-space charge-transfer.[74–77] A series of systems based on the *ortho*-substitution of benzene was studied in the groups of Kochi and Nöll (Figure IV.8).

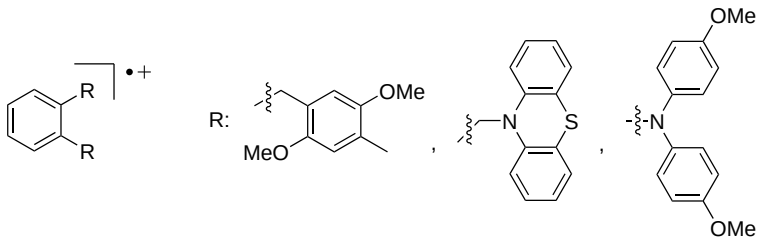

Figure IV.8. Examples of mixed-valent *ortho*-substituted benzenes exhibiting through-space communication.

In **N1** and **N2** the phenylene bridge is connected via a methylene spacer with the redox-active moiety, introducing a certain degree of flexibility and decreasing the through-bond electronic coupling. This allows a conformation, where the aromatic systems of the donor adopt a coplanar orientation, necessary for the orbital overlap. The *ortho*-phenylenediamine compound **N3**, in which the nitrogen atoms are directly connected to the phenylene bridge, was found to belong to Class III in low-polarity solvents.[77] The electronic coupling is only slightly weaker compared to its *para*-substituted analogue.[50] The bulkiness of the aryl substituents limits conjugation of the nitrogen lone-pair of electrons with the bridge π-system. As this is a key requirement for efficient through-bond coupling, it was argued that the through-space pathway has a considerable contribution.
In order to study the through-space pathway with further decreased through-bond contribution, we recently analyzed a series of mixed-valent compounds with naphthalene as an aromatic backbone (Figure IV.9).[74] Naphthalene-based mixed-valent systems are known to exhibit through-bond electronic couplings not dependent on the number of single bonds between the substituents, but on the alternating double bond sequence.[78] No such sequence is possible for a 1,8-substitution pattern, reducing this pathway to a great extent.

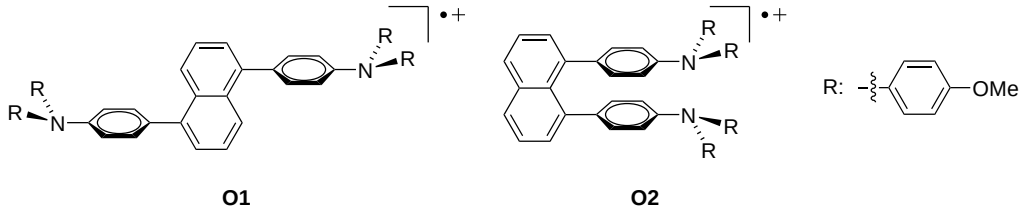

Figure IV.9. Examples of the *ortho*-substituted benzenes showing through-space communication in their mixed-valent form.

O2 was found to be a Class II system with significant through-space coupling. In contrast to **N3** (Figure IV.8), the interaction is not limited to an overlap of the nitrogen lone-pairs. DFT-calculations indicated that the carbon atoms in α-positions to the naphthalene bridge display a substantial fraction of the spin density. The overall electronic communication was comparable in the 1,5-substituted compound **O2**. The determination of the exact pathway remains difficult, for reasons such as conformational flexibility or a possible substantial contribution of the through-bond pathway.

V A Mixed-Valence Triple-Decker as a Model Compound for n-π-n Interactions

The vast majority of mixed-valence compounds investigated for through-space interactions were designed on either the possibility of π-stacked aryl building blocks or the close contact of the redox-active moieties.[79] The interaction of an aromatic π-system with a lone-pair of electrons was primarily investigated in the field of protein research.[80,81] The spin density of the monocations of triarylamines that are most commonly used in organic mixed-valence studies is mainly located at the nitrogen atom. A spatially close-orientated π-system to the occupied non-bonding nitrogen p-orbital should facilitate an overlap between these orbitals.
The compounds presented in this work exhibit a triple-decker-like stacked geometry, where a central aryl ring is 'sandwiched' by the two amine moieties (Figure V.1).

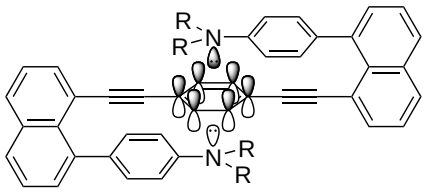

Figure V.1. Schematic depiction of the triple-decker geometry.

This design should allow an orientation where the non-bonding nitrogen p-orbital of the nitrogen atom in both donor moieties points towards the π-system of the central aryl ring. This approximately linear alignment of the orbitals should result in a significant through-space electronic coupling.
Charge-transfer in the monocationic species is expected to occur mainly through the resulting n-π-n interaction. A through-bond pathway is highly disfavoured for three reasons: (1) the weak through-bond electronic coupling in the 1,8-substitution pattern in naphthalenes[74]; (2) the orthogonality of the π-systems of the naphthalene moieties and the aryl rings due to steric hinderance; (3) the large number of chemical bonds between the two redox centers. Any contribution from through-bond charge-transfer shall be accounted for by the use of the 1,5-substituted isomer, wherein only through-bond charge-transfer can occur, as a reference molecule.

V.1 First Generation Triple-Decker System

For the first generation system, phenothiazine (PTZ) was chosen as the redox-active unit. The butterfly-shaped geometry of the fused ring system in the neutral form should lead to a more centrally-directed orientation of the nitrogen lone pair in comparison with the commonly used open propeller-shaped triarylamines. Additionally, the through-bond electronic coupling is further decreased by the change from an open triarylamine to phenothiazine, because the latter has a comparatively smaller orbital overlap of the nitrogen p-orbital with the bridge π-orbitals.[68] A second, outwardly directed, orientation would be possible but is sterically disfavoured. For the central aryl unit, an unsubstituted phenylene and the highly electron rich 1,2,4,5-tetramethoxybenzene (tmb) were chosen. Comparison between homologous systems incorporating these two bridging units should give further insight in the dependence of through-space charge-transfer on the electronic properties of the bridge. Higher electron density on the mediating bridge should enhance hole-transfer, as the tunneling barrier is decreased. If the oxidation potential of the bridge becomes close to that of the redox-active moiety, charge-delocalization might also involve the central π-system, in addition to the amines.

V.1.1 Synthesis

Both triple-decker compounds were synthesized using analogous strategies, where the central ethyne-substituted aryl is introduced in the last step.
In this synthetic route, the boronic ester **PTZ-Ph-BE** was the first building block. It was obtained in an overall yield of 29% over four steps (Scheme V.1).

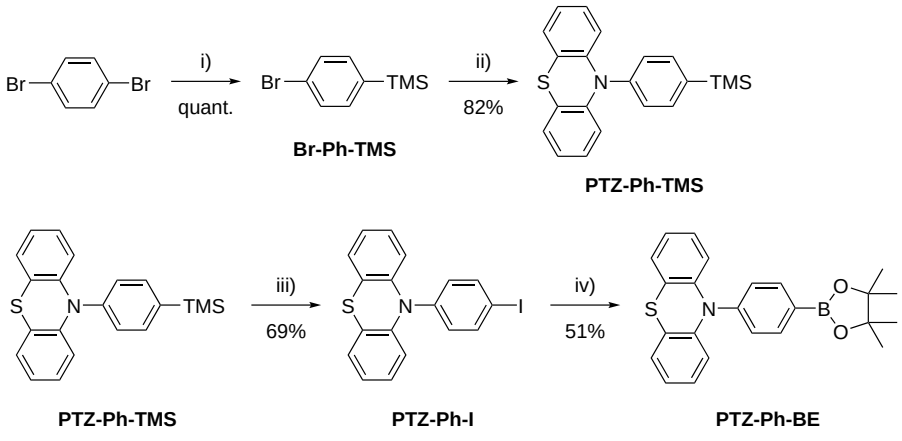

Scheme V.1. Synthesis of **PTZ-Ph-BE**; i) *n*-BuLi, Me_3SiCl, Et_2O, -78 °C; ii) phenothiazine, NaO*t*-Bu, $[Pd(dba)_2]$, $HP(t\text{-}Bu)_3BF_4$, toluene, 80 °C; iii) ICl, -78 °C, CH_2Cl_2; iv) bis(pinacolato)diboron, KOAc, $[Pd(PPh_3)_2Cl_2]$, DMSO, 80 °C.

The key step in the overall synthesis was the statistically-controlled Suzuki-Miyaura cross-coupling reaction between **PTZ-Ph-BE** and **1,8-Naph-I_2** (Scheme V.2 (ii)). The desired product was only obtained in 34% yield, even after using an excess of **1,8-Naph-I_2**. Formation of the doubly-coupled product appears to be kinetically favoured, despite the second coupling being sterically hindered.

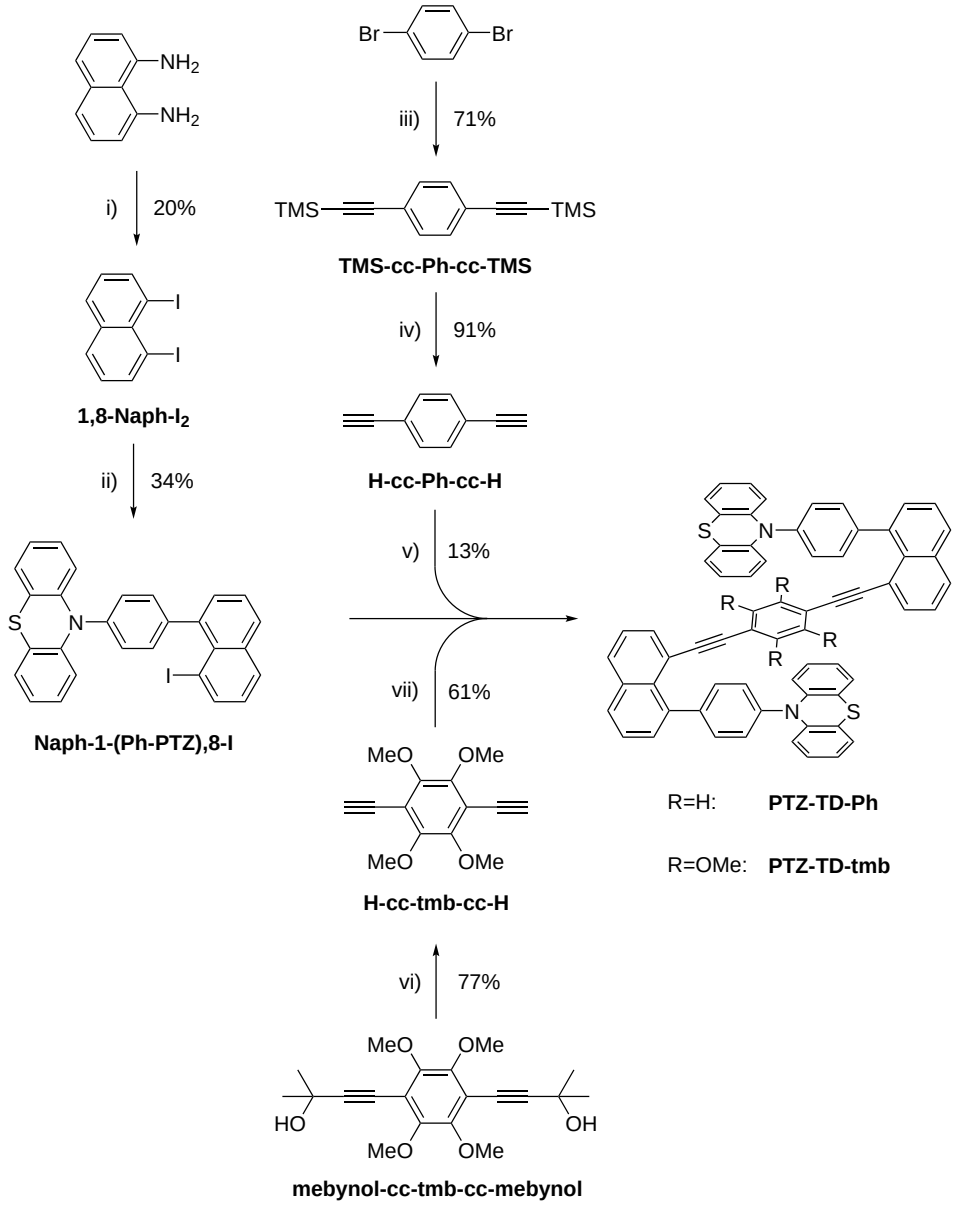

Scheme V.2. Synthesis of **PTZ-TD-Ph**; i) $NaNO_2$, KI, H_2SO_4, 0 °C; ii) **PTZ-Ph-BE**, Na_2CO_3, $[Pd(PPh_3)_4]$, THF/H_2O, 80 °C; iii) trimethylsilylacetylene, $[Pd(PPh_3)_2Cl_2]$, CuI, THF/*i*-Pr_2NH, 45 °C; iv) KF, THF/MeOH, 60 °C; v) $[Pd(PPh_3)_2Cl_2]$, CuI, $NEt_3/CHCl_3$, 65 °C; vi): NaOH, toluene, 110 °C; vii) $[Pd(PPh_3)_2Cl_2]$, CuI, NEt_3/DMSO, 90 °C.

The final Sonogashira-Hagihara coupling with the respective diethynyl bridge formed **PTZ-TD-Ph** in 13% (Scheme V.2 (v)) and **PTZ-TD-tmb** in 61% yield (Scheme V.2 (vii)). The lower yield of **PTZ-TD-Ph** was accounted for by its low solubility, resulting in purification difficulties.

For the reference molecules **PTZ-Ref-Ph** and **PTZ-Ref-tmb**, a different route (Scheme V.3) had to be taken, as mono-coupling between **PTZ-Ph-BE** and **1,5-Naph-I$_2$** was unsuccessful. In the alternative route, the central bridging unit was first coupled with the naphthalenes before the phenothiazine sidearmes were attached. To decrease the probability of polymerization in the Sonogashira-Hagihara reaction, a naphthalene derivative bearing one iodo and one triflate group (**Naph-1-OTf,5-I**) was prepared. Only **PTZ-Ref-tmb** was isolated using this route, in 68% yield. The linear arrangement of the reference compound favours aggregation, which results in a lower solubility compared to the molecules with triple-decker geometry. Potentially formed **PTZ-Ref-Ph** could not be purified for this reason.

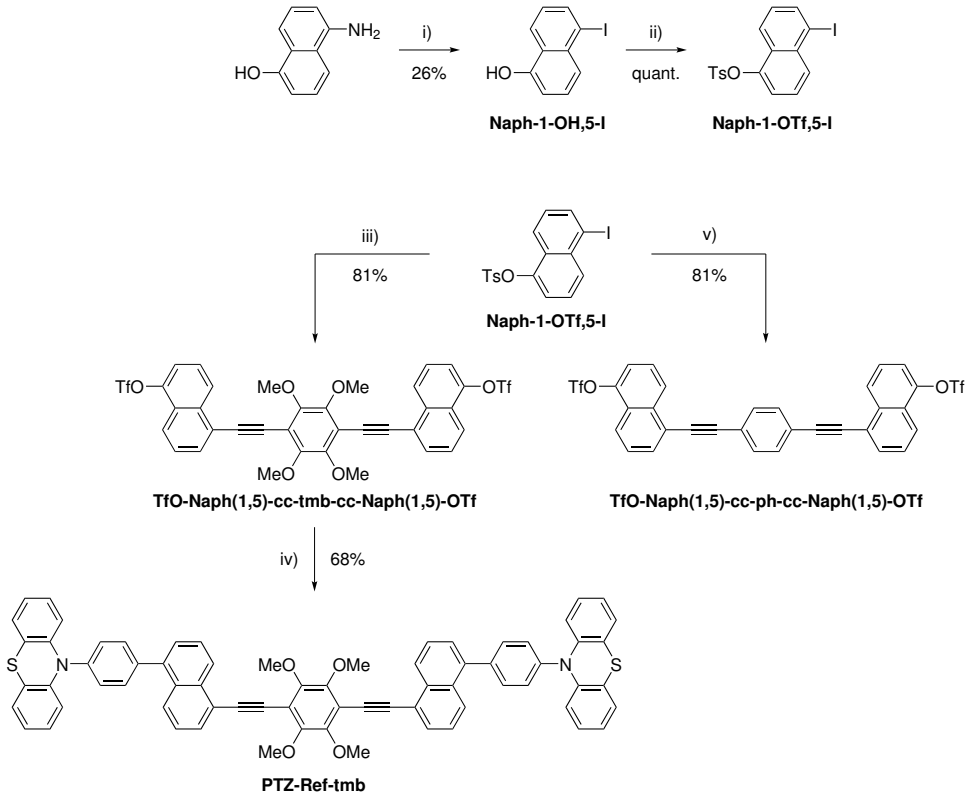

Scheme V.3. Synthesis of **PTZ-Ref-tmb**; i) $NaNO_2$, KI, aq. HCl, 0 °C; Tf_2O, CH_2Cl_2/pyridine, 0 °C, iii) **H-cc-tmb-cc-H**, $[Pd(PPh_3)_2Cl_2]$, CuI, NEt_3/THF, 90 °C; iv) **PTZ-Ph-BE**, Cs_2CO_3, $[Pd(dppf)Cl_2]\cdot CH_2Cl_2$, DMF, 60 °C; v) **H-cc-Ph-cc-H**, $[Pd(PPh_3)_2Cl_2]$, CuI, NEt_3/THF, 90 °C.

Single crystals were obtained from **[PTZ-TD-Ph][SbCl$_6$]$_2$** and **PTZ-TD-tmb** by diffusion of pentane into the respective CH_2Cl_2 solution of the compound and measured by X-ray diffractometry. Comparison between the X-ray crystal structures of the triple-decker compounds reveals that for **PTZ-TD-Ph**$^{2+}$, the central aryl ring has a roughly parallel orientation to the phenothiazine plane. This alignment enables a charge-transfer pathway across the two stacked π-systems. This conformation is not present for **PTZ-TD-tmb**, which may be caused by the steric bulk, provided by the methoxy-substituent.

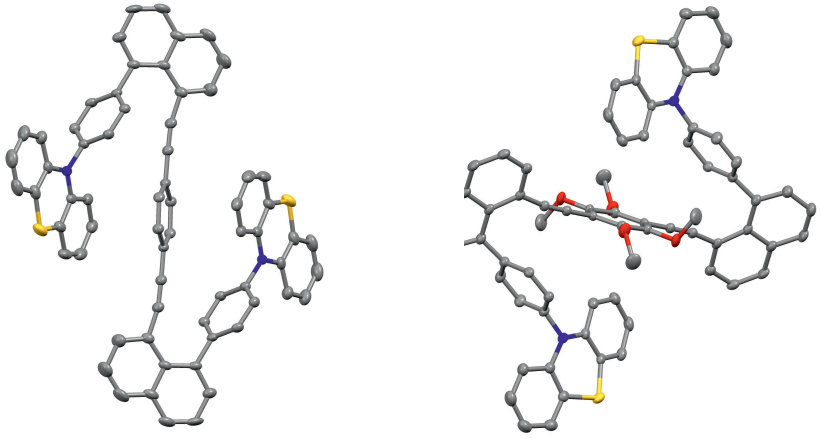

PTZ-TD-Ph^{2+} **PTZ-TD-tmb**

Figure V.2. X-ray crystal structures of **PTZ-TD-Ph**$^{2+}$ with two $SbCl_6^-$ as counter-ions and neutral **PTZ-TD-tmb**, with thermal ellipsoids drawn at 50% probability; solvent, counter-ions and hydrogen atoms omitted for clarity.

V.1.2 Electrochemistry

Cyclic voltammetry was used to determine the oxidation potentials for the triple-decker compounds **PTZ-TD-Ph** and **PTZ-TD-tmb**. Both compounds show a single quasi-reversible oxidation at an identical potential of $E_{1/2}^{(+/0)}$ = 0.72 V vs SCE in CH_2Cl_2. The lack of resolution of two consecutive oxidation waves is accounted for by negligible electrostatic interaction and electronic communication between the amines. This unobserved potential difference for the one-electron oxidations of the two redox-active moieties of a mixed-valence compound depends on the thermodynamic stability of the mixed-valent species.[82] A low stability of the monocations could also be partially responsible for the unresolved potential splitting.

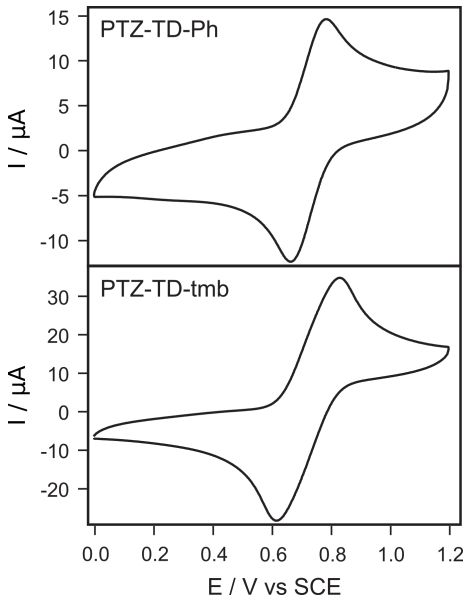

Figure V.3. Cyclic voltammograms of **PTZ-TD-Ph** and **PTZ-TD-tmb** measured in deaerated CH_2Cl_2 with 0.1 M of $TBAPF_6$ as electrolyte; potential sweep rate of 0.1 V/s.

The behaviour of **PTZ-TD-tmb** during the electrochemical measurement was surprisingly similar to **PTZ-TD-Ph** (Figure V.3). The voltammogram also shows only a single oxidation, and no additional oxidation that could be assigned to the tmb-unit is visible within the solvent window. The isolated 1,2,4,5-tetramethoxybenzene has an oxidation potential of 0.81 V vs SCE.[83] This phenomenon of a missing tmb-oxidation was also observed in previous studies and may be due to an overlap with the oxidation of phenothiazine.[84]

Table V.1: Electrochemical oxidation potentials of phenothiazine-based triple-decker molecules, measured in deaerated CH_2Cl_2 with 0.1 M of $TBAPF_6$ as electrolyte; potential sweep rate of 0.1 V/s.

Compound	$E_{1/2}^{(+/0)}$/V vs SCE	ΔE_p/mV
PTZ-TD-Ph	0.72	125
PTZ-TD-tmb	0.72	215

Two close lying signals should cause broadening, but the measured voltammograms **PTZ-TD-tmb** gave almost identical signals compared to **PTZ-TD-Ph** - even though the

separation of the peak potentials ΔE_p increased. The **PTZ-Ref-tmb** reference compound could not be measured due to solubility issues.

V.1.3 UV-Vis-NIR-Spectroscopy

Measurements in CH_2Cl_2

The neutral compounds **PTZ-TD-Ph** and **PTZ-TD-tmb** exhibit no optical absorption at wavelengths larger than 500 nm. Single oxidation of the compounds leads to their respective mixed-valence forms. Of particular interest is the NIR region, where an IVCT band is expected. Upon titration of a $SbCl_5$ solution (2.0 mM in CH_2Cl_2) as a chemical oxidant, two bands at 790 nm and 890 nm appear that can be assigned to $PTZ^{\cdot+}$.[85]

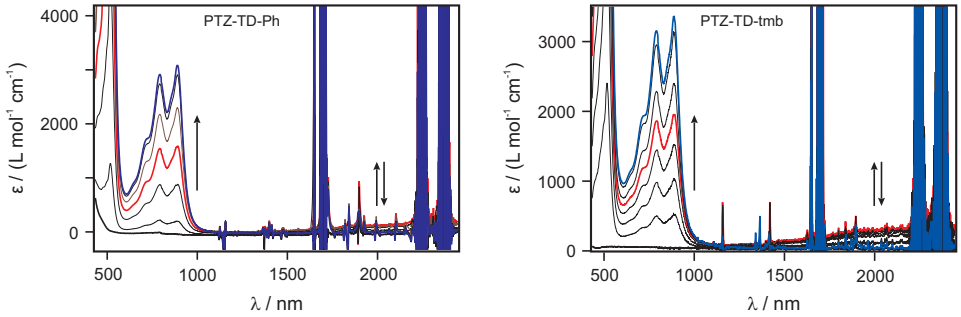

Figure V.4. UV-Vis-NIR spectra of **PTZ-TD-Ph** and **PTZ-TD-tmb** upon titration of $SbCl_5$ in CH_2Cl_2; red traces after single oxidation; blue traces after double oxidation.

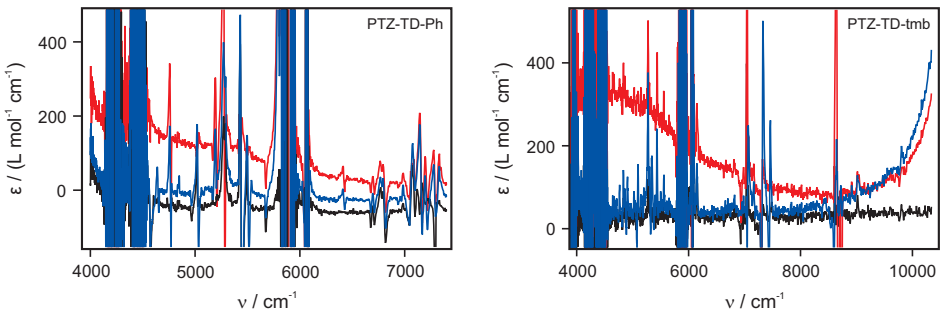

Figure V.5. Enlargement of the NIR region of the spectra shown in Figure V.4; black traces show neutral compounds; red traces after single oxidation; blue traces after double oxidation.

For both compounds, an additional band is visible in the NIR region. These bands reach maximum intensity at about one equivalent of added oxidant (red traces) and vanish

again after adding twice the amount (Figure V.4 and Figure V.5), while the bands related to $PTZ^{\cdot+}$ further increase in intensity. This behaviour of the low energy bands is characteristic for IVCT bands.
Analysis of the IVCT bands shows that, for both compounds, a single Gaussian curve is sufficient to fit the band shape (Figure V.6). The results of the Gaussian fits are listed in Table IV.1. For the calculation of the electronic coupling, the distance between the two nitrogen atoms extracted from the X-ray crystal structures (Figure V.2) was used. This is only an approximation, because for triarylamine systems the *NN*-distance does not represent the separation of the redox units very well, as the charge is expected to be delocalized across the bridge to some extent.[86,87] In organic through-bond mixed-valence systems, a somewhat lower value of the distance between the redox-active moieties is expected, as discussed in section IV.1. For the triple-decker compounds, the situation is more complicated as the exact pathway of charge-transfer is not known. As the the general geometry stays the same, using the *NN*-distance should be sufficient to compare the **PTZ-TD-Ph** and **PTZ-TD-tmb** monocations.

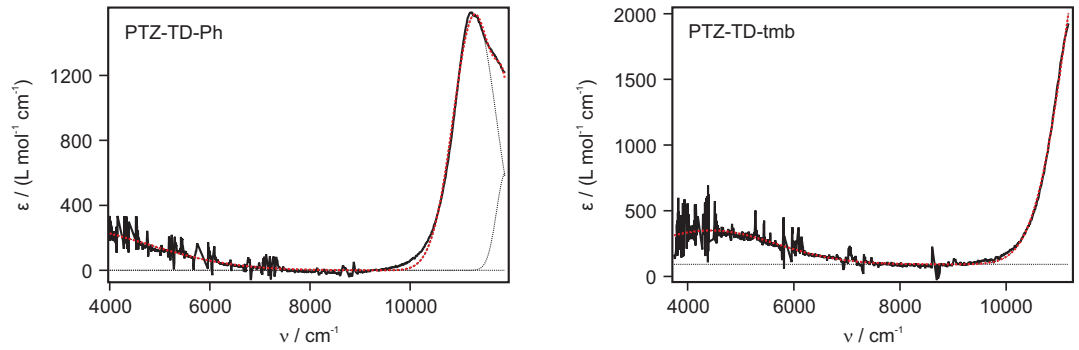

Figure V.6. Gaussian fits of the IVCT bands of **PTZ-TD-Ph** and **PTZ-TD-tmb**; black dotted lines: individual Gaussian curves; red dotted lines: sum of the Gaussian curves; vibrational solvent signals were manually removed for clarity.

Table V.2: Fit parameters of the Gaussian curves for the IVCT bands of **PTZ-TD-Ph** and **PTZ-TD-tmb**, and calculated parameters.

Compound	ν_{max} [cm^{-1}]	ε_{max} [M^{-1} cm^{-1}]	$\Delta\nu_{1/2}$ [cm^{-1}]	r_{NN} [Å]*	H_{AB} [cm^{-1}]
PTZ-TD-Ph	3030	266	4041	10.2	116
PTZ-TD-tmb	4434	258	2906	11.3	105

* values obtained from X-ray crystal structures.

Both mixed-valence compounds can be classified as Class II due to the low energy of the IVCT bands, their symmetrical band shape and low H_{AB} values. The fitting of IVCT bands revealed similar but less electronic coupling in the **PTZ-TD-tmb** monocation compared to the **PTZ-TD-Ph** monocation. This is surprising, as the higher electron density on the central aryl ring should lower the barrier for hole-transfer in the molecule. A possible explanation for this can be provided by the X-ray crystal structures (Figure V.2). The methoxy substituents provide enough steric bulk to prevent a close contact with the two phenothiazine units, as observed for **PTZ-TD-Ph**. A greater distance and less overlap of the π-systems weakens the electronic coupling between both redox-active units. In addition, the orientation of the π-systems associated with the phenothiazine nitrogen prevents an overlap of the nitrogen lone pair of electrons with the tmb-π-system.

Reliable conclusions cannot be drawn from the crystal structures, as neither of them are of the mixed-valent species of interest, and due to potential differences between the configuration in the solid state and in solution. However, they gave new insights into the possible orientations and therefore explanations of the obtained data.

A comparison with the methoxy-substituted reference compound **PTZ-Ref-tmb** was not possible, as the solubility in CH_2Cl_2 was too low to obtain a UV-Vis spectrum. Due to the insolubility of **PTZ-Ref-tmb** in CH_2Cl_2, other solvents were investigated.

Measurements in chlorobenzene

Chlorobenzene was found to be the only solvent able to dissolve **PTZ-Ref-tmb**. A repetition of the titration experiment in chlorobenzene showed no observable IVCT band for all three compounds (Figure V.7). Little absorption in the NIR region is present for all three compounds. This could be an effect of the addition of the CH_2Cl_2 solution of the oxidizing agent that shifts the overall baseline and adds CH_2Cl_2-based vibrational signals. The **PTZ-Ref-dmb** titration shows less defined signals of the oxidized PTZ that tail into the NIR region. As the tmb-bridge is less shielded in the reference molecule, its oxidation is expected to occur faster in comparison to the triple-decker system. Low-energy absorption of the delocalized radical after bridge oxidation or the absorption of degradation products could explain spectral differences to **PTZ-TD-tmb**.

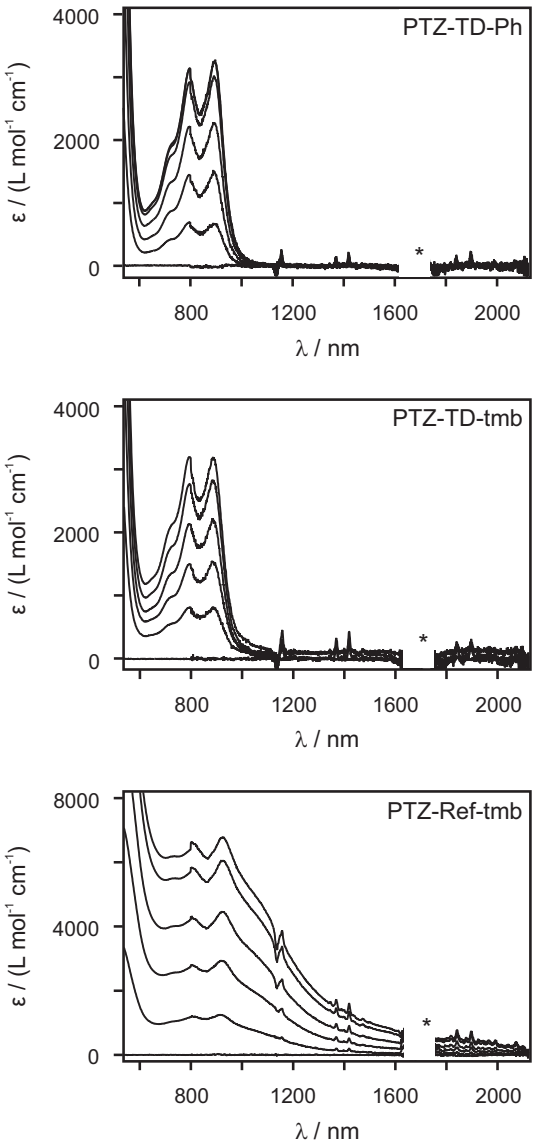

Figure V.7. UV-Vis-NIR spectra measured in chlorobenzene at 22 °C; neutral form of the compounds was used as baseline; black traces: difference to neutral form after addition of up to 2.5 eq. of the chemical oxidant; asterisk: removed due to intense solvent vibrational features.

As the dipole moments of dichloromethane and chlorobenzene have only negligible difference, this solvent effect is most likely not due to stabilizing/destabilizing effects of the charge on one PTZ-moiety. A possible explanation could be that the presence of an aromatic solvent reduces the electronic coupling of the two PTZ-units, respectively, with the mediating central aromatic bridging unit. The electron-deficient chlorobenzene might intercalate in the void between the both electron-rich PTZ and tmb, stabilized by electrostatic interactions. This might be an effect of an increase of the distance between the two redox-centers.

V.1.4 EPR-Spectroscopy

Measurements in CH_2Cl_2

The EPR spectrum of the **PTZ-TD-Ph** monocation shows a five line nitrogen pattern (Figure V.8) according to $2nI+1$, where n is the number of atoms and I its nuclear spin.[88] This means the unpaired electron interacts with both amine nitrogen atoms (n=2; $I(^{14}N)$=1) on the EPR time scale. The five line pattern is only possible for Class II or III mixed-valence compounds.[51] A Class I compound would show only three lines, as the radical is fully localized on a single nitrogen atom. This is the case for the **PTZ-TD-tmb** monocation, which is surprising as an IVCT band with greater intensity than for the phenyl bridged molecule was clearly visible in the UV-Vis-NIR spectrum. As the nature of the observed electron-transfer is different for UV-Vis and EPR spectroscopy (optical vs. thermal), this is not necessarily a contradiction. It was demonstrated that for triarylamine-based mixed-valent systems with weak electronic coupling, a five-line pattern in EPR at room temperature can change to a three-line pattern at low temperatures.[51] However, the presence of an IVCT band usually suggests that thermal electron-transfer is fast, thus one should observe a five-line-pattern in the EPR experiment.[53] The presence of optical electron-transfer, while exhibiting localized behavior in the EPR measurement, has not been reported and may be an effect of the through-space interaction. By increasing the temperature it may be possible to change the pattern to five lines for the **PTZ-TD-tmb** monocation, but as the solvent for the measurement was CH_2Cl_2 (T_B=312.8 K), this hypothesis could not be examined.

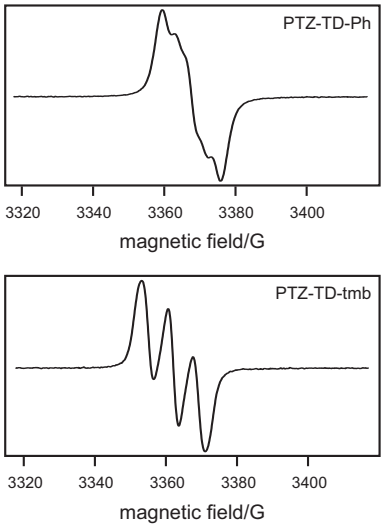

Figure V.8. EPR spectra recorded in CH_2Cl_2 at 20 °C after chemical oxidation with 0.8 equivalents $SbCl_5$; microwave frequencies were (**PTZ-TD-Ph**) 9.4565 GHz, and (**PTZ-TD-tmb**) 9.4487 GHz.

E_{th} was calculated for **PTZ-TD-Ph**$^{\cdot+}$ and **PTZ-TD-tmb**$^{\cdot+}$ according to equation IV.3 (Table V.3). The calculated values may only be an estimation, due to the uncertainty of H_{AB}, but the general relation is in agreement with the EPR measurements. **PTZ-TD-Ph**$^{\cdot+}$ exhibits a higher degree of delocalization in the EPR experiment and a lower E_{th} was calculated compared to **PTZ-TD-tmb**$^{\cdot+}$.

Table V.3: Barrier for thermal electron-transfer calculated with values obtained from fits of the IVCT bands.

	PTZ-TD-Ph$^{\cdot+}$	**PTZ-TD-tmb**$^{\cdot+}$
E_{th}/cm^{-1}	646	1006

Measurements in chlorobenzene

The EPR measurements were repeated with the full set of molecules in chlorobenzene. All monocationic compounds show a three line pattern (Figure V.9). Interestingly no spectrum can be explained with a radical fully localized on a single nitrogen atom. Two conclusions can be drawn from this second measurement. Firstly, the change from CH_2Cl_2 to chlorobenzene decreases the electronic coupling in the mixed-valent species. For **PTZ-TD-Ph**$^{\cdot+}$, the unpaired electron was delocalized over two nitrogen atoms in CH_2Cl_2, and localized on a single nitrogen in chlorobenzene. This is in line with the results from the UV-Vis-NIR measurements, which means that neither a light- nor a temperature-induced charge-transfer is present.

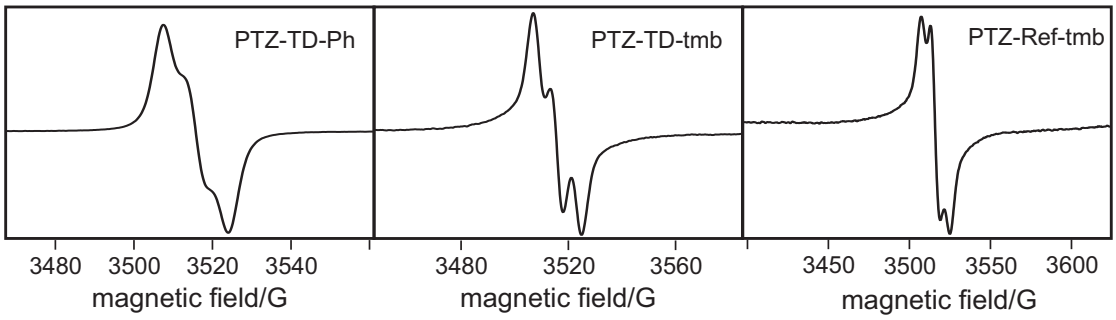

Figure V.9. EPR spectra recorded in chlorobenzene at 20 °C after chemical oxidation with $SbCl_5$, microwave frequencies were (**PTZ-TD-Ph**) 9.8714 GHz, (**PTZ-TD-tmb**) 9.8717 GHz, and (**PTZ-Ref-tmb**) 9.8724 GHz.

Second, the use of chlorobenzene as a solvent changes the charge-distribution in the molecule, as the spectra of **PTZ-TD-tmb** also differ. As pictured in Figure V.2, the PTZ-plane is almost orthogonally orientated to the central and the *N*-substituted aryl-ring. The aromatic solvent may cause a more coplanar orientation of the PTZ-moiety with one or both of the π-systems, leading to a less localized spin on the nitrogen atom.

V.2 Second Generation Triple-Decker System

To overcome solubility problems, the redox-active amine unit was changed to a twofold hexyl-substituted carbazole (CBZ). Carbazoles can be easily substituted with alkyl chains to enhance the solubility in organic solvents. Tetramethoxybenzene has a lower oxidation potential than *N*-aryl carbazoles, and therefore cannot be used as the bridging unit. 1,4-dimethoxybenzene (dmb) is slightly harder to oxidize (1.34 V vs. SCE)[89] than a comparable carbazole to the one used (1.13 V vs. SCE)[90] and was therefore chosen as second bridging unit. Furthermore, the potential difference between redox-active moiety (CBZ) and electron-rich bridge (dmb) is greater compared to the first generation, to avoid similar complications as described above.

V.2.1 Synthesis

CBZ-Ph-BE was synthesized according to Figure V.10, over four steps in an overall yield of 12%. The first two steps, consisting of a Friedel-Crafts acylation followed by a reduction, have been previously reported.[91] Successive carbazole *N*-arylation and Miyaura-couplings were used to form the boronic ester.

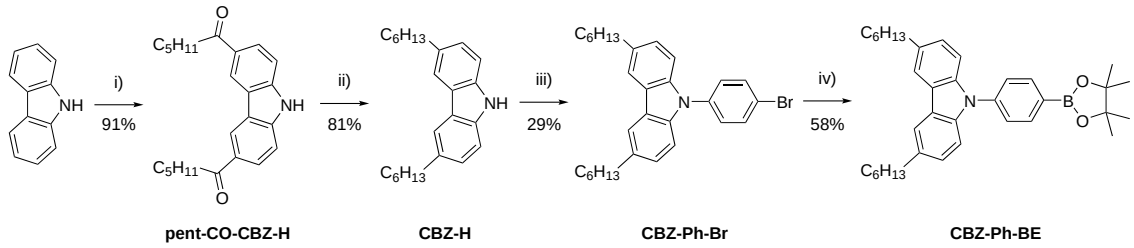

Figure V.10. Synthesis of **CBZ-Ph-BE**; i) $AlCl_3$, hexanoyl chloride, CH_2Cl_2, 0 °C; ii) $LiALH_4$, $AlCl_3$, THF, 0 °C; iii) 1-bromo-4-fluorobenzene, Cs_2CO_3, DMF, 160 °C; iv) bis(pinacolato)diboron, KOAc, $[Pd(PPh_3)_2Cl_2]$, DMSO, 80 °C.

In a first attempt, *N*-arylation by nucleophilic substitution reaction between **CBZ-H** and 1-bromo-4-fluorobenzene was examined for the synthesis of **CBZ-Ph-Br**. Due to low yields after increasing reaction times (Figure V.10 (iii)), analogous to the synthesis of **PTZ-Ph-TMS**, a Buchwald-Hartwig amination of **CBZ-H** with **Br-Ph-TMS** was examined as an alternative. After the failure of multiple attempts at the deprotection of the TMS-group with ICl, the initial route was revived. Optimisation of reaction conditions led to a satisfactory yield (29%) of the desired product.

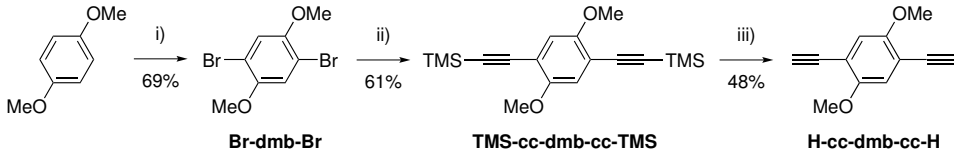

Figure V.11. Synthesis of **H-cc-dmb-cc-H**; i) Br_2, acetic acid, 0 °C; ii) trimethylsilylacetylene, $[Pd(PPh_3)_2Cl_2]$, CuI, *i*-Pr_2NH, THF, 45 °C; iii) KF, THF/MeOH, 55 °C.

The bridge building block **H-cc-dmb-cc-H** was synthesized in three steps. After bromination of 1,4-dimethoxybenzene, the synthetic route of **H-cc-Ph-cc-H** was adapted (Scheme V.2).

All triple-decker and reference molecules with the carbazole residues could be synthesized (Figure V.12 and Figure V.13) by the established route from the phenothiazine based compounds. The enhanced solubility caused by the hexyl-chains enabled purification by column chromatography for all compounds.

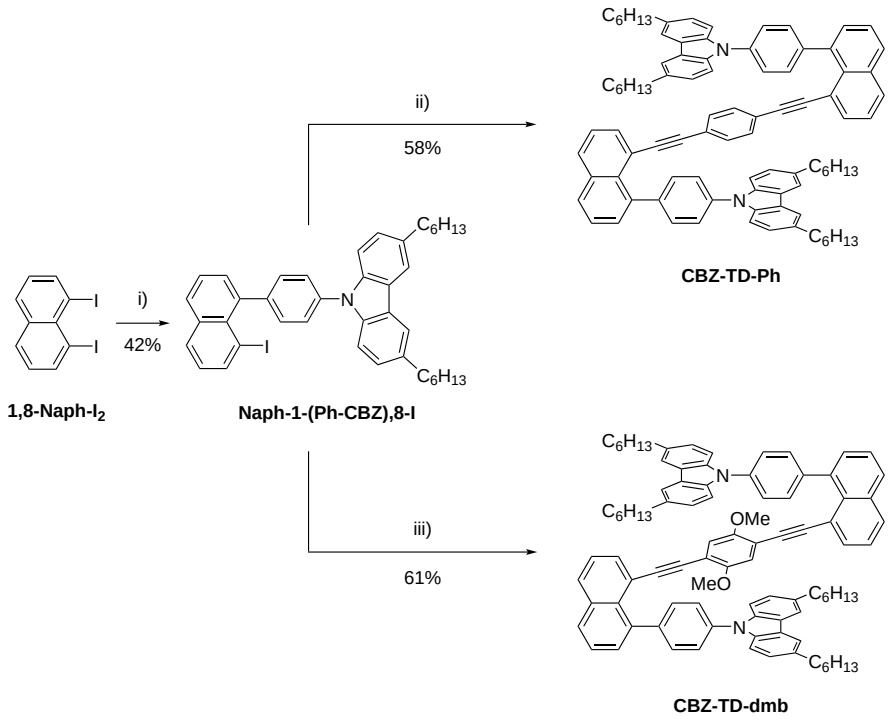

Figure V.12. Synthesis of **CBZ-TD-Ph** and **CBZ-TD-dmb**; i) **CBZ-Ph-BE**, Na_2CO_3, $Pd(PPh_3)_4$, THF/H_2O, 80 °C; ii) **H-cc-Ph-cc-H**, $[Pd(PPh_3)_2Cl_2]$, CuI, NEt_3, 90 °C; iii) **H-cc-dmb-cc-H**, $[Pd(PPh_3)_2Cl_2]$, CuI, diisopropylamine, 90 °C.

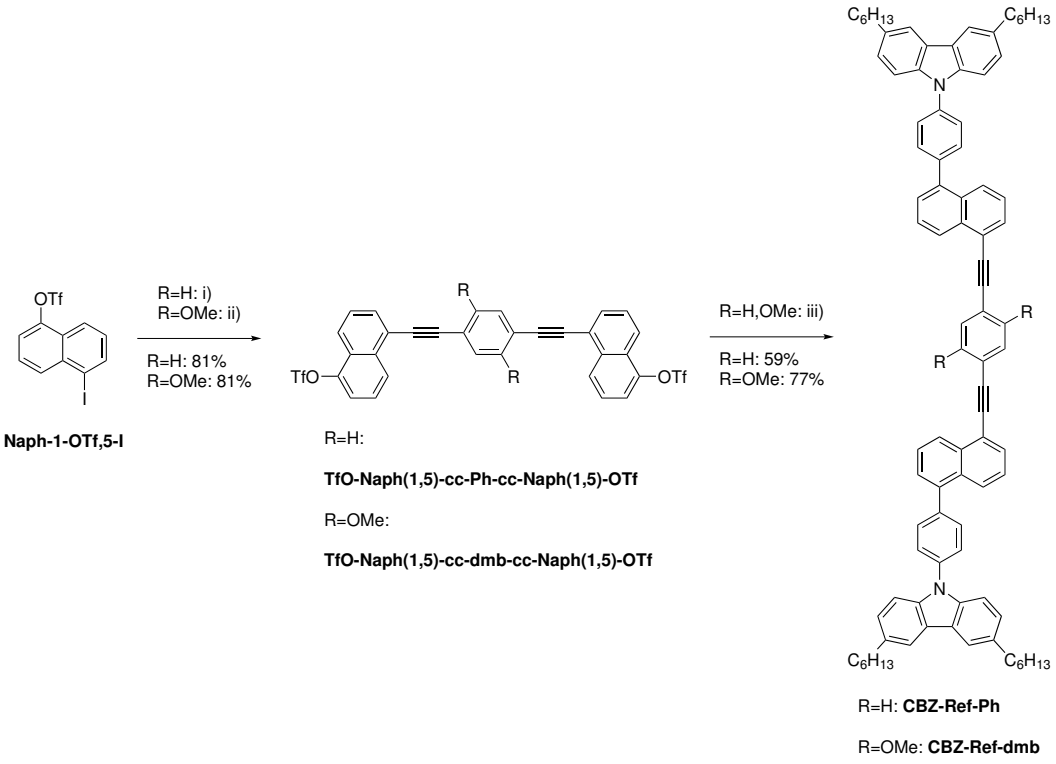

Naph-1-OTf,5-I

R=H:

TfO-Naph(1,5)-cc-Ph-cc-Naph(1,5)-OTf

R=OMe:

TfO-Naph(1,5)-cc-dmb-cc-Naph(1,5)-OTf

R=H: **CBZ-Ref-Ph**

R=OMe: **CBZ-Ref-dmb**

Figure V.13. Synthesis of **CBZ-Ref-Ph** and **CBZ-Ref-dmb**; i) **H-cc-Ph-cc-H**, $[Pd(PPh_3)_2Cl_2]$, CuI, NEt_3/THF, 90 °C; ii) **H-cc-dmb-cc-H**, $[Pd(PPh_3)_2Cl_2]$, CuI, NEt_3/THF, 90 °C; iii) **CBZ-Ph-BE**, Cs_2CO_3, $[Pd(dppf)Cl_2]\cdot CH_2Cl_2$, DMF, 60 °C.

V.2.2 Electrochemistry

The oxidative cyclic voltammograms for the carbazole-based series of molecules are presented in Figure V.14 (values listed in Table V.4).

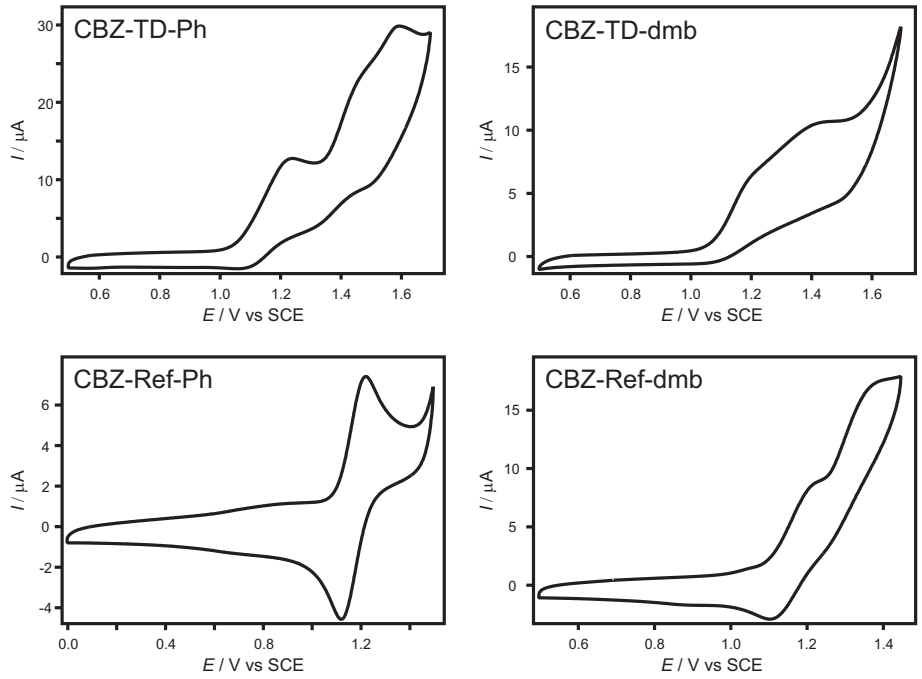

Figure V.14. Cyclic voltammograms of 2nd generation triple-decker and reference molecules measured in deaerated CH_2Cl_2 with 0.1 M of $TBAPF_6$ as electrolyte; potential sweep rate of 0.1 V/s.

The only fully reversible oxidation could be measured for **CBZ-Ref-Ph**. The determined oxidation potential of 1.17 V vs SCE is in line with comparable 3,6-alkyl substituted *N*-phenyl carbazoles,[90] meaning that the extension of the π-system at the phenyl substituent has only a negligible influence on the electrochemical properties of the amine. Furthermore, only a single oxidation associated with the carbazole unit is visible. This changed for the second reference molecule, **CBZ-Ref-dmb**. In addition to a second non-reversible oxidation, the first oxidation broadens and is less pronounced than for **CBZ-Ref-Ph**. The second oxidation at roughly 1.38 V vs SCE can be assigned to the dmb-unit.[89]

Reversibility is completely lost when moving from the reference compounds to the triple-decker compounds. Measurements with narrower potential windows or a change in scan rate had no effect on the reversibility. The first carbazole-based oxidation has a constant potential. For **CBZ-TD-Ph**, one clear additional oxidation with a small shoul-

der can be observed. **CBZ-TD-dmb** was the least stable compound upon electrochemical oxidation, with two very broad and undefined oxidation signals.

Table V.4: Electrochemical oxidation potentials of carbazole-based triple-decker and reference molecules, measured in deaerated CH_2Cl_2 with 0.1 M of $TBAPF_6$ as electrolyte; potential sweep rate of 0.1 V/s.

Compound	$E_{1/2}^{(+/0)}$/V vs SCE	$E_{1/2}^{(2+/+)}$/V vs SCE	$E_{1/2}^{(3+/2+)}$/V vs SCE
CBZ-TD-Ph	1.23*	1.46*	1.59*
CBZ-TD-dmb	1.20*	1.43*	-
CBZ-Ref-Ph	1.17	-	-
CBZ-Ref-dmb	1.16	1.38*	-

* values obtained from anodic peak potential.

The change from phenyl to dmb as a central aryl bridging unit had no influence on the oxidation potential of the carbazole, but it does have a destabilizing effect on the oxidized molecule. The triple-decker compounds further exhibit lower stability upon oxidation than their respective reference compounds. Evidence for electronic communication in the singly oxidized triple-deckers could not be obtained from the electrochemical measurements.

V.2.3 UV-vis-NIR-Spectroscopy and Spectroelectrochemistry

All neutral compounds show no absorption at wavelengths longer than 420 nm. An analogous titration with $SbCl_5$, as described for the 1st generation compounds, is expected to show a band around 820 nm with a distinct shoulder to shorter wavelengths[68] for the carbazole monocation, as well as the IVCT band for the triple-decker molecules in the NIR region. The behaviour of **CBZ-TD-Ph**, and all other carbazole-based compounds, towards chemical oxidation was different to that of the phenothiazine-based compounds. Oxidation occurred much slower and more oxidant was needed to evoke a spectral change. Therefore, the time between the additions of oxidant was increased to 20 minutes. Spectra of all compounds (Figure V.15) show the expected 800 nm absorption for the carbazole monocation.[90] It has to be noted that the first change in absorption could only be observed after addition of 1.5 equivalents of oxidant. Upon oxidation, an additional band emerges at ~ 1100 nm which shifts to shorter wavelengths after addition of seven equivalents of $SbCl_5$. This band cannot be assigned as IVCT, as it is only visible after addition of more than a single equivalent of oxidant and does not clearly vanish after oxidation of both carbazole units. This point was most likely never reached during the experiment, as the band at 800 nm never stopped increasing in intensity

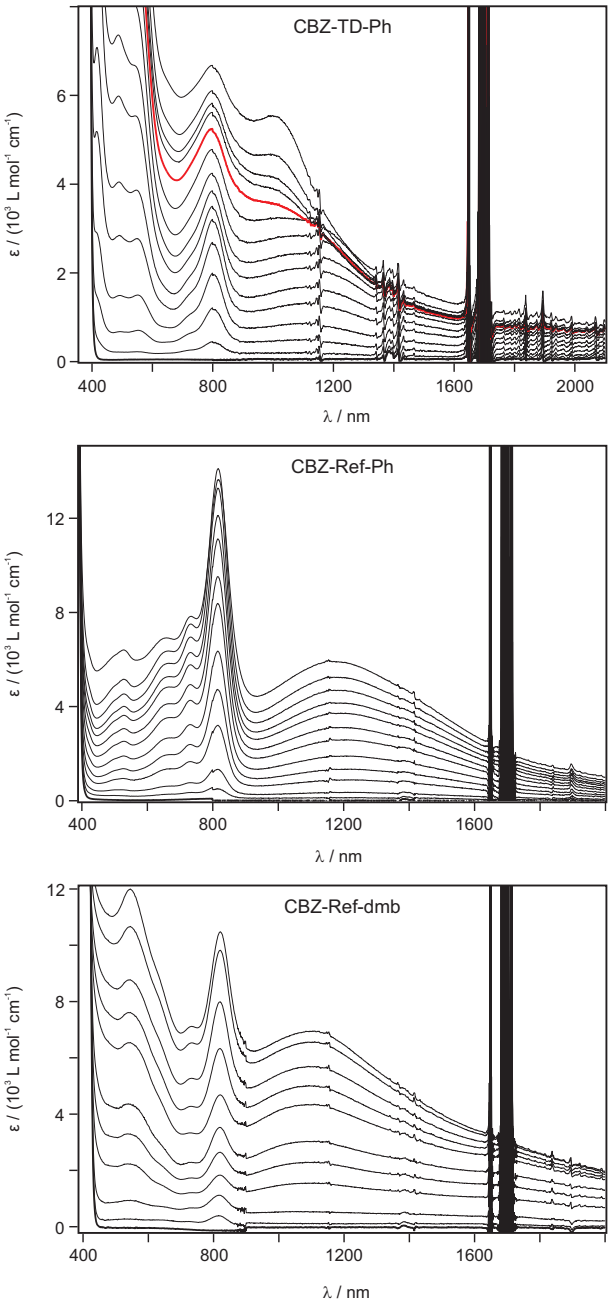

Figure V.15. UV-Vis-NIR spectra of **CBZ-TD-Ph**, **CBZ-Ref-Ph** and **CBZ-Ref-dmb** upon titration with $SbCl_5$ in CH_2Cl_2; red trace in the top titration marks the point of beginning bandshift.

upon addition of more $SbCl_5$. The stronger argument against an IVCT nature of the 1100 nm band is the spectrum of **CBZ-Ref-Ph**. In general, the two titrations exhibit close resemblance at wavelengths longer than 700 nm. The only difference is the shift of the low energy band for **CBZ-TD-Ph** at the end of the titration. This could also mean that a second oxidation of the molecules is not possible using $SbCl_5$. The difficulties of this experiment were somewhat surprising, as it was previously reported that carbazole oxidation with $SbCl_5$ is possible in nearly quantitative isolated yield and was even successfully implemented in mixed-valence studies.[68,92] As no real conclusion could be obtained from the titration experiment, spectroelectrochemical measurements were performed with **CBZ-TD-Ph** and **CBZ-Ref-Ph**. The spectra obtained from the titration experiment were reproduced by the spectroelectrochemical measurements (Figure V.16). The decrease of the low-energy band of **CBZ-TD-Ph** is more pronounced and could be a sign of degradation upon oxidation. This could exclude possible lack of oxidative strength of $SbCl_5$ as the cause for the problems of the previous experiment.

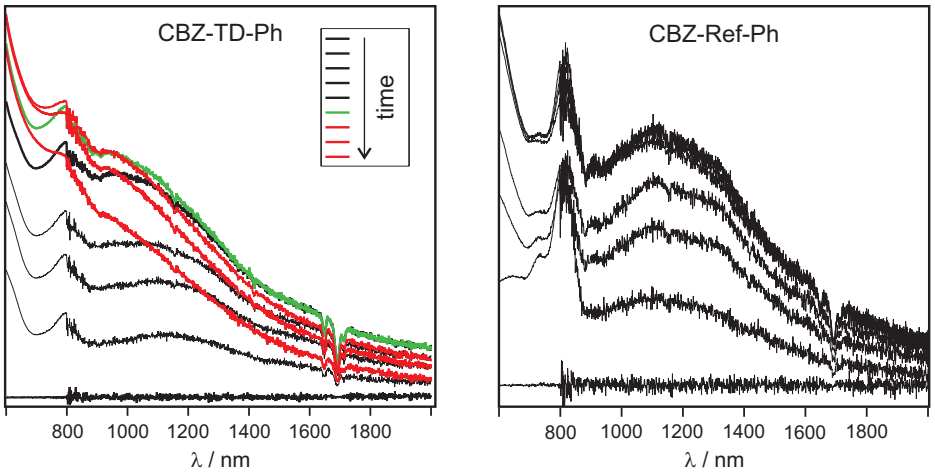

Figure V.16. UV-Vis-NIR-spectroelectrochemical spectra of **CBZ-TD-Ph** and **CBZ-Ref-Ph** measured in CH_2Cl_2 with an applied potential of 1.4 V vs SCE.

V.2.4 EPR-Spectroscopy

EPR measurements gave important information for the interpretation of the data obtained for this 2nd generation of mixed-valent compounds. As shown in Figure V.17, all monocations showed only a single line pattern in their EPR spectra. This is in strong contradiction to the expected three or five line patterns as measured for the phenothiazine-based compounds (V.1.4).

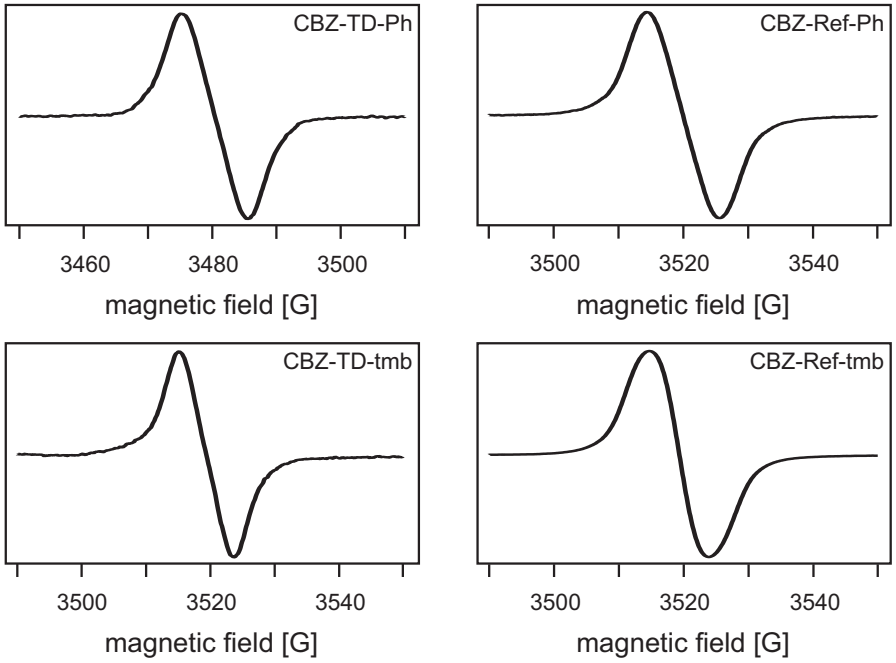

Figure V.17. EPR spectra recorded in CH_2Cl_2 solution at 20 °C after chemical oxidation with 0.8 equivalents $SbCl_5$, microwave frequencies were (**CBZ-TD-Ph**) 9.7603 GHz, (**CBZ-TD-dmb**) 9.8704 GHz, (**CBZ-Ref-Ph**) 9.8717 GHz, and (**CBZ-Ref-dmb**) 9.8701 GHz.

These results point towards localization of the unpaired electron elsewhere than on the nitrogen atom. No reference of an EPR spectrum for a monocation of an *N*-aryl carbazole is available, but it was reported that the *N*-phenylcarbazole monocation showed no nitrogen splitting either.[93] This could explain why, although this technique is quite common for characterisation of amine based mixed-valence compounds, was not used for the two existing examples of carabazole mixed-valence compounds.[68,90]

V.2.5 Conclusion and Future Prospects

Two triple-decker compounds based on a phenothiazine redox-active moiety, along with one of the corresponding linear reference compounds were synthesized. The monocations of the triple-decker compounds obtained from chemical oxidation show weak IVCT bands in the NIR-region when measured in CH_2Cl_2. EPR spectra suggested a different degree of delocalization of the radical for the two mixed-valent triple-decker compounds. When the measurements were repeated in chlorobenzene, a solvent capable of dissolving the reference compound, no IVCT bands could be detected for any of the molecules, nor was delocalization in EPR measurements observed.
Due to the poor solubility of these compounds, a 2nd generation of triple-decker molecules based on carbazole as a redox-active moiety, including both reference compounds, were synthesized. All measurements for this second generation could be performed in CH_2Cl_2. No conclusive results could be obtained, as chemical oxidation occurred on a timescale of minutes, and an increasing signal of oxidized amine was visible for amounts of oxidizing agent greater than two equivalents. There are no obvious reasons for this behaviour concerning the redox potentials of carbazole and $SbCl_5$, further supported by previous studies with similar redox couples. EPR measurements even suggest that the generated carbazole radical is not primarily located on the nitrogen atom, but somewhere on the aromatic backbone.
Although significant advances towards a mixed-valence system with a triple-decker geometry showing through-space charge-delocalization could be achieved with this project, a clear proof of the n-π-n interaction is still pending. A previously undiscovered stacking of three π-systems is another possibility for the charge-transfer pathway in the presented system. Temperature-dependent EPR measurements for the phenothiazine-based compounds are of particular interest, as **PTZ-TD-Ph**$^{\cdot+}$ could be one of the rare examples among mixed-valence systems, exhibiting the possibility to determine the rate constant for thermal electron-transfer from both EPR and optical absorption spectroscopy.

VI Experimental

VI.1 Methods

General Methods

All commercially purchased chemicals were used without further purification. $[Pd(PPh_3)_4]$ and mebynol-cc-tmb-cc-mebynol were synthesized within the group. All anhydrous solvents were purchased, except DCM, THF and Et_2O, which were obtained in-house using a solvent purification system by Innovative Technology. Silica gel (40–63 μm, silicycle) was used for column chromatography. Thin-layer chromatography was carried out on silica gel plates (60 F_{254}) from Merck. Deaerating of solvents for chemical reactions was performed by passing nitrogen gas through the solution for 10 minutes.

NMR Spectroscopy

^{1}H-NMR and ^{13}C-NMR spectra were measured on a 400 MHz Bruker Avance III instrument at 298 K. Chemical shifts (δ) are given in ppm and were referenced to the NMR-solvent residual peak, proton-proton coupling constants are given in Hz. The multiplicity of the signals is labelled as follows: singlet (s), doublet (d), triplet (t), quartet (q) and multiplet (m).

UV-Vis-NIR Spectroscopy

UV-Vis-NIR spectra were recorded as solutions on a Cary 5000 instrument from Varian.

Elemental Analysis

C,H,N elemental analyses were conducted by Ms Sylvie Mittelheisser on a Vario Micro Cube instrument.

Electrochemistry

Cyclic voltammetry was measured with a Versastat3-200 potentiostat from Princeton Applied Research. The same instrument was used in combination with the Cary 5000 for spectroelectrochemical measurements. All voltammograms were obtained using 0.1 M tetrabutylammonium hexafluorophosphate in the respective solvent stated. The sweep rate was 0.1 V/s if not stated otherwise. A glassy carbon electrode was used as

the working electrode, with a silver wire counter electrode and an SCE reference electrode for electrochemical measurements. For spectroelectrochemical measurements, a platinum-net used as the working electrode, with a platinum wire counter electrode and an SCE reference electrode.

Mass Spectrometry

ESI mass spectra were recorded on a Bruker esquire 3000 plus. High resolution ESI mass spectra were measured on a Bruker maxis 4G QTOF EDI by Dr. Heinz Nadig. MALDI spectra were recorded on a Bruker microflex instrument by Dr. Christopher Larsen using a *trans*-2-[3-(4-*t*-butylphenyl)-2-methyl-2-propenylidene]malononitrile (DCTB) matrix.

EPR Spectroscopy

EPR-spectra were recorded on a Bruker CW EPR Elexsys-500 by Mr Pascal Richard. All measurements were performed at room temperature as 1 mM solutions in the respective solvent stated.

Pump-Probe Spectroscopy

Pump-probe measurements were performed with a LP920-KS spectrometer from Edinburgh Instruments, equipped with an iCCD camera from Andor. The light source for sample excitation was a frequency-doubled Quantel Brilliant b laser. All measurements were performed in Schlenk-cuvettes as solutions, deaerated by four freeze-pump-thaw cycles.

VI.2 Synthesis for Project 1

Method A

An aryl halide (1.00 eq.), a boric acid/boronic ester (1.00 eq.) and Na_2CO_3 (10.0 eq.) were dissolved in a 5:3 v:v mixture of THF and H_2O under a nitrogen atmosphere. The mixture was deaerated for 20 minutes (min.), $[Pd(PPh_3)_4]$ (5 mol%) added and heated at 85 °C overnight. After cooling to r.t. the product was extracted into CH_2Cl_2, the combined organic phases dried over Na_2SO_4, and the solvents removed under reduced pressure.

Method B

The trimethyl(aryl)silane (1.00 eq.) was dissolved in anhydrous CH_2Cl_2 and cooled to −78 °C. A solution of ICl (2.50 eq. per TMS group) in anhydrous CH_2Cl_2 was added dropwise. The reaction was stirred for 30 min. at that temperature and quenched by addition of saturated (sat.) $Na_2S_2O_3$ solution. The organic phase was separated, dried over Na_2SO_4, and the solvent removed under reduced pressure.

Method C

An aryl halide (1.00 eq.), bis(pinacolato)diboron (1.50 eq.), $[Pd(PPh_3)_2Cl_2]$ (10 mol%) and KOAc (4.00 eq.) were suspended in anhydrous, deaerated dimethyl sulfoxide (12 mL/mmol substrate) under a nitrogen atmosphere. The reaction mixture was stirred at 80 °C overnight. After cooling to r.t. water was added and the product extracted into CH_2Cl_2. The combined organic phases were washed with water, dried over Na_2SO_4, and the solvent removed under reduced pressure.

biph-Br

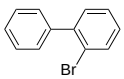

biph-Br was synthesized by a adapting a literature procedure.[94]
Under a nitrogen atmosphere, phenylboronic acid (0.50 g, 4.10 mmol), 1,2-dibromobenzene (1.93 g, 8.18 mmol) and Na_2CO_3 (1.00 g, mmol) were dissolved in a 5:2 (v:v) THF/H_2O mixture (16 mL). After deaerating for 5 min, the reaction was stirred at 80 °C overnight. The reaction mixture was diluted with H_2O and the product extracted

into CH_2Cl_2. The combined organic phases were dried over Na_2SO_4 and the solvents removed under reduced pressure. The crude product was purified using column chromatography (SiO_2, pure pentane). The product was isolated as a colorless oil (589 mg, 2.50 mmol, 62%).

^{1}**H-NMR** (400 MHz, CD_2Cl_2): δ 7.68 (dd, J = 8.0, 1.2 Hz, 1H), 7.49-7.30 (m, 7H), 7.23 (ddd, J = 8.0, 7.1, 2.0 Hz, 1H) ppm.

FlO

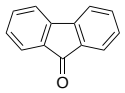

FlO was synthesized by a adapting a literature procedure.[95]
9*H*-Fluorene (1.66 g, 10.0 mmol) and KI (332 mg, 2.00 mmol) were suspended in MeCN (30 mL). *tert*-butyl hydroperoxid (4.15 mL, 30.0 mmol, 70% in H_2O) was added and the reaction mixture stirred overnight. Remaining peroxide was quenched by addition of sat. aq. $Na_2S_2O_3$ solution. The product extracted into CH_2Cl_2 and the combined organic phases dried over Na_2SO_4. The solvents were removed under reduced pressure and the crude product purified using column chromatography (SiO_2, pentane:EtOAc, 10:1). The product was isolated as yellow solid (1.70 g, 9.43 mmol, 94%).

^{1}**H-NMR** (400 MHz, $CDCl_3$): δ 7.66 (dt, J = 7.3, 0.9 Hz, 2H), 7.55-7.45 (m, 4H), 7.30 (td, J = 7.3, 1.3 Hz, 2H) ppm.

Br-FlH-Br

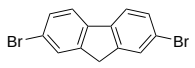

9*H*-Fluorene (7.50 g, 45.1 mmol) was dissolved in CH_2Cl_2 (75 mL) and cooled to 0 °C. Under exclusion of light, a solution of bromine (5.00 mL, 99.5 mmol) in CH_2Cl_2 (45 mL) was added dropwise. The reaction mixture was stirred at r.t. overnight and sat. $Na_2S_2O_3$ solution added. The phases were separated and the product extracted into CH_2Cl_2. The combined organic phases were washed with H_2O and dried over Na_2SO_4. The solvent was evaporated and the residue recrystallized from EtOH, which

afforded the product as a colorless solid (10.3 g, 31.8 mmol, 70%).

^{1}**H-NMR** (400 MHz, $CDCl_3$): δ 7.68-7.65 (m, 2H), 7.60 (d, J = 8.1 Hz, 2H), 7.54-7.46 (m, 2H), 3.87 (s, 2H) ppm.

Br-FlO-Br

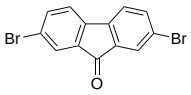

Br-FlO-Br was synthesized by a adapting a literature procedure.[95]
Br-FlH-Br (3.50 g, 10.4 mmol) was dissolved in the minimum volume of CH_2Cl_2 required, then diluted with MeCN (50 mL). KI (0.35 g, 2.11 mmol) and *tert*-butyl hydroperoxide (4.30 mL, 31.0 mmol, 70% in H_2O) were added and the reaction mixture was stirred at 50 °C overnight. Remaining peroxide was quenched by addition of $Na_2S_2O_3$ solution. The product was extracted into CH_2Cl_2 and the combined organic phases dried over Na_2SO_4. The solvents were removed under reduced pressure and the crude product purified using column chromatography (SiO_2, pentane:CH_2Cl_2, 3:1). The product was isolated as a yellow solid (2.94 g, 8.70 mmol, 81%).

^{1}**H-NMR** (400 MHz, $CDCl_3$): δ 7.77 (dd, J = 1.9, 0.5 Hz, 2H), 7.63 (dd, J = 7.9, 1.9 Hz, 2H), 7.39 (dd, J = 7.9, 0.5 Hz, 2H) ppm.

spiro-Fl

spiro-Fl was synthesized by a adapting a literature procedure.[38]
Under a nitrogen atmosphere, magnesium turnings (64 mg, 2.63 mmol) were activated by stirring with an iodine crystal. A solution of **biph-Br** (589 mg, 2.53 mmol) in anhydrous Et_2O (5 mL) was added slowly while the reaction mixture was heated at 35 °C. After heating at reflux for 2 h, a solution of **FlO** (500 mg, 2.77 mmol) in anhydrous Et_2O (5 mL) was added dropwise and the resulting mixture was heated at reflux overnight. After cooling to r.t. the precipitate was filtered and washed with Et_2O. The solid ma-

terial was added to an ice-cold aq. NH_4Cl solution and stirred for 2 h. The precipitate was filtered and washed with H_2O. The solid material was transferred to a flask and dissolved in a minimum volume of refluxing acetic acid. HCl solution (0.2 mL, 38%) was added to the solution and stirred for an additional 10 minutes. After cooling to r.t., the precipitate was filtered and washed with H_2O. The pure product was obtained by recrystallization from EtOH as a colorless solid (350 mg, 1.11 mmol, 44%).

^{1}**H-NMR** (400 MHz, $CDCl_3$): δ 7.85 (dt, J = 7.6, 0.9 Hz, 4H), 7.37 (td, J = 7.6, 1.1 Hz, 4H), 7.11 (td, J = 7.6, 1.1 Hz, 4H), 6.73 (dt, J = 7.6, 0.9 Hz, 4H) ppm.

TMS-Ph-BA

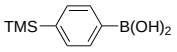

1,4-Dibromobenzene (5.59 g, 23.8 mmol) was dissolved in anhydrous THF (60 mL) under a nitrogen atmosphere and cooled to −78 °C. *n*-BuLi (10 mL, 2.5 M in hexane, 25 mmol) was added dropwise and stirred for 10 min. Me_3SiCl (3.15 mL, 25.0 mmol) was added dropwise and the reaction was allowed to reach r.t. before it was cooled down again to −78 °C. Another portion of *n*-BuLi (10.5 mL, 2.5 M in hexane, 26.3 mmol) was added dropwise. After stirring for 20 min at this temperature, B(O*i*-Pr)$_3$ (4.66 mL, 20.2 mmol) was added dropwise. The reaction was allowed to warm to r.t., stirred overnight, and then quenched by addition of H_2O. The product was extracted into CH_2Cl_2, the combined organic phases were dried over Na_2SO_4 and the solvents removed under reduced pressure. The crude product was purified using column chromatography (SiO_2, CH_2Cl_2 to EtOAc) to obtain the product as a white solid (2.60 g, 13.4 mmol, 56%).

^{1}**H-NMR** (400 MHz, $CDCl_3$): δ 8.22-8.18 (m, 2H), 7.70-7.66 (m, 2H), 0.33 (s, 9H) ppm.

TMS-biph-Br

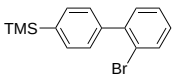

TMS-biph-Br was synthesized using method A, with 1,2-dibromobenzene (3.63 g, 15.5 mmol) as aryl halide and **TMS-Ph-BA** (2.50 g, 12.9 mmol) as boronic acid.

The crude product was purified using column chromatography (SiO_2; pentane) to afford the product as a colorless oil (2.00 g, 6.55 mmol, 51%).

^{1}**H-NMR** (400 MHz, $CDCl_3$): δ 7.69-7.65 (m, 1H), 7.60-7.57 (m, 2H), 7.42-7.39 (m, 2H), 7.38-7.31 (m, 2H), 7.20 (ddd, J = 8.0, 6.9, 2.2 Hz, 1H), 0.31 (s, 9H) ppm.

TMS-biph-MC

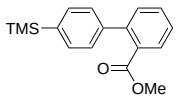

TMS-biph-Br (1.50 g, 4.91 mmol) was dissolved in anhydrous THF (15 mL) under a nitrogen atmosphere and cooled to –78 °C. *n*-BuLi (2.00 mL, 2.5 M in hexane, 5.00 mmol) was added dropwise and stirred for 10 min. Dimethylcarbonate (0.84 mL, 9.82 mmol) was added dropwise and the reaction slowly warmed to -40 °C. The reaction was stirred at that temperature for 2 h and warmed to r.t. overnight. Sat. aq. NH_4Cl solution was added to the reaction mixture, the product extracted into CH_2Cl_2. The combined organic phases were dried over Na_2SO_4 and the solvents removed under reduced pressure. Column chromatography (SiO_2; pentane:EtOAc, 20:1 to 15:1) yielded the product as a colorless oil (700 mg, 2.46 mmol, 50%).

^{1}**H-NMR** (400 MHz, $CDCl_3$): δ 7.82 (ddd, J = 7.8, 1.4, 0.5 Hz, 1H), 7.57-7.53 (m, 2H), 7.52 (dd, J = 7.6, 1.4 Hz, 1H), 7.41 (ddd, J = 7.6, 1.3 Hz, 1H), 7.38 (ddd, J = 7.5, 1.4, 0.6 Hz, 1H), 7.33-7.29 (m, 2H), 3.65 (s, 3H), 0.30 (s, 9H) ppm.

bis-TMS-biph-CO

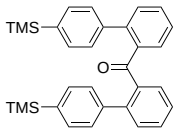

TMS-biph-Br (780 g, 2.55 mmol) was dissolved in anhydrous THF (15 mL) under a nitrogen atmosphere and cooled to –78 °C. *n*-BuLi (1.03 mL, 2.5 M in hexane, 2.58 mmol) was added dropwise and stirred for 10 min A solution of **TMS-biph-MC** (700 mg, 2.46 mmol) in anhydrous THF (10 mL) was added dropwise and the reaction slowly warmed to -40 °C. The reaction was stirred at that temperature for 2 h and warmed to

r.t. overnight. sat. aq. NH_4Cl solution was added and the aqueous phase extracted with CH_2Cl_2. The combined organic phases were dried over Na_2SO_4 and the solvents removed under reduced pressure. Column chromatography (SiO_2; pentane:EtOAc, 20:1 to 15:1) yielded the product as a colorless oil (810 mg, 1.69 mmol, 69%).

^{1}**H-NMR** (400 MHz, CD_2Cl_2): δ 7.42 (ddd, J = 7.7, 1.4, 0.5 Hz, 2H), 7.39-7.31 (m, 6H), 7.21 (dt, J = 7.6, 1.3 Hz, 2H), 7.16 (ddd, J = 7.5, 1.3, 0.5 Hz, 2H), 7.12-7.04 (m, 4H) 0.24 (s, 18H) ppm.

bis-Br-biph-CO

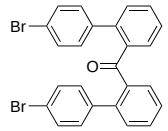

bis-Br-biph-CO was synthesized by a adapting a literature procedure.[39]
bis-TMS-biph-CO (810 mg, 1.69 mmol) and NaOAc (278 mg, 3.39 mmol) were suspended in anhydrous THF (20 mL) under a nitrogen atmosphere and cooled to 0 °C. Bromine (0.37 mL, 7.09 mmol) was added dropwise and the reaction stirred for 2 h. NEt_3 (1.50 mL) and sat. aq. Na_2CO_3 solution were added and the mixture diluted with water. After extraction into Et_2O, the combined organic phases were washed with sat. aq. $Na_2S_2O_3$ solution, dried over Na_2SO_4 and the solvents removed under reduced pressure. Column chromatography (SiO_2; pentane:EtOAc:CH_2Cl_2 15:1:1) yielded the product as a white solid (704 mg, 1.43 mmol, 85%).

^{1}**H-NMR** (400 MHz, $CDCl_3$): δ 7.44-7.38 (m, 4H), 7.35-7.30 (m, 4H), 7.28 (dd, J = 7.6, 1.3 Hz, 2H), 7.14 (ddd, J = 7.6, 1.3, 0.6 Hz, 2H), 6.99-6.94 (m, 4H) ppm.

Br-spiro(A)-Br

Br-spiro(A)-Br was synthesized from two different substrates:
1. **Br-spiro(A)-Br** was synthesized by a adapting a literature procedure.[38]

spiro-Fl (859 mg, 2.72 mmol) was dissolved in $CHCl_3$ (10 mL) and cooled to 0 °C. $FeCl_3$ (1.30 mg, 8.01 µmol) was added and, under exclusion of light, a solution of bromine (0.29 mL, 5.74 mmol) in $CHCl_3$ (2 mL) was added dropwise over 45 min. The reaction was warmed to r.t. overnight and quenched by addition of sat. aq. $Na_2S_2O_3$ solution. The phases were separated, the organic phase dried over Na_2SO_4 and the solvent removed under reduced pressure. The resulting solid was recrystallized three times from cyclohexane to afford the product as a white solid (678 mg, 1.43 mmol, 53%).
2. **Br-spiro(A)-Br** was synthesized by adapting a literature procedure.[39]
bis-Br-biph-CO (532 mg, 1.08 mmol) was heated in methanesulfonic acid (20 mL) at 120 °C overnight. After cooling to r.t., the precipitate was filtered and washed with water. It was redissolved in CH_2Cl_2, dried over Na_2SO_4 and the solvent removed under reduced pressure to obtain the pure product as a white solid (320 mg, 0.67 mmol, 62%).

^{1}**H-NMR** (400 MHz, $CDCl_3$): δ 7.81 (dt, J = 7.6, 0.9 Hz, 2H), 7.70 (dd, J = 8.1, 0.5 Hz, 2H), 7.51 (dd, J = 8.1, 1.8 Hz, 2H), 7.39 (dt, J = 7.5, 1.1 Hz, 2H), 7.15 (dt, J = 7.5, 1.1 Hz, 2H), 6.84 (dd, J = 1.9, 0.5 Hz, 2H), 6.71 (dt, J = 7.6, 0.9 Hz, 1H) ppm.

Br-spiro(L)-Br

Br-spiro(L)-Br was synthesized by adapting a literature procedure.[38]
Under a nitrogen atmosphere, magnesium tunings (190 mg, 7.92 mmol) were activated by stirring with an iodine crystal. A solution of **biph-Br** (1.75 g, 7.49 mmol) in anhydrous Et_2O (15 mL) was added slowly while heating at 35 °C. After heating at reflux for 2 h, a solution of **Br-FlO-Br** (2.78 g, 8.22 mmol) in anhydrous THF (35 mL) was added dropwise and the resulting mixture heated at reflux overnight. After cooling to r.t., EtOH (5 mL) was added and the solvents removed under reduced pressure. The solid material was added to an ice-cold sat. aq. NH_4Cl solution and stirred for 2 h. The precipitate was filtered and washed with H_2O. The solid material was transferred to a flask and dissolved in a minimum volume of refluxing acetic acid. Aqueous HCl solution (4 mL, 38%) was added to the solution and stirred for an additional 10 minutes. After cooling to r.t., the precipitate was filtered and washed with H_2O. The pure product was obtained by recrystallization from EtOH as an off-white solid (2.02 g, 4.26 mmol, 57%).

^{1}**H-NMR** (400 MHz, $CDCl_3$): δ 7.85 (ddd, J = 7.6, 1.1, 0.8 Hz, 2H), 7.67 (dd, J = 8.1,

0.5 Hz, 2H), 7.49 (dd, J = 8.1, 1.8 Hz, 2H), 7.41 (td, J = 7.5, 1.1 Hz, 2H), 7.15 (dd, J = 7.5, 1.1 Hz, 2H), 6.84 (dd, J = 1.8, 0.5 Hz, 2H), 6.72 (dt, J = 7.6, 0.8 Hz, 2H) ppm.

Br-Fl-Br

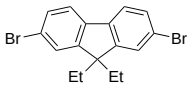

Br-Fl-Br was synthesized by adapting a literature procedure.[96]
Br-FlH-Br (1.62 g, 5.00 mmol), bromoethane (1.36 g, 12.5 mmol) and KI (0.11 g, 0.60 mmol) were suspended in DMSO (15 mL). KOH (1.26 g, 22.5 mmol) was added portionwise, while vigorously stirring the reaction mixture. After stirring for 2 h, the reaction mixture was diluted with DMSO (5 mL) and stirring was continued overnight. The mixture was poured into ice water and the product extracted into CH_2Cl_2. The combined organic phases were washed three times with H_2O, dried over Na_2SO_4 and the solvent removed under reduced pressure. Column chromatography (SiO_2; pure pentane) afforded the product as a white solid (1.29 g, 3.39 mmol, 68%).

^{1}**H-NMR** (400 MHz, $CDCl_3$): δ 7.53 (dd, J = 8.0, 0.7 Hz, 2H), 7.48-7.43 (m, 4H), 1.99 (q, J = 7.4 Hz, 4H), 0.32 (t, J = 7.4 Hz, 6H) ppm.

TMS-Fl-B(OH)$_2$

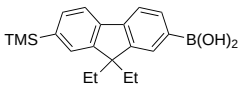

Br-Fl-Br (2.50 g, 6.57 mmol) was dissoved in anhydrous THF (30 mL) under a nitrogen atmosphere. At −78 °C, *n*-BuLi (2.70 mL, 2.50 M in hexane, 6.75 mmol) was added dropwise. After stirring for 20 min, Me_3SiCl (0.87 mL, 6.85 mmol) was added dropwise. The mixture was allowed to warm to room temperature. After stirring for an additional 1 h, the mixture was cooled to −78 °C again, and *n*-BuLi (2.70 mL, 2.50 M in hexane, 6.75 mmol) was added dropwise. After stirring for 20 min, B(O*i*-Pr)$_3$ (4.66 mL, 20.2 mmol) was added dropwise. After warming to r.t. overnight, the reaction was quenched by addition of water. The product was extracted into CH_2Cl_2 and the combined organic phases were dried over Na_2SO_4. After removal of solvents, the residue was purified using column chromatography (SiO_2; pentane:EtOAc, 7:3) affording the

product as a white solid (1.29 g, 3.81 mmol, 58%).

^{1}**H-NMR** (400 MHz, $CDCl_3$): δ 8.32 (dd, J = 7.5, 1.0 Hz, 1H), 8.26-8.21 (m, 1H), 7.91 (dd, J = 7.6, 0.7 Hz, 1H), 7.81 (dd, J = 7.4, 0.8 Hz, 1H), 7.59-7.51 (m, 2H), 2.28 (m, 4H), 0.38 (m, 16H) ppm.

TAA-H

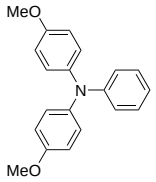

TAA-H was synthesized by a adapting a literature procedure.[74]
Bis(4-methoxyphenyl)amine (1.00 g, 4.36 mmol), NaO*t*Bu (6.28 g, 65.4 mmol) and [Pd(dba)$_2$] (100 mg, 172 µmol, 4 mol%) were suspended in anhydrous toluene (24 mL) under a nitrogen atmosphere. Bromobenzene (0.46 mL, 4.36 mmol) was added and the mixture deaerated for 15 min. [HP(*t*Bu)$_3$]BF_4 (50.0 mg, 172 µmol) was added and the reaction stirred at 85 °C overnight. Water was added and the mixture extracted with CH_2Cl_2. The combined organic phases were dried over Na_2SO_4 and the solvents removed under reduced pressure. The crude product was purified using column chromatography (SiO_2; pentane:CH_2Cl_2 1:1) to afford the product as a colorless solid (0.99 g, 3.24 mmol, 74%).

^{1}**H-NMR** (400 MHz, acetone-d_6): δ 7.20-7.14 (m, 2H), 7.04-6.99 (m, 4H), 6.94-6.81 (m, 7H), 3.78 (s, 6H) ppm.

TAA-I

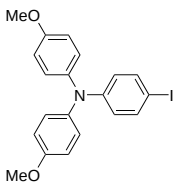

TAA-I was synthesized by adapting a literature procedure.[74]
Iodine (0.50 g, 1.97 mmol) and bis(trifluoroacetoxy)iodobenzene (0.84 g, 1.97 mmol)

were dissolved in anhydrous CH_2Cl_2 (20 mL) under exclusion of light, and stirred for 1 h. A solution of **TAA-H** (0.99 g, 3.24 mmol) in anhydrous CH_2Cl_2 (30 mL) was added and the reaction heated at reflux for 1 h. After cooling to r.t., additional iodine (0.50 g, 1.97 mmol) and bis(trifluoroacetoxy)iodobenzene (0.84 g, 1.97 mmol) was added and the reaction heated at reflux for another 1 h. After quenching with sat. aq. $Na_2S_2O_3$ solution, it was extracted with CH_2Cl_2. The combined organic phases were dried over Na_2SO_4 and the solvents removed under reduced pressure. The crude product was purified using column chromatography (SiO_2; pentane:CH_2Cl_2 1:1) to afford the product as off-white solid (1.16 g, 2.69 mmol, 83%).

^{1}**H-NMR** (400 MHz, acetone-d_6): δ 7.50-7.43 (m, 2H), 7.09-7.04 (m, 4H), 6.95-6.89 (m, 4H), 6.66-6.59 (m, 2H), 3.79 (s, 6H) ppm.

TAA-Fl-TMS

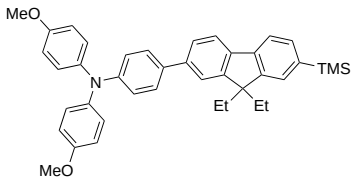

TAA-Fl-TMS was synthesized using method A, with **TAA-I** (1.00 g, 2.32 mmol) as aryl halide and **TMS-Fl-B(OH)$_2$** (0.81 g, 2.40 mmol) as boronic acid. The crude product was purified using column chromatography (SiO_2; pentane:CH_2Cl_2 1:1) to afford the product as a yellow oil (1.32 g, 2.21 mmol, 95%).

^{1}**H-NMR** (400 MHz, acetone-d_6): δ 7.83 (dd, J = 7.9, 0.6 Hz, 1H), 7.79 (dd, J = 7.4, 0.8 Hz, 1H), 7.68 (dd, J = 1.7, 0.6 Hz, 1H), 7.63-7.56 (m, 4H), 7.54 (dd, J = 7.5, 1.0 Hz, 1H), 7.12-7.06 (m, 4H), 6.98-6.90 (m, 6H), 3.80 (s, 6H), 2.14 (m, 4H), 0.32 (m, 14H).
^{13}**C-NMR** (101 MHz, acetone-d_6): δ 206.3, 157.4, 151.7, 150.1, 149.4, 143.1, 141.8, 141.1, 141.0, 139.7, 134.2, 133.1, 128.5, 127.7, 126.2, 121.7, 121.1, 120.0, 115.8, 57.1, 55.9, 33.4, 9.1, -0.6 ppm.

TAA-Fl-I

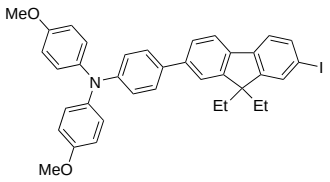

TAA-Fl-I was synthesized using method B, with **TAA-Fl-TMS** (1.20 g, 2.01 mmol) as substrate. The crude product was purified using column chromatography (SiO_2; pentane:CH_2Cl_2 1:1) to afford the product as a yellow oil (1.30 g, 2.00 mmol, 99%).

^{1}**H-NMR** (400 MHz, acetone-d_6): δ 7.84 (dd, J = 8.0, 0.6 Hz, 1H), 7.82 (dd, J = 1.7, 0.5 Hz, 1H), 7.72 (dd, J = 8.0, 1.6 Hz, 1H), 7.68 (dd, J = 1.7, 0.7 Hz, 1H), 7.65-7.55 (m, 4H), 7.13-7.04 (m, 4H), 6.99-6.88 (m, 6H), 3.80 (s, 6H), 2.21-2.07 (m, 4H), 0.32 (t, J = 7.3 Hz, 6H).
^{13}**C-NMR** (101 MHz, acetone-d_6): δ 157.4, 153.7, 151.0, 149.5, 142.3, 141.8, 141.5, 137.1, 133.9, 133.2, 128.5, 127.7, 126.4, 122.6, 121.6, 121.4, 121.3, 115.8, 92.8, 57.5, 55.9, 33.3, 8.99 ppm.
MS (ESI): m/z (%) = 651.2 (100, $[M]^+$), calcd for $C_{37}H_{34}NO_2I$ 651.2.

TAA-Fl-BA

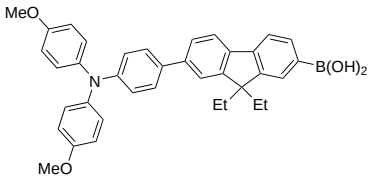

TAA-Fl-I (1.30 g, 2.00 mmol) was dissolved in anhydrous THF (20 mL) and cooled to −78 °C. *n*-BuLi (0.80 mL, 2.5 M in hexane) was added dropwise and the mixture stirred for 20 min. B(O*i*-Pr)$_3$ (1.40 mL, 9.13 mmol) was added dropwise and the reaction was allowed to warm to r.t. overnight. The reaction was quenched with H_2O and the product extracted into CH_2Cl_2. The combined organic phases were dried over Na_2SO_4 and the solvents were removed under reduced pressure. The crude product was purified using column chromatography (SiO_2; pentane:EtOAc 7:3 to 1:2) to afford the product as a yellow glass (214 mg, 0.38 mmol, 19%).

^{1}H-NMR (400 MHz, acetone-d_6): δ 7.81-7.78 (m, 1H), 7.75 (dd, J = 7.6, 1.1 Hz, 1H), 7.69 (dd, J = 7.9, 0.6 Hz, 1H), 7.63 (dd, J = 7.7, 0.7 Hz, 1H), 7.53 (dd, J = 1.8, 0.7 Hz, 1H), 7.49-7.42 (m, 3H), 6.96-6.89 (m, 4H), 6.84-6.73 (m, 6H), 3.65 (s, 6H), 2.05-1.94 (m, 4H), 0.16 (t, J = 7.3 Hz, 6H) ppm.
^{13}C-NMR (101 MHz, acetone-d_6): δ 171.3, 157.2, 151.9, 149.7, 149.22, 144.3, 141.0, 140.9, 134.1, 134.0, 129.4, 128.3, 127.5, 126.0, 121.5, 121.3, 121.1, 119.6, 115.7, 56.8, 55.8, 33.4, 29.8, 8.9 ppm.
MS (ESI): m/z (%) = 569.2 (100, $[M]^+$), calcd for $C_{43}H_{46}NO_4B$ 569.3.

TAA-Fl-BE

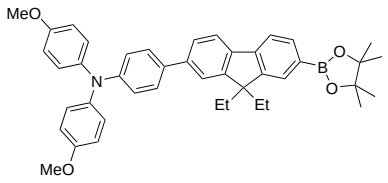

TAA-Fl-BE was synthesized using method C, with **TAA-Fl-I** (753 mg, 1.16 mmol) as aryl halide.
The product was obtained after column chromatography (SiO_2; pentane:EtOAc 6:1) as a yellow glass (622 mg, 0.30 mmol, 82%).
^{1}H-NMR (400 MHz, acetone-d_6): δ 7.87 (dd, J = 7.9,0.6 Hz, 1H), 7.83-7.75 (m, 3H), 7.72-7.69 (m, 1H), 7.66-7.57 (m, 3H), 7.15-7.05 (m, 4H), 7.02-6.87 (m, 6H), 3.80 (s, 6H), 2.23-2.08 (m, 4H), 1.36 (s, 12H), 0.30 (t, J = 7.3 Hz, 6H) ppm.

bpy-Br

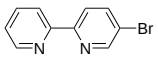

bpy-Br was synthesized by a adapting a literature procedure.[97]
A solution of 2-pyridylzinc bromide in THF (15 mL, 0.5 M, 7.50 mmol) was added to 2-iodo-5-bromopyridine (1.70 g, 6.00 mmol) and $[Pd(PPh_3)_4]$ (75.0 mg, 60.0 µmol, 1 mol%) under a nitrogen atmosphere. The reaction was stirred at r.t. overnight. After quenching the reaction by adding sat. aq. NH_4Cl solution, the mixture was extracted with CH_2Cl_2 and the combined organic phases washed with 0.1 M EDTA solution, dried over Na_2SO_4 and the solvents removed under reduced pressure. The crude product was purified using column chromatography (SiO_2; pentane:EtOAc 4:1 + 2% NEt_3)

to afford the product as an off-white solid (1.17 g, 4.97 mmol, 83%).

^{1}H-NMR (400 MHz, $CDCl_3$): δ 8.73 (dd, J = 2.4, 0.7 Hz, 1H), 8.68 (ddd, J = 4.9, 1.8, 0.9 Hz, 1H), 8.38 (dt, J = 8.1, 1.1 Hz, 1H), 8.34 (dd, J = 8.6, 0.8 Hz, 1H), 7.95 (dd, J = 8.5, 2.4 Hz, 1H), 7.83 (td, J = 7.8, 1.8 Hz, 1H), 7.34 (ddd, J = 7.5, 4.8, 1.2 Hz, 1H) ppm.

bpy-Fl-TMS

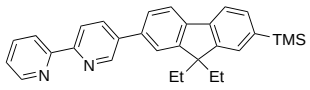

bpy-Fl-TMS was synthesized using method A, with **bpy-Br** (87 mg, 0.37 mmol) as aryl halide and **TMS-Fl-B(OH)$_2$** (130 mg, 0.38 mmol) as boronic acid. The crude product was purified using column chromatography (SiO_2; pentane:EtOAc 4:1 + 2% NEt_3) to afford the product as a light yellow solid (161 mg, 0.36 mmol, 97%).

^{1}H-NMR (400 MHz, CD_2Cl_2): δ 9.00 (dd, J = 2.4, 0.9 Hz, 1H), 8.69 (ddd, J = 4.8, 1.8, 0.9 Hz, 1H), 8.56-8.46 (m, 2H), 8.12 (dd, J = 8.3, 2.4 Hz, 1H), 7.89-7.81 (m, 2H), 7.76 (dd, J = 7.4, 0.8 Hz, 1H), 7.72-7.65 (m, 2H), 7.58-7.50 (m, 2H), 7.33 (ddd, J = 7.5, 4.8, 1.2 Hz, 1H), 2.11 (q, J = 7.4 Hz, 4H), 0.37 (t, J = 7.3 Hz, 6H), 0.33 (s, 9H) ppm.
^{13}C-NMR (101 MHz, CD_2Cl_2): δ 156.5, 155.3, 151.8, 149.9, 149.8, 148.2, 142.0, 140.3, 137.4(1), 137.3(9), 137.2, 135.5, 132.7, 128.3, 126.5, 124.2, 122.1, 121.4, 121.3, 120.9, 119.7, 56.8, 33.2, 9.0, -0.64 ppm.
MS (ESI): m/z (%) = 449.2 (100, $[M]^+$), calcd for $C_{30}H_{32}N_2Si$ 449.2.

bpy-Fl-I

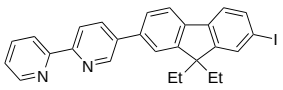

bpy-Fl-I was synthesized using method B, with **bpy-Fl-TMS** (312 mg, 0.70 mmol) as substrate. The crude product was purified using column chromatography (SiO_2; pentane:EtOAc 4:1 + 2% NEt_3) to afford the product as a yellow glass (348 mg, 0.69 mmol, quant.).

^{1}H-NMR (400 MHz, CD_2Cl_2): δ 8.99 (dd, J = 2.4, 0.8 Hz, 1H), 8.69 (ddd, J = 4.8, 1.8, 0.9 Hz, 1H), 8.56-8.46 (m, 2H), 8.11 (dd, J = 8.3, 2.4 Hz, 1H), 7.88-7.81 (m, 2H), 7.76-7.63 (m, 4H), 7.54 (dd, J = 7.9, 0.5 Hz, 1H), 7.33 (ddd, J = 7.5, 4.8, 1.2 Hz, 1H), 2.18-2.01 (m, 4H), 0.36 (t, J = 7.3 Hz, 6H) ppm.
^{13}C-NMR (101 MHz, CD_2Cl_2): δ 156.4, 155.4, 153.3, 151.0, 149.8, 148.1, 141.3, 141.2, 137.7, 137.4, 137.2, 136.6, 135.6, 132.9, 126.7, 124.3, 122.2, 121.0, 121.4, 121.0, 93.4, 57.2, 33.2, 27.5, 8.9 ppm.
MS (ESI): m/z (%) = 503.1 (100, $[M+H]^+$), calcd for $C_{27}H_{24}N_2I$ 503.1.

bpy-Fl-BE

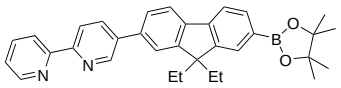

bpy-Fl-BE was synthesized using method C, with **bpy-Fl-I** (252 mg, 0.50 mmol) as aryl halide.
The product was obtained after column chromatography (SiO_2; pentane:EtOAc 4:1 + 2% NEt_3) as a yellow glassy gum (151 mg, 0.30 mmol, 60%).

^{1}H-NMR (400 MHz, CD_2Cl_2): δ 9.00 (dd, J = 2.4, 0.8 Hz, 1H), 8.68 (ddd, J = 4.8, 1.8, 0.9 Hz, 1H), 8.56-8.45 (m, 2H), 8.12 (dd, J = 8.3, 2.4 Hz, 1H), 7.91-7.81 (m, 2H), 7.81-7.76 (m, 3H), 7.73-7.64 (m, 2H), 7.33 (ddd, J = 7.5, 4.8, 1.2 Hz, 1H), 2.14 (q, J = 7.4 Hz, 4H), 1.37 (s, 12H), 0.34 (t, J = 7.3 Hz, 6H) ppm.
^{13}C-NMR (101 MHz, CD_2Cl_2): δ 156.5, 155.3, 152.1, 149.9, 149.8, 148.2, 144.4, 142.1, 137.6, 137.4, 137.3, 135.6, 134.3, 129.5, 126.5, 124.2, 122.1, 121.4, 121.3, 121.2, 119.8, 84.4, 56.9, 33.2, 25.3, 8.9 ppm.
MS (ESI): m/z (%) = 503.21 (100, $[M]^+$), calcd for $C_{33}H_{35}N_2O_2B$ 503.29.

Br-spiro(A)-Fl-TAA

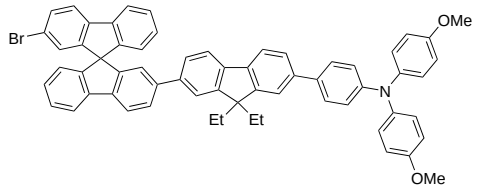

Br-spiro(A)-Fl-TAA was synthesized using method A, with **Br-spiro(A)-Br** (95 mg, 0.20 mmol) as aryl halide and **TAA-Fl-BA** (100 mg, 0.18 mmol) as boronic acid. The crude product was purified using column chromatography (SiO_2; pentane:CH_2Cl_2 1:1) to afford the product as yellowish glass (110 mg, 0.12 mmol, 67%).

^{1}**H-NMR** (400 MHz, acetone-d_6): δ 8.09 (dd, J = 8.0, 0.6 Hz, 1H), 8.01 (tt, J = 7.7, 0.9 Hz, 2H), 7.94 (d, J = 8.2 Hz, 1H), 7.83 (dd, J = 8.0, 1.7 Hz, 1H), 7.75 (dd, J = 7.9, 0.6 Hz, 1H), 7.74-7.68 (m, 1H), 7.63 (dd, J = 1.7, 0.7 Hz, 1H), 7.59-7.52 (m, 5H), 7.46-7.37 (m, 3H), 7.20-7.12 (m, 3H), 7.09-7.02 (m, 4H), 6.95-6.86 (m, 7H), 6.74 (dt, J = 7.6, 0.9 Hz, 1H), 6.67 (dt, J = 7.6, 0.9 Hz, 1H), 3.77 (s, 6H), 0.24 (t, J = 7.3 Hz, 6H) ppm. The CH_2-group signals could not be resolved due to an overlap with the acetone solvent signals.
^{13}**C-NMR** (101 MHz, acetone-d_6): δ 157.3, 152.1, 151.7(1), 151.7(0), 149.7, 149.5, 149.4, 149.3, 142.4(3), 142.4(0), 142.1(4), 142.1(0), 141.9, 141.8, 141.7, 140.8, 140.7, 140.4, 134.0, 132.1, 129.5, 129.3, 129.2, 129.1, 128.4(4), 128.4(0), 127.8, 127.6, 127.0, 126.2, 124.9, 124.6, 123.2, 123.0, 122.0(3), 122.0(0), 121.9, 121.6, 121.5(1), 121.5(0), 121.1, 115.8, 67.0, 57.2, 55.9, 33.4, 9.1 ppm.
MS (ESI): m/z (%) = 917.3 (100, $[M]^+$), calcd for $C_{62}H_{48}NO_2Br$ 917.3.

bpy-Fl-spiro(A)-Fl-TAA

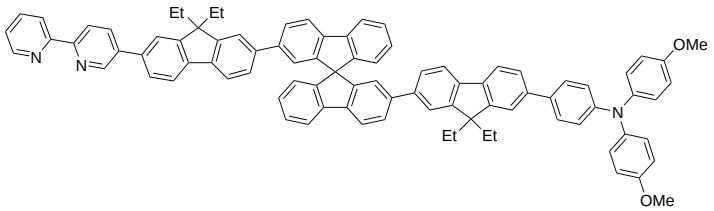

bpy-Fl-spiro(A)-Fl-TAA was synthesized using method A, with **Br-spiro(A)-Fl-TAA** (60 mg, 0.12 mmol) as aryl halide and **bpy-Fl-BE** (100 mg, 0.11 mmol) as boronic ester. The crude product was purified using column chromatography (SiO_2; pentane:EtOAc 2:1 + 2% NEt_3) to afford the product as a yellow solid (95 mg, 78 µmol, 72%).

^{1}**H-NMR** (400 MHz, CD_2Cl_2): δ 8.99 (dd, J = 2.4, 0.9 Hz, 1H), 8.69 (ddd, J = 4.8, 1.8, 0.9 Hz, 1H), 8.55-8.48 (m, 2H), 8.11 (dd, J = 8.3, 2.4 Hz, 1H), 8.03 (ddd, J = 8.0, 2.4, 0.6 Hz, 2H), 7.96 (dq, J = 7.7, 0.9 Hz, 2H), 7.83-7.77 (m, 3H), 7.77-7.63 (m, 6H), 7.57-7.40 (m, 10H), 7.32 (ddd, J = 7.5, 4.8, 1.2 Hz, 1H), 7.20-7.13 (m, 4H), 7.12-7.06 (m, 4H), 7.03-6.96 (m, 2H), 6.90-6.83 (m, 4H), 6.79 (dt, J = 7.6, 0.9 Hz, 2H),

3.79 (s, 6H), 2.13-2.02 (m, 8H), 0.36-0.27 (m, 12H) ppm.

AC1

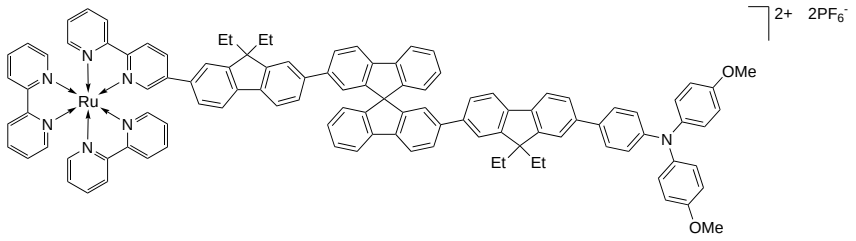

bpy-Fl-spiro(A)-Fl-TAA (23.2 mg, 45 µmol) and $[Ru(bpy)_2Cl_2] \cdot 2H_2O$ (64 mg, 52.7 µmol) were suspended in ethylene glycol (4 mL) under a nitrogen atmosphere. The mixture was heated at 120 °C for 4 h. After cooling down to 70 °C, acetone (4 mL) was added and stirring was continued at that temperature for 12 h. CH_2Cl_2 (3 mL) was added and the reaction was stirred for additional 4 h at 65 °C. The reaction mixture was cooled to r.t. and subjected to column chromatography, starting with acetone as eluent until non-reacted ligand was removed from the column. Afterwards, the eluent was changed to acetone:H_2O 10:1 to remove the precursor complex, and finally to acetone:H_2O 10:1 + 1% sat. KNO_3 solution to elute the desired complex. The organic solvents were removed under reduced pressure and the complex precipitated by addition of a sat. aq. KPF_6 solution. The complex was extracted into CH_2Cl_2. The organic phase was dried over Na_2SO_4 and the solvent removed under reduced pressure to obtain the product as a red solid (77 mg, 37 µmol, 83%).

^{1}**H-NMR** (400 MHz, MeCN-d_3): δ 8.55-8.45 (m, 6H), 8.34 (dd, J = 8.6, 2.1 Hz, 1H), 8.11-8.00 (m, 9H), 7.88-7.81 (m, 4H), 7.80-7.70 (m, 8H), 7.58-7.37 (m, 16H), 7.25-7.15 (m, 3H), 7.10-7.04 (m, 6H), 6.93-6.86 (m, 6H), 6.70 (ddt, J = 7.7, 3.8, 0.9 Hz, 2H), 3.77 (s, 6H), 0.19 (td, J = 7.3, 1.1 Hz, 6H), 0.12 (t, J = 7.3 Hz, 6H) ppm. The CH_2-group signals could not be resolved due to an overlap with the acetonitrile solvent signal.
HR-MS (ESI TOF): m/z (%) = 813.7993 (100, $[M\text{-}2\,PF_6^-]^2+$), calcd for $C_{109}H_{87}N_7O_2Ru^{2+}$ 813.7979.
EA (%): calcd for $C_{109}H_{87}N_7O_2F_{12}P_2Ru \cdot 1.5\ H_2O \cdot 3\ C_3H_6O$ C, 66.88; H, 5.14; N, 4.63; found: C, 66.98; H, 5.48; N, 4.66.

Br-spiro(L)-Fl-TAA

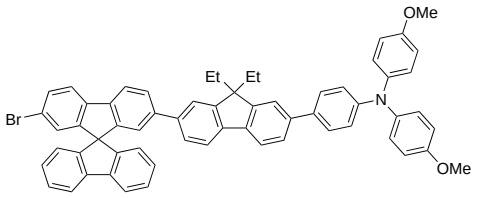

Br-spiro(L)-Fl-TAA was synthesized using method A, with **Br-spiro(L)-Br** (132 mg, 0.23 mmol) as aryl halide and **TAA-Fl-BA** (130 mg, 0.27 mmol) as boronic acid. The crude product was purified using column chromatography (SiO_2; pentane:CH_2Cl_2 10:1 to 4:1) to afford the product as a light yellow solid (104 mg, 0.11 mmol, 49%).

^{1}**H-NMR** (400 MHz, CD_2Cl_2): δ 7.95 (dd, J = 8.0, 0.6 Hz, 1H), 7.91 (dt, J = 7.6, 1.0 Hz, 2H), 7.78 (dd, J = 8.1, 0.5 Hz, 1H), 7.74 (dd, J = 8.0, 1.7 Hz, 1H), 7.69 (dd, J = 7.9, 0.6 Hz, 1H), 7.64 (dd, J = 7.9, 0.7 Hz, 1H), 7.55-7.46 (m, 5H), 7.45-7.36 (m, 4H), 7.17 (dt, J = 7.5, 1.1 Hz, 2H), 7.10-7.04 (m, 4H), 7.02 (dd, J = 1.7, 0.6 Hz, 1H), 7.00-6.94 (m, 2H), 6.87-6.76 (m, 7H), 3.79 (s, 6H), 2.09-1.98 (m, 4H), 0.28 (t, J = 7.3 Hz, 6H) ppm. **MS (ESI)**: m/z (%) = 917.10 (100, $[M]^+$), calcd for $C_{62}H_{48}NO_2Br$ 917.29.

bpy-Fl-spiro(L)-Fl-TAA

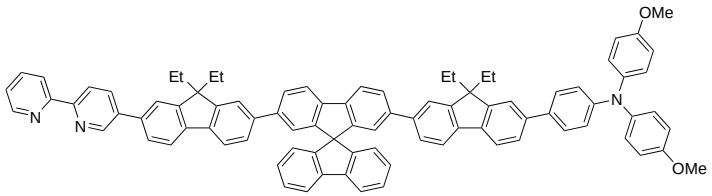

bpy-Fl-spiro(L)-Fl-TAA was synthesized using method A, with **Br-spiro(L)-Fl-TAA** (104 mg, 0.11 mmol) as aryl halide and **bpy-Fl-BE** (68 mg, 0.14 mmol) as boronic ester. The crude product was purified using column chromatography (SiO_2; pentane:EtOAc 2:1 + 2% NEt_3 to 3:2 + 2% NEt_3) to afford the product as a yellow solid (132 mg, 0.11 mmol, 96%).

^{1}**H-NMR** (400 MHz, CD_2Cl_2): δ 9.00 (dd, J = 2.4, 0.9 Hz, 1H), 8.69 (ddd, J = 4.8, 1.9, 1.0 Hz, 1H), 8.53 (dd, J = 8.3, 0.8 Hz, 1H), 8.50 (dt, J = 8.0, 1.1 Hz, 1H), 8.12

(dd, J = 8.3, 2.4 Hz, 1H), 8.03 (ddd, J = 8.1, 1.9, 0.6 Hz, 2H), 7.96 (dt, J = 7.6, 0.9 Hz, 2H), 7.88-7.75 (m, 4H), 7.74-7.63 (m, 5H), 7.57-7.39 (m, 10H), 7.33 (ddd, J = 7.4, 4.8, 1.2 Hz, 1H), 7.19 (dt, J = 7.5, 1.1 Hz, 2H), 7.12-7.03 (m, 6H), 7.02-6.96 (m, 2H), 6.90-6.83 (m, 6H), 3.79 (s, 6H), 2.14-2.03 (m, 8H), 0.32 (dt, J = 10.5, 7.3 Hz, 12H) ppm.
MS (ESI): m/z (%) = 1214.40 (100, $[M+H]^+$), calcd for $C_{89}H_{72}N_3O_2$ 1214.56.

LC1

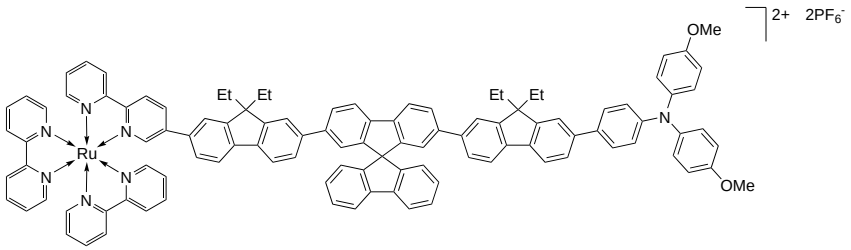

bpy-Fl-spiro(L)-Fl-TAA (24.1 mg, 46.4 µmol) and $[Ru(bpy)_2Cl_2] \cdot 2H_2O$ (62 mg, 51.0 µmol) were suspended in ethylene glycol (4 mL) under a nitrogen atmosphere. The mixture was heated at 120 °C for 4 h. After cooling to 70 °C, acetone (4 mL) was added and stirring was continued at that temperature for 12 h. CH_2Cl_2 (2 mL) was added and the reaction was stirred overnight at 65 °C. The reaction mixture was cooled to r.t. and subjected to column chromatography, starting with acetone as eluent until non-reacted ligand was removed from the column. Afterwards, the eluent was changed to acetone:H_2O 10:1 to remove the precursor complex, and finally to acetone:H_2O 10:1 + 1% sat. KNO_3 solution to elute the desired complex. The organic solvents were removed under reduced pressure and the complex precipitated by addition of a sat. aq. KPF_6 solution. The complex was extracted into CH_2Cl_2. The organic phase was dried over Na_2SO_4 and the solvent removed under reduced pressure to obtain the product as a red solid (87 mg, 45.4 µmol, 98%).

^{1}**H-NMR** (400 MHz, MeCN-d_3): δ 8.56-8.46 (m, 6H), 8.35 (dd, J = 8.6, 2.1 Hz, 1H), 8.12-7.99 (m, 9H), 7.90-7.70 (m, 12H), 7.60-7.37 (m, 16H), 7.25 (d, J = 1.4 Hz, 1H), 7.20 (dt, J = 7.5, 1.1 Hz, 2H), 7.10-7.04 (m, 4H), 7.01-6.98 (m, 2H), 6.94-6.86 (m, 6H), 6.78 (dt, J = 7.6, 0.9 Hz, 2H), 3.78 (s, 6H), 0.21 (t, J = 7.3, 6H), 0.14 (t, J = 7.3 Hz, 6H) ppm. The CH_2-group signals could not be resolved due to an overlap with the acetonitrile solvent signal.
HR-MS (ESI TOF): m/z (%) = 813.7991 (100, $[M\text{-}2\,PF_6^-]^{2+}$), calcd for $C_{109}H_{87}N_7O_2Ru^{2+}$

813.7979.
EA (%): calcd for $C_{109}H_{87}N_7O_2F_{12}P_2Ru \cdot 2\ H_2O \cdot 2\ C_3H_6O$ C, 66.72; H, 5.02; N, 4.74; found: C, 66.74; H, 5.36; N, 4.93.

TMS-Fl-spiro(L)-Fl-TMS

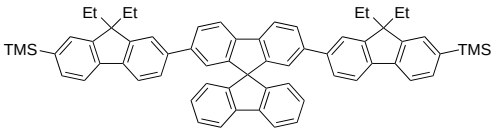

TMS-Fl-spiro(L)-Fl-TMS was synthesized using method A, with **Br-spiro(L)-Br** as aryl halide (292 mg, 0.61 mmol) and **TMS-Fl-B(OH)$_2$** (412 mg, 1.35 mmol) as boronic acid. The crude product was purified using column chromatography (SiO_2; pentane:CH_2Cl_2 5:1) to afford the product as a white solid (458 mg, 0.51 mmol, 83%).

^{1}**H-NMR** (400 MHz, CD_2Cl_2): δ 8.00 (dd, J = 8.0, 0.7 Hz, 2H), 7.94 (dt, J = 7.7, 0.9 Hz, 2H), 7.74 (dd, J = 8.0, 1.7 Hz, 2H), 7.65 (ddd, J = 7.8, 3.4, 0.7 Hz, 4H), 7.50-7.36 (m, 10H), 7.17 (td, J = 7.5, 1.1 Hz, 2H), 7.00 (dd, J = 1.7, 0.6 Hz, 2H), 6.84 (dt, J = 7.7, 0.9 Hz, 2H), 2.08-1.95 (m, 8H), 0.29 (s, 18H), 0.25 (t, J = 7.3 Hz, 12H) ppm.
^{13}**C-NMR** (101 MHz, CD_2Cl_2): δ 151.3, 150.5, 149.7, 149.3, 142.6, 142.2, 141.9, 141.4, 141.2, 140.5, 139.8, 132.5, 128.5, 128.4, 128.2, 127.7, 126.5, 124.6, 122.8, 121.9, 121.0, 120.8, 120.4, 119.5, 66.8, 56.7, 33.1, 8.9, -0.7 ppm.

I-Fl-spiro(L)-Fl-I

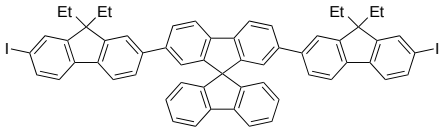

I-Fl-spiro(L)-Fl-I was synthesized using method B, with **TMS-Fl-spiro(L)-Fl-TMS** (351 mg, 0.39 mmol) as aryl halide. The temperature was kept at −78 °C during the reaction. The crude product was purified using column chromatography (SiO_2; pentane:CH_2Cl_2 5:1) to afford the product as a white solid (390 mg, 0.39 mmol, quant.).

^{1}**H-NMR** (400 MHz, CD_2Cl_2): δ 8.00 (dd, J = 7.9, 0.7 Hz, 2H), 7.94 (dt, J = 7.7, 0.9 Hz, 2H), 7.74 (dd, J = 8.0, 1.7 Hz, 2H), 7.69-7.59 (m, 6H), 7.48-7.36 (m, 8H), 7.17 (td,

J = 7.5, 1.1 Hz, 2H), 7.00 (dd, J = 1.7, 0.7 Hz, 2H), 6.84 (dt, J = 7.6, 0.9 Hz, 2H), 1.99 (dq, J = 7.0, 3.5 Hz, 8H), 0.25 (t, J = 7.3 Hz, 12H) ppm.
^{13}**C-NMR** (101 MHz, CD_2Cl_2): δ 153.2, 150.6, 149.2, 142.6, 141.8, 141.4, 141.3, 141.0, 140.4, 136.5, 132.8, 128.5(1), 128.4(7), 127.8, 126.8, 124.6, 122.8, 121.9, 121.8, 121.1, 120.8, 120.5, 93.0, 66.8, 57.1, 33.1, 27.5, 8.8 ppm.

bpy-Fl-Fl-spiro(L)-Fl-I

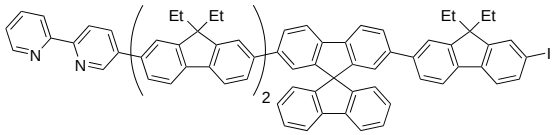

bpy-Fl-Fl-spiro(L)-Fl-I was synthesized using method A, with **I-Fl-spiro(L)-Fl-I** (285 mg, 283 µmol) as aryl halide and **bpy-Fl-BE** (150 mg, 299 µmol) as boronic ester. The crude product was purified using column chromatography (SiO_2; pentane:EtOAc 2:1 + 2% NEt_3) to afford the product as an off-white solid (58 mg, 46 µmol, 16%).

^{1}**H-NMR** (400 MHz, CD_2Cl_2): δ 9.01 (dd, J = 2.5, 0.8 Hz, 1H), 8.70-8.67 (m, 1H), 8.53 (dd, J = 8.2, 0.9 Hz, 1H), 8.51-8.47 (m, 1H), 8.14 (dd, J = 8.3, 2.3 Hz, 1H), 8.02 (dd, J = 8.0, 2.6 Hz, 2H), 7.97-7.93 (m, 2H), 7.90-7.82 (m, 3H), 7.80-7.61 (m, 13H), 7.49-7.38 (m, 7H), 7.34 (ddd, J = 7.4, 4.8, 1.2 Hz, 1H), 7.18 (td, J = 7.5, 1.2 Hz, 2H), 7.04-6.99 (m, 2H), 6.85 (dt, J = 7.6, 0.8 Hz, 2H), 2.26-1.98 (m, 12H), 0.41 (dt, J = 7.3, 3.0 Hz, 6H), 0.32 (t, J = 7.3 Hz, 6H), 0.25 (t, J = 7.3 Hz, 6H) ppm.
MS (ESI): m/z (%) = 1257.22 (100, $[M]^+$), calcd for $C_{86}H_{69}N_2I$ 1257.45.

bpy-Fl-Fl-spiro(L)-Fl-Fl-TAA

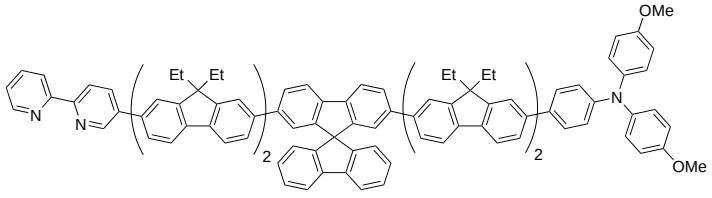

bpy-Fl-Fl-spiro(L)-Fl-Fl-TAA was synthesized using method A, with **bpy-Fl-Fl-spiro(L)-Fl-I** (138 mg, 0.11 mmol) as aryl halide and **TAA-Fl-BE** (107 mg, 0.17 mmol) as boronic ester. The crude product was purified using column chromatography (SiO_2;

pentane:EtOAc 2:1 + 2% NEt_3) to afford the product as a yellow solid (89 mg, 54 μmol, 49%).

^{1}**H-NMR** (400 MHz, CD_2Cl_2): δ 9.01 (dd, J = 2.4, 0.9 Hz, 1H), 8.69 (ddd, J = 4.8, 1.8, 1.0 Hz, 1H), 8.54 (dd, J = 8.3, 0.8 Hz, 1H), 8.49 (dt, J = 8.0, 1.1 Hz, 1H), 8.14 (dd, J = 8.3, 2.4 Hz, 1H), 8.03 (d, J = 8.0 Hz, 2H), 7.96 (dt, J = 7.7, 0.9 Hz, 2H), 7.90-7.83 (m, 3H), 7.81-7.75 (m, 6H), 7.73-7.62 (m, 12H), 7.62-7.41 (m, 10H), 7.34 (ddd, J = 7.5, 4.8, 1.2 Hz, 1H), 7.20 (td, J = 7.5, 1.1 Hz, 2H), 7.11-7.06 (m, 4H), 7.05-7.02 (m, 2H), 7.02-6.97 (m, 2H), 6.90-6.82 (m, 6H), 3.80 (s, 6H), 2.24-2.04 (m, 16H), 0.46-0.28 (m, 24H) ppm.
MS (MALDI): m/z (%) = 1654.542 (84, $[M]^+$), calcd for $C_{123}H_{103}N_3O_2$ 1654.808.

TMS-Fl-spiro(A)-Fl-TMS

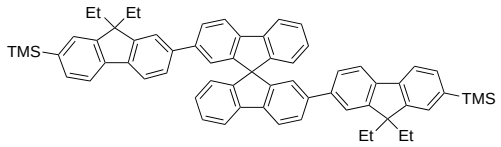

TMS-Fl-spiro(A)-Fl-TMS was synthesized using method A, with **Br-spiro(A)-Br** as aryl halide (500 mg, 1.05 mmol) and **TMS-Fl-BA** (785 mg, 2.32 mmol) as boronic acid. The crude product was purified using column chromatography (SiO_2; pentane:CH_2Cl_2 5:1) to afford the product as a white solid (886 mg, 0.98 mmol, 94%).

^{1}**H-NMR** (400 MHz, CD_2Cl_2): δ 8.01 (dd, J = 7.9, 0.6 Hz, 2H), 7.95 (dt, J = 7.6, 0.9 Hz, 2H), 7.77 (dd, J = 8.0, 1.7 Hz, 2H), 7.66 (dt, J = 7.9, 0.8 Hz, 4H), 7.51-7.40 (m, 10H), 7.16 (dt, J = 7.5, 1.1 Hz, 2H), 7.12 (dd, J = 1.8, 0.6 Hz, 2H), 6.77 (dt, J = 7.6, 0.9 Hz, 2H), 6.76 (dt, J = 7.6, 0.9 Hz, 2H), 2.06-1.98 (m, 8H), 0.30 (s, 18H), 0.26 (dt, J = 7.3, 2.5 Hz, 12H) ppm.
^{13}**C-NMR** (101 MHz, CD_2Cl_2): δ 151.4, 149.9, 149.9, 149.7, 142.2, 142.1, 142.0, 141.8, 141.4, 140.5, 139.8, 132.5, 128.4, 128.2, 127.7, 126.6, 124.4, 123.0, 121.9, 121.1, 120.8, 120.4, 119.5, 66.9, 56.7, 33.1, 8.9, -0.7 ppm.

I-Fl-spiro(A)-Fl-I

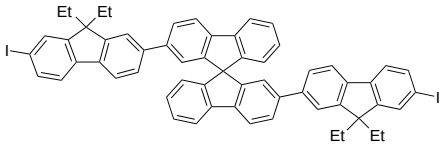

I-Fl-spiro(A)-Fl-I was synthesized using method B, with **TMS-Fl-spiro(A)-Fl-TMS** (510 mg, 566 µmol) as aryl halide. The temperature was kept at −78 °C during the reaction. The crude product was purified using column chromatography (SiO_2; pentane:CH_2Cl_2 5:1) to afford the product as a white solid (408 mg, 405 µmol, 72%).

^{1}**H-NMR** (400 MHz, CD_2Cl_2): δ 8.01 (d, J = 8.0 Hz, 2H), 7.95 (dt, J = 7.7, 0.9 Hz, 2H), 7.76 (dd, J = 8.0, 1.7 Hz, 2H), 7.69-7.59 (m, 6H), 7.47-7.38 (m, 8H), 7.15 (dt, J = 7.5, 1.1 Hz, 2H), 7.12 (d, J = 1.6 Hz, 2H), 2.06-1.90 (m, 8H), 0.24 (td, J = 7.3, 2.1 Hz, 12H) ppm.
^{13}**C-NMR** (101 MHz, CD_2Cl_2): δ 153.1, 150.5, 149.9, 149.8, 142.0, 141.9, 141.8, 141.4, 141.0, 140.4, 136.4, 132.7, 128.5, 128.5, 127.8, 126.8, 124.4, 123.0, 121.9, 121.8, 121.1, 120.8, 120.6, 92.9, 66.8, 57.1, 33.1, 8.8 ppm.

I-Fl-spiro(A)-Fl-Fl-bpy

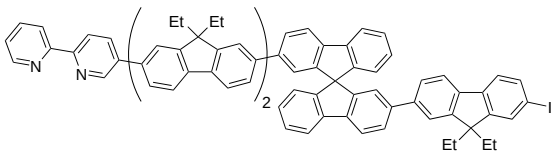

I-Fl-spiro(A)-Fl-Fl-bpy was synthesized using method A, with **I-Fl-spiro(A)-Fl-I** (400 mg, 397 µmol) as aryl halide and **bpy-Fl-BE** (120 mg, 239 µmol) as boronic ester. The crude product was purified using column chromatography (SiO_2; pentane:EtOAc 2:1 + 2% NEt_3) to afford the product as an off-white solid (102 mg, 81 µmol, 20%).

^{1}**H-NMR** (400 MHz, CD_2Cl_2): δ 9.02 (dd, J = 2.4, 0.9 Hz, 1H), 8.69 (ddd, J = 4.8, 1.8, 0.9 Hz, 1H), 8.54 (dd, J = 8.2, 0.9 Hz, 1H), 8.50 (dt, J = 8.0, 1.1 Hz, 1H), 8.14 (dd, J = 8.3, 2.3 Hz, 1H), 8.02 (dd, J = 8.0, 1.9 Hz, 2H), 7.95 (dt, J = 7.7, 1.0 Hz, 2H), 7.89-7.83 (m, 3H), 7.81-7.74 (m, 3H), 7.73-7.62 (m, 10H), 7.51-7.41 (m, 7H), 7.34 (ddd, J = 7.5, 4.8, 1.2 Hz, 1H), 7.20-7.11 (m, 4H), 6.80-6.75 (m, 2H), 2.24-2.05 (m, 8H),

0.43 (t, J = 7.3 Hz, 6H), 0.32 (td, J = 7.3, 2.3 Hz, 6H), 0.25 (td, J = 7.4, 2.2 Hz, 6H) ppm. Only 4 of the 6 CH_2-groups could be resolved, due to overlap with the methyl-group peak of EtOAc at 2.01 ppm.

TAA-Fl-Fl-spiro(A)-Fl-Fl-bpy

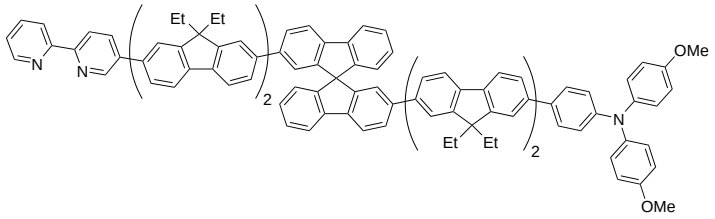

TAA-Fl-Fl-spiro(A)-Fl-Fl-bpy was synthesized using method A, with **I-Fl-spiro(A)-Fl-Fl-bpy** (102 mg, 81 µmol) as aryl halide and **TAA-Fl-BE** (62 mg, 95 µmol) as boronic ester. The crude product was purified using column chromatography (SiO_2; pentane:EtOAc 2:1 + 2% NEt_3) to afford the product as a yellow solid (52.0 mg, 31.4 µmol, 38%).

^{1}**H-NMR** (400 MHz, CD_2Cl_2): δ 9.03 (dd, J = 2.3, 0.8 Hz, 1H), 8.72-8.68 (m, 1H), 8.55 (d, J = 8.3 Hz, 1H), 8.51 (dd, J = 8.0, 1.1 Hz, 1H), 8.14 (dd, J = 8.3, 2.4 Hz, 1H), 8.04 (d, J = 8.0 Hz, 2H), 7.97 (d, J = 7.6 Hz, 2H), 7.91-7.83 (m, 4H), 7.82-7.75 (m, 5H), 7.73-7.63 (m, 12H), 7.60-7.41 (m, 10H), 7.34 (ddd, J = 7.5, 4.7, 1.2 Hz, 1H), 7.21-7.14 (m, 4H), 7.13-7.06 (m, 4H), 7.04-6.98 (m, 2H), 6.92-6.83 (m, 4H), 6.79 (d, J = 7.5 Hz, 2H), 3.80 (s, 6H), 2.25-2.05 (m, 16H), 0.47-0.37 (m, 12H), 0.37-0.29 (m, 12H) ppm.
MS (ESI): m/z (%) = 1655.46 (19, $[M+H]^+$), calcd for $C_{123}H_{104}N_3O_2^+$ 1655.82.

LC2

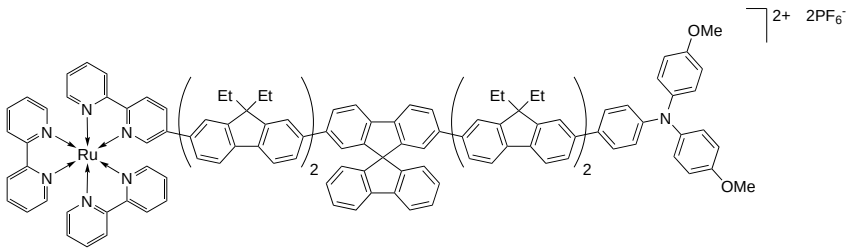

TAA-Fl-Fl-spiro(L)-Fl-Fl-bpy (70.0 mg, 42.3 µmol) and $[Ru(bpy)_2Cl_2]\cdot 2H_2O$ (21 mg,

40.4 µmol) were suspended in ethylene glycol (5 mL) and acetone (10 mL), and stirred at 85 °C for 1 h. CH_2Cl_2 (5 mL) was added and the reaction was stirred overnight at 65 °C. The reaction mixture was cooled to r.t. and subjected to column chromatography, starting with acetone as eluent until non-reacted ligand was removed from the column. Afterwards, the eluent was changed to acetone:H_2O 10:1 to remove the precursor complex, and finally to acetone:H_2O 10:1 + 1% sat. KNO_3 solution to elute the desired complex. The organic solvents were removed under reduced pressure and the complex precipitated by addition of a sat. aq. KPF_6 solution. The complex was extracted into CH_2Cl_2. The organic phase was dried over Na_2SO_4 and the solvent removed under reduced pressure to obtain the product as a red solid (60 mg, 25.4 µmol, 63%).

^{1}H-NMR (400 MHz, CD_2Cl_2): δ 8.56-8.45 (m, 6H), 8.35 (dd, J = 8.5, 2.0 Hz, 1H), 8.13-8.05 (m, 5H), 8.03 (d, J = 8.0 Hz, 2H), 7.96 (d, J = 7.7 Hz, 2H), 7.88-7.42 (m, 39H), 7.36 (dd, J = 7.9, 1.7 Hz, 1H), 7.27 (d, J = 1.7 Hz, 1H), 7.19 (t, J = 7.5 Hz, 2H), 7.13-7.07 (m, 3H), 7.05 (d, J = 1.6 Hz, 2H), 7.01-6.96 (m, 2H), 7.02-6.98 (m, 2H), 6.90-6.85 (m, 5H), 3.80 (s, 6H), 2.20-2.06 (m, 16H), 0.43-0.29 (m, 24H) ppm.
HR-MS (ESI TOF): m/z (%) = 1034.4254 (71, $[M\text{-}2\,PF_6^-]^{2+}$), calcd for $C_{143}H_{119}N_7O_2Ru^{2+}$ 1034.4256.
EA (%): calcd for $C_{143}H_{119}N_7O_2F_{12}P_2Ru \cdot 3\,C_3H_6O$ C, 72.08; H, 5.45; N, 3.87; found: C, 72.01; H, 5.73; N, 4.14.

AC2

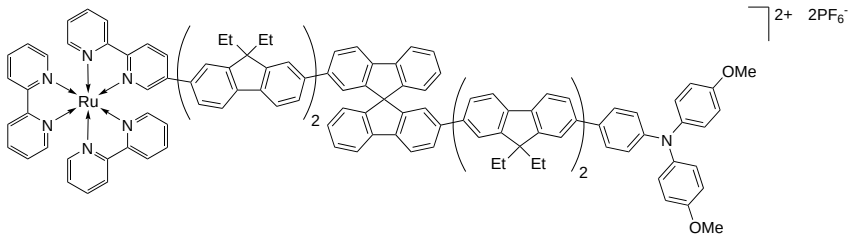

TAA-Fl-Fl-spiro(A)-Fl-Fl-bpy (52.0 mg, 31.4 µmol) and $[Ru(bpy)_2(MeCN)_2](OTf)_2$ (25.0 mg, 31.5 µmol) were dissolved in a mixture of 1,2-dichloroethane (3 mL), acetone (2 mL) and ethylene glycole (2 mL), and stirred at 85 °C overnight. The reaction mixture was cooled to r.t. and subjected to column chromatography, starting with acetone as eluent until non-reacted ligand was removed from the column. Afterwards, the eluent was changed to acetone:H_2O 10:1 to remove the precursor complex, and finally to acetone:H_2O 10:1 + 1% sat. KNO_3 solution to elute the desired complex. The organic solvents were removed under reduced pressure and the complex precipitated by addi-

tion of a sat. aq. KPF_6 solution. The complex was extracted into CH_2Cl_2. The organic phase was washed with hydrochloric acid (2 M) and NaOH solution (1 M), dried over Na_2SO_4 and the solvent removed under reduced pressure to obtain the product as a red solid (15.0 mg, 6.4 μmol, 16%).

^{1}**H-NMR** (400 MHz, CD_2Cl_2): δ 8.54-8.42 (m, 6H), 8.33 (dd, J = 8.5, 2.1 Hz, 1H), 8.13-8.04 (m, 5H), 8.01 (dd, J = 8.1, 3.1 Hz, 2H), 7.95 (d, J = 7.6 Hz, 2H), 7.87-7.23 (m, 42H), 7.19-7.05 (m, 8H), 7.01-6.96 (m, 2H), 6.88-6.82 (m, 3H), 6.76 (d, J = 7.5 Hz, 2H), 3.78 (s, 6H), 2.18-1.97 (m, 16H), 0.44-0.25 (m, 24H) ppm.
HR-MS (ESI TOF): m/z (%) = 1034.4249 (100, $[M\text{-}2PF_6^-]^{2+}$), calcd for $C_{143}H_{119}N_7O_2Ru^{2+}$ 1034.4256.
EA (%): calcd for $C_{143}H_{119}N_7O_2F_{12}P_2Ru \cdot 4\ H_2O \cdot 5\ C_3H_6O$ C, 72.43; H, 6.04; N, 3.74; found: C, 72.22; H, 6.43; N, 3.82.

Br-Fl-Fl-TMS

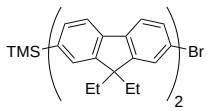

Br-Fl-Fl-TMS was synthesized using method A, with **Br-Fl-Br** as aryl halide (1.08 g, 2.84 mmol) and **TMS-Fl-B(OH)$_2$** (300 mg, 0.89 mmol) as boronic acid. A solvent mixture of toluene (20 mL) and water (1.5 mL) was used. The crude product was purified using column chromatography (SiO_2; pure pentane to pentane:CH_2Cl_2 15:1) to afford the product as a white solid (408 mg, 0.69 mmol, 77%).

^{1}**H-NMR** (400 MHz, CD_2Cl_2): δ 7.75-7.63 (m, 3H), 7.62-7.52 (m, 5H), 7.47-7.39 (m, 4H), 2.12-1.94 (m, 8H), 0.32-0.20 (m, 21H) ppm.
^{13}**C-NMR** (101 MHz, CD_2Cl_2): δ 153.1, 151.5, 150.9, 149.8, 142.3, 141.6, 141.4, 141.1, 141.0, 140.2, 139.9, 132.6, 130.6, 128.2, 126.9, 126.8, 126.6, 122.1, 122.0, 121.6, 121.5, 120.5(7), 120.5(5), 119.5, 57.2, 56.8, 33.3, 33.2, 9.00, 8.9, -0.6 ppm.

BE-Fl-Fl-TMS

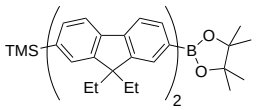

BE-Fl-Fl-TMS was synthesized using method C, with **Br-Fl-Fl-TMS** (200 mg, 0.34 mmol) as aryl halide.
The product was obtained after column chromatography (SiO_2; pentane:CH_2Cl_2 3:2 to 1:1) as a white solid (144 mg, 0.22 mmol, 67%).

^{1}**H-NMR** (400 MHz, CD_2Cl_2): δ 7.86-7.73 (m, 6H), 7.72-7.65 (m, 4H), 7.56-7.52 (m, 2H), 2.20-2.09 (m, 8H), 1.38 (s, 12H), 0.41-0.30 (m, 21H) ppm.
^{13}**C-NMR** (101 MHz, CD_2Cl_2): δ 151.8, 151.5, 149.8, 149.8, 144.8, 142.4, 141.7, 141.4, 141.2, 141.1, 139.8, 134.3, 132.6, 129.4, 128.2, 126.7, 126.6, 122.0(8), 122.0(6), 120.9, 120.6, 119.6, 119.5, 84.3, 56.9, 56.8, 33.3, 33.2, 25.4, 9.0(3), 8.9(7), -0.6 ppm.

bpy-Fl-Fl-TMS

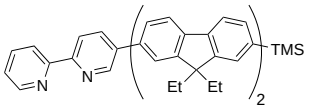

bpy-Fl-Fl-TMS was synthesized using method A, with **bpy-Br** (110 mg, 467 μmol) as aryl halide and **BE-Fl-Fl-TMS** (299 mg, 467 μmol) as boronic acid. The crude product was purified using column chromatography (SiO_2; pentane:CH_2Cl_2 1:1 + 2% NEt_3) to afford the product as a light yellow solid (241 mg, 360 μmol, 97%).

^{1}**H-NMR** (400 MHz, CD_2Cl_2): δ 9.02 (dd, J = 2.4, 0.8 Hz, 1H), 8.69 (ddd, J = 4.8, 1.8, 0.9 Hz, 1H), 8.54 (dd, J = 8.3, 0.8 Hz, 1H), 8.50 (dt, J = 8.0, 1.1 Hz, 1H), 8.14 (dd, J = 8.3, 2.4 Hz, 1H), 7.91-7.81 (m, 4H), 7.77-7.66 (m, 7H), 7.56-7.51 (m, 2H), 7.34 (ddd, J = 7.5, 4.8, 1.2 Hz, 1H), 2.25-2.09 (m, 8H), 0.43 (t, J = 7.3 Hz, 6H), 0.38 (t, J = 7.3 Hz, 6H), 0.33 (s, 9H) ppm.

bpy-Fl-Fl-I

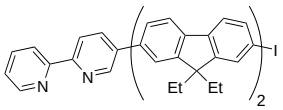

bpy-Fl-Fl-I was synthesized using method B, with **bpy-Fl-Fl-TMS** (461 mg, 689 μmol) as substrate. The crude product was purified using column chromatography (SiO_2; CH_2Cl_2:pentane 3:2 + 2% NEt_3) to afford the product as a yellow solid (500 mg, 689 μmol, quant.).

^{1}**H-NMR** (400 MHz, CD_2Cl_2): δ 9.02 (dd, J = 2.4, 0.8 Hz, 1H), 8.69 (ddd, J = 4.8, 1.8, 0.9 Hz, 1H), 8.56-8.48 (m, 1H), 8.14 (dd, J = 8.3, 2.4 Hz, 1H), 7.92-7.76 (m, 4H), 7.76-7.62 (m, 9H), 7.53 (d, J = 8.9 Hz, 1H), 7.34 (ddd, J = 7.5, 4.8, 1.2 Hz, 1H), 2.24-2.04 (m, 8H), 0.42 (t, J = 7.3 Hz, 6H), 0.37 (t, J = 7.3 Hz, 6H) ppm.
MS (MALDI): m/z (%) = 723.286 (100, $[M+H]^+$), calcd for $C_{44}H_{40}N_2I$ 723.223.

bpy-Fl-Fl-BE

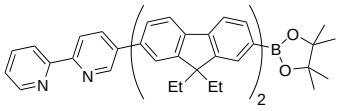

bpy-Fl-Fl-BE was synthesized using method C, with **bpy-Fl-Fl-I** (500mg, 689 μmol) as aryl halide.
The product was obtained after column chromatography (SiO_2; pentane:EtOAc (3:1 to 2:1) + 2% NEt_3) as a yellow solid (293 mg, 405 μmol, 78%).

^{1}**H-NMR** (400 MHz, CD_2Cl_2): δ 9.02 (dd, J = 2.4, 0.8 Hz, 1H), 8.69 (ddd, J = 4.8, 1.8, 0.9 Hz, 1H), 8.56-8.48 (m, 2H), 8.14 (dd, J = 8.3, 2.4 Hz, 1H), 7.91-7.83 (m, 4H), 7.81-7.67 (m, 9H), 7.34 (ddd, J = 7.5, 4.8, 1.2 Hz, 1H), 2.26-2.11 (m, 8H), 1.38 (s, 12H), 0.43 (t, J = 7.3 Hz, 6H), 0.40-0.31 (m, 6H) ppm.
MS (MALDI): m/z (%) = 722.478 (100, $[M]^+$), calcd for $C_{50}H_{51}N_2O_2B$ 722.404.

TAA-BE

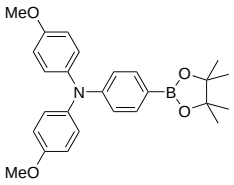

TAA-BE was synthesized using method C, with **TAA-I** (500 mg, 1.16 mmol) as aryl halide.
The product was obtained after column chromatography (SiO_2; pentane:CH_2Cl_2 1:1 to CH_2Cl_2) as a light orange oil (390 mg, 0.90 mmol, 78%).

^{1}**H-NMR** (400 MHz, acetone-d_6): δ 7.56-7.50 (m, 2H), 7.11-7.06 (m, 4H), 6.95-6.90 (m, 4H), 6.79-6.75 (m, 2H), 3.80 (s, 6H), 1.30 (s, 12H) ppm.

TAA-Fl-Fl-TMS

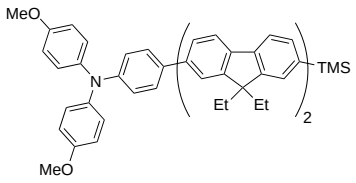

TAA-Fl-Fl-TMS was synthesized from two different substrates:
1. **TAA-Fl-Fl-TMS** was synthesized using method A, with **TMS-Fl-Fl-Br** (344 mg, 579 µmol) as aryl halide and **TAA-BE** (290 mg, 672 µmol) as boronic acid. The crude product was purified using column chromatography (SiO_2; pentane:CH_2Cl_2 1:1) to afford the product as a light yellow glass (473 mg, 578 µmol, quant.).
2. **TAA-Fl-Fl-TMS** was synthesized using method A, with **TAA-Fl-I** (730 mg, 1.12 mmol) as aryl halide and **TMS-Fl-B(OH)$_2$** (420 mg, 1.24 mmol) as boronic acid. The crude product was purified using column chromatography (SiO_2; pentane:CH_2Cl_2 1:1) to afford the product as a light yellow glass (902 mg, 1.10 mmol, 97%).

^{1}**H-NMR** (400 MHz, acetone-d_6): δ 7.93-7.81 (m, 6H), 7.77 (dd, J = 7.9, 1.7 Hz, 2H), 7.71 (q, J = 0.7 Hz, 1H), 7.67-7.59 (m, 4H), 7.56 (dd, J = 7.5, 1.0 Hz, 1H), 7.12-7.07 (m, 4H), 6.99-6.91 (m, 6H), 3.81 (s, 6H), 2.27-2.13 (m, 8H), 0.42-0.28 (m, 21H) ppm.
MS (ESI): m/z (%) = 817.32 (100, $[M]^+$), calcd for $C_{57}H_{59}NO_2Si$ 817.43.

TAA-Fl-Fl-I

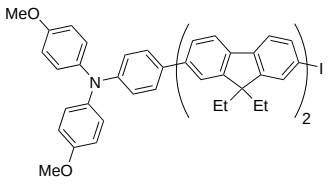

TAA-Fl-Fl-I was synthesized using method B, with **TAA-Fl-Fl-TMS** (1.00 g, 1.22 mmol) as substrate. The crude product was purified using column chromatography (SiO_2; CH_2Cl_2:pentane 1:1) to afford the product as a yellow glass (630 mg, 723 μmol, 59%).

^{1}**H-NMR** (400 MHz, acetone-d_6): δ 7.93-7.84 (m, 6H), 7.81-7.60 (m, 8H), 7.13-7.07 (m, 4H), 6.98-6.92 (m, 6H), 3.81 (s, 6H), 2.26-2.12 (m, 8H), 0.40-0.30 (m, 12H) ppm.

TAA-Fl-Fl-BE

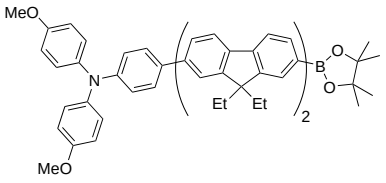

TAA-Fl-Fl-BE was synthesized using method C, with **TAA-Fl-Fl-I** (630 mg, 723 μmol) as aryl halide.
The product was obtained after purification by column chromatography (SiO_2; CH_2Cl_2:pentane 1:1 to 2:1) as a yellow glass (463 mg, 531 μmol, 73%).

^{1}**H-NMR** (400 MHz, acetone-d_6): δ 7.93 (d, J = 7.9 Hz, 1H), 7.90-7.74 (m, 9H), 7.70 (d, J = 1.6 Hz, 1H), 7.64-7.58 (m, 3H), 7.12-7.06 (m, 4H), 7.00-6.95 (m, 2H), 6.95-6.90 (m, 4H), 3.79 (s, 6H), 2.25-2.13 (m, 8H), 1.37 (s, 12H), 0.37 (t, J = 7.3 Hz, 6H), 0.32 (t, J = 7.3 Hz, 6H) ppm.
MS (MALDI): m/z (%) = 871.425 (100, $[M]^+$), calcd for $C_{60}H_{62}NO_4B$ 871.477.

I-Fl-spiro(A)-Fl-Fl-Fl-bpy

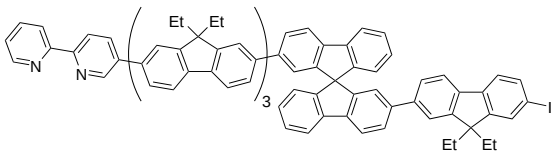

I-Fl-spiro(A)-Fl-Fl-Fl-bpy was synthesized using method A, with **I-Fl-spiro(A)-Fl-I** (240 mg, 238 µmol) as aryl halide and **bpy-Fl-Fl-BE** (138 mg, 191 µmol) as boronic ester. Toluene (2 mL) was added to the solvent mixture for better solubility of the substrates.
The crude product was purified using column chromatography (SiO_2; pentane:EtOAc 2:1 + 2% NEt_3) to afford the product as a light yellow solid (110 mg, 74.4 µmol, 39%).

^{1}**H-NMR** (400 MHz, CD_2Cl_2): δ 9.02 (dd, J = 2.4, 0.8 Hz, 1H), 8.69 (ddd, J = 4.8, 1.8, 0.9 Hz, 1H), 8.54 (dd, J = 8.3, 0.8 Hz, 1H), 8.50 (dt, J = 8.0, 1.1 Hz, 1H), 8.14 (dd, J = 8.3, 2.4 Hz, 1H), 8.03 (dd, J = 8.0, 0.6 Hz, 1H), 7.97 (dt, J = 7.6, 0.9 Hz, 1H), 7.92-7.63 (m, 30H), 7.52-7.42 (m, 4H), 7.34 (ddd, J = 7.5, 4.8, 1.2 Hz, 1H), 7.20-7.14 (m, 2H), 6.78 (dt, J = 7.7, 0.9 Hz, 1H), 2.29-2.06 (m, 16H), 0.50-0.38 (m, 15H), 0.38-0.27 (m, 9H) ppm.

TAA-Fl-Fl-Fl-spiro(A)-Fl-Fl-Fl-bpy

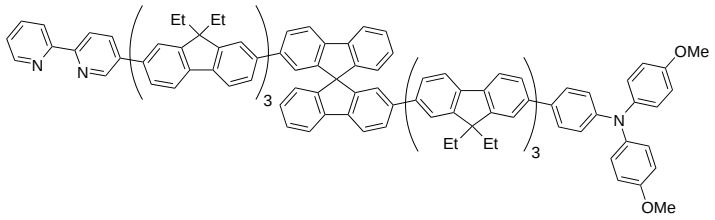

TAA-Fl-Fl-Fl-spiro(A)-Fl-Fl-Fl-bpy was synthesized using method A, with **I-Fl-spiro(A)-Fl-Fl-Fl-bpy** (106 mg, 71.7 µmol) as aryl halide and **TAA-Fl-Fl-BE** (68 mg, 78.0 µmol) as boronic ester. Toluene (2 mL) was added to the solvent mixture for better solubility of the substrates.
The crude product was purified using column chromatography (SiO_2; pentane:EtOAc (2:1 to 3:2) + 2% NEt_3) to afford the product as a yellow solid (75.0 mg, 35.8 µmol, 50%).

^{1}**H-NMR** (400 MHz, CD_2Cl_2): δ 9.03 (dd, J = 2.4, 1.0 Hz, 1H), 8.70 (ddd, J = 4.8, 1.8, 1.0 Hz, 1H), 8.55 (dd, J = 8.0, 1.0 Hz, 1H), 8.51 (dd, J = 8.0, 1.2 Hz, 1H), 8.15 (dd, J = 8.3, 2.3 Hz, 1H), 8.04 (dd, J = 8.0, 1.2 Hz, 2H), 7.97 (dt, J = 7.8, 1.0 Hz, 2H), 7.92-7.41 (m, 43H), 7.34 (ddd, J = 7.5, 4.8, 1.2 Hz, 1H), 7.21-7.14 (m, 4H), 7.13-7.07 (m, 4H), 7.01 (dd, J = 8.4, 1.5 Hz, 2H), 6.90-6.84 (m, 4H), 6.82-6.76 (m, 2H), 3.80 (s, 6H), 2.27-2.06 (m, 24H), 0.49-0.39 (m, 24H), 0.38-0.30 (m, 12H) ppm.

I-Fl-spiro(L)-Fl-Fl-Fl-bpy

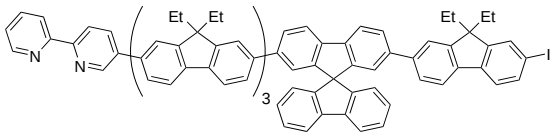

I-Fl-spiro(L)-Fl-Fl-Fl-bpy was synthesized using method A, with **I-Fl-spiro(L)-Fl-I** (207 mg, 205 µmol) as aryl halide and **bpy-Fl-Fl-BE** (144 mg, 200 µmol) as boronic ester.
The crude product was purified using column chromatography (SiO_2; pentane:EtOAc 2:1 + 2% NEt_3) to afford the product as a light yellow solid (63.0 mg, 42.6 µmol, 21%).

^{1}**H-NMR** (400 MHz, CD_2Cl_2): δ 9.02 (d, J = 2.4 Hz, 1H), 8.69 (dt, J = 4.7, 1.2 Hz, 1H), 8.54 (d, J = 8.3 Hz, 1H), 8.50 (dd, J = 8.1, 1.1 Hz, 1H), 8.15 (dd, J = 8.3, 2.4 Hz, 1H), 8.02 (dd, J = 8.0, 2.7 Hz, 2H), 7.95 (d, J = 7.7 Hz, 2H), 7.92-7.82 (m, 5H), 7.80-7.61 (m, 19H), 7.48-7.41 (m, 5H), 7.34 (ddd, J = 7.7, 4.8, 1.1 Hz, 1H), 7.19 (td, J = 7.6, 1.1 Hz, 2H), 7.02 (dd, J = 9.1, 1.6 Hz, 2H), 6.86 (d, J = 7.6 Hz, 2H), 2.25-2.04 (m, 16H), 0.47-0.39 (m, 12H), 0.33 (t, J = 7.3 Hz, 6H), 0.25 (t, J = 7.3 Hz, 6H) ppm.

TAA-Fl-Fl-Fl-spiro(L)-Fl-Fl-Fl-bpy

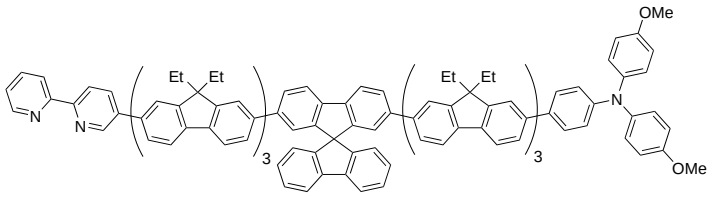

TAA-Fl-Fl-Fl-spiro(L)-Fl-Fl-Fl-bpy was synthesized using method A, with **I-Fl-spiro(L)-Fl-Fl-Fl-bpy** (63.0 mg, 42.6 µmol) as aryl halide and **TAA-Fl-Fl-BE** (40 mg, 45.9 µmol)

as boronic ester.
The crude product was purified using column chromatography (SiO_2; pentane:EtOAc 2:1 + 2% NEt_3) to afford the product as a yellow solid (45.0 mg, 21.5 μmol, 50%).

^{1}H-NMR (400 MHz, CD_2Cl_2): δ 9.02 (dd, J = 2.3, 0.9 Hz, 1H), 8.69 (ddd, J = 4.9, 1.8, 0.9 Hz, 1H), 8.54 (dd, J = 8.3, 0.8 Hz, 1H), 8.50 (dt, J = 8.0, 1.1 Hz, 1H), 8.15 (dd, J = 8.3, 2.4 Hz, 1H), 8.03 (d, J = 8.0 Hz, 2H), 7.97 (dt, J = 7.7, 0.9 Hz, 2H), 7.91-7.63 (m, 32H), 7.60-7.51 (m, 5H), 7.49-7.41 (m, 6H), 7.34 (ddd, J = 7.5, 4.8, 1.2 Hz, 2H), 7.20 (td, J = 7.5, 1.1 Hz, 2H), 7.12-7.06 (m, 4H), 7.04 (d, J = 1.6 Hz, 2H), 7.02-6.98 (m, 2H), 6.90-6.84 (m, 5H), 3.80 (s, 6H), 2.28-2.04 (m, 24H), 0.48-0.20 (m, 36H) ppm.
MS (MALDI): m/z (%) = 2096.556 (100, $[M+H]^+$), calcd for $C_{157}H_{135}N_3O_2$ 2096.067.

AC3

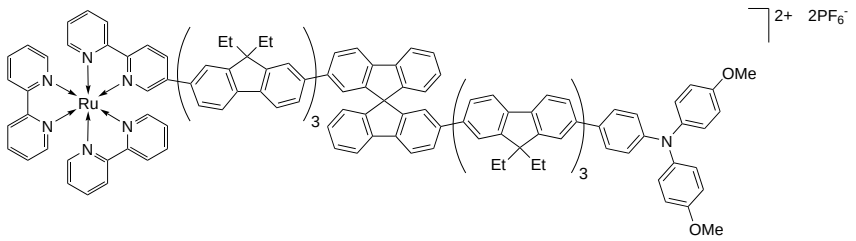

A solution of **TAA-Fl-Fl-Fl-spiro(A)-Fl-Fl-Fl-bpy** (74.0 mg, 35.3 μmol) and $[Ru(bpy)_2(MeCN)_2](OTf)_2$ (28.0 mg, 35.3 μmol) in 1,2-dichloroethane (3 mL), acetone (2 mL) and ethylene glycole (2 mL) was stirred at 85 °C overnight. The reaction mixture was cooled to r.t. and subjected to column chromatography, starting with acetone as eluent until non-reacted ligand was removed from the column. Afterwards, the eluent was changed to acetone:H_2O 10:1 to remove the precursor complex, and finally to acetone:H_2O 10:1 + 1% sat. aq. KNO_3 solution to elute the desired complex. The organic solvents were removed under reduced pressure and the complex precipitated by addition of a sat. aq. KPF_6 solution. The complex was extracted into CH_2Cl_2. The organic phase was washed with hydrochloric acid (2 M) and NaOH solution (1 M), dried, and the solvent removed under reduced pressure to obtain the product as a red solid (18.0 mg, 6.4 μmol, 18%).

^{1}H-NMR (400 MHz, CD_2Cl_2): δ 8.56-8.45 (m, 6H), 8.35 (dd, J = 8.5, 2.0 Hz, 1H), 8.15-8.06 (m, 5H), 8.04 (d, J = 8.00 Hz, 2H), 7.97 (dd, J = 7.6, 1.1 Hz, 2H), 7.89-7.34 (m, 52H), 7.27 (d, J = 1.7 Hz, 1H), 7.21-7.14 (m, 4H), 7.12-7.07 (m, 4H), 7.04-6.98 (m, 2H), 6.90-6.84 (m, 4H), 6.78 (d, J = 7.5 Hz, 2H), 3.80 (s, 6H), 2.28-2.00 (m, 24H), 0.46-0.38

(m, 18H), 0.38-0.28 (m, 18H) ppm.
HR-MS (ESI TOF): *m/z* (%) = 1254.5507 (100, $[M\text{-}2\ PF_6^-]^{2+}$), calcd for $C_{177}H_{151}N_7O_2Ru^{2+}$ 1254.5512.
EA (%): calcd for $C_{177}H_{151}N_7O_2F_{12}P_2Ru \cdot 1.7\ H_2O \cdot 5\ C_3H_6O$ C, 73.91; H, 5.96; N, 3.14; found: C, 74.29; H, 6.34; N, 3.40.

VI.3 Synthesis for Project 2

Standardized reaction conditions are listed and labeled in section VI.2.

Br-Ph-TMS

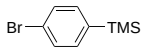

1,4-Dibromobenzene (2.50 g, 10.6 mmol) was dissolved in anhydrous Et_2O (20 mL) under a nitrogen atmosphere. The solution was cooled to −78 °C and *n*-BuLi (4.40 mL, 2.5 M in hexane, 11.0 mmol) was added dropwise. After 15 min, Me_3SiCl (1.41 mL, 11.1 mmol) was added dropwise. The reaction mixture was allowed to warm to r.t. and stirred for an additional 2 h. Water was added, and the product was extracted into CH_2Cl_2. The combined organic phases were dried over Na_2SO_4, and the solvents removed under reduced pressure. The product was obtained as a colorless oil (2.41 g, 10.6 mmol, quant.) and used without further purification.

^{1}**H-NMR** (400 MHz, $CDCl_3$): δ (ppm) = 7.51-7.45 (m, 2H), 7.40-7.34 (m, 2H), 0.25 (s, 9H) ppm.

PTZ-Ph-TMS

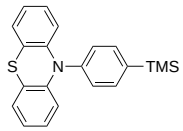

Phenothiazine (1.90 g, 9.53 mmol), NaO*t*Bu (13.7 g, 0.14 mol) and $[Pd(dba)_2]$ (160 mg, 0.28 mmol, 3 mol%) were suspended in anhydrous toluene (53 mL) under a nitrogen atmosphere and deaerated for 15 min. **Br-Ph-TMS** (2.19 g, 9.60 mmol) and $[HP(tBu)_3]BF_4$ (80.0 mg, 0.28 mmol) were added and the reaction stirred at 80 °C overnight. After cooling to r.t., water was added and the product extracted into CH_2Cl_2. The combined organic phases were dried over Na_2SO_4, and the solvents removed under reduced pressure. Purification by column chromatography (SiO_2; pentane:CH_2Cl_2 10:1) afforded the product as an off-white solid (2.72 g, 7.81 mmol, 82%).

^{1}**H-NMR** (400 MHz, acetone-d_6): δ 7.88-7.80 (m, 2H), 7.44-7.36 (m, 2H), 7.07 (dd, J = 7.5, 1.6 Hz, 2H), 6.94 (ddd, J = 8.1, 7.4, 1.7 Hz, 2H), 6.87 (dt, J = 7.4, 1.3 Hz, 2H),

6.28 (dd, J = 8.2, 1.3 Hz, 2H), 0.35 (s, 9H) ppm.

PTZ-Ph-I

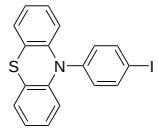

PTZ-Ph-I was synthesized using method B, with **PTZ-Ph-TMS** (2.72 g, 7.81 mmol) as aryltrimethylsilane. Purification by column chromatography (SiO_2; pentane:CH_2Cl_2 5:1) afforded the product as a light-yellow solid (2.16 g, 5.40 mmol, 69%).

^{1}**H-NMR** (400 MHz, acetone-d_6): δ 8.05-7.97 (m, 2H), 7.27-7.18 (m, 2H), 7.10 (dd, J = 7.6, 1.6 Hz, 2H), 6.99 (ddd, J = 8.2, 7.4, 1.7 Hz, 2H), 6.91 (dt, J = 7.5, 1.3 Hz, 2H), 6.38 (dd, J = 8.2, 1.2 Hz, 2H) ppm.

PTZ-Ph-BE

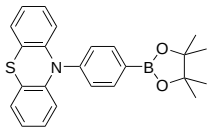

PTZ-Ph-BE was synthesized by applying method C with **PTZ-Ph-I** (1.00 g, 2.49 mmol) as aryl halide.

Purification by column chromatography (SiO_2; pentane:CH_2Cl_2 2:1) afforded the product as a white solid (0.51 g, 1.27 mmol, 51%).

^{1}**H-NMR** (400 MHz, acetone-d_6): δ 8.01-7.95 (m, 2H), 7.43-7.36 (m, 2H), 7.12 (dd, J = 7.5, 1.6 Hz, 2H), 6.99 (td, J = 7.8, 1.7 Hz, 2H), 6.92 (dt, J = 7.5, 1.3 Hz, 2H), 6.40 (dd, J = 8.1, 1.3 Hz, 2H), 1.38 (s, 12H) ppm.

1,8-Naph-I_2

Naph-1,8-I_2 was synthesized by adapting a literature procedure.[74]
To a suspension of 1,8-diaminonaphthalene (2.00 g, 12.6 mmol) in an aqueous H_2SO_4 solution (100 mL, 6.9 M) at 0 °C, a solution of $NaNO_2$ (2.60 g, 37.7 mmol) in water (5 mL) was added dropwise. The mixture was stirred for 5 min prior to dropwise addition of a KI solution (12.8 g, 77.1 mmol) in water (10 mL). After heating the reaction mixture at 80 °C for 2 min, it was cooled to r.t. and the product extracted into CH_2Cl_2. The combined organic phases were washed three times with an aqueous HCl solution (10%), sat. aqueous $Na_2S_2O_3$ solution, and aqueous NaOH solution (1 M). The solvents were removed under reduced pressure after drying over anhydrous Na_2SO_4. Purification by column chromatography (SiO_2; pentane:CH_2Cl_2 5:1) afforded the product as a yellow solid (0.94 g, 2.47 mmol, 20%).

^{1}**H-NMR** (400 MHz, CD_2Cl_2): δ 8.43 (dd, J = 7.3, 1.2 Hz, 2H), 7.85 (dd, J = 8.2, 1.3 Hz, 2H), 7.08 (dd, J = 8.2, 7.3 Hz, 2H) ppm.

Naph-1-(Ph-PTZ),8-I

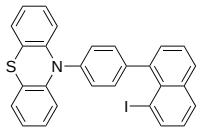

Naph-1-(Ph-PTZ),8-I was synthesized using method A, with **Naph-1,8-I_2** as aryl halide (200 mg, 0.53 mmol) and **PTZ-Ph-BE** (200 mg, 0.50 mmol) as boronic ester.
Purification by column chromatography (SiO_2; pentane:CH_2Cl_2 9:1 to 4:1) afforded the product as a light-yellow solid (90 mg, 0.17 mmol, 34%).

^{1}**H-NMR** (400 MHz, CD_2Cl_2): δ 8.27 (dd, J = 7.3, 1.3 Hz, 1H), 7.99 (ddd, J = 8.0, 1.2, 0.4 Hz, 1H), 7.94 (dd, J = 7.3, 2.2 Hz, 1H), 7.63-7.55 (m, 4H), 7.48-7.43 (m, 2H), 7.17 (dd, J = 8.1, 7.3 Hz, 1H), 7.04 (dd, J = 7.4, 1.7 Hz, 2H), 6.94-6.80 (m, 4H), 6.53 (d, J = 8.1 Hz, 2H) ppm.
^{13}**C-NMR** (101 MHz, CD_2Cl_2): δ 144.8, 143.1, 142.1, 141.2, 140.6, 136.2, 134.4, 132.1,

131.8, 130.6, 130.5, 130.0, 127.4, 127.3, 127.2, 125.8, 123.1, 120.9, 117.1, 92.5 ppm.

TMS-cc-Ph-cc-TMS

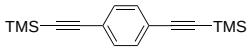

1,4-Dibromobenzene (1.00 g, 3.76 mmol), trimethylsilylacetylene (1.45 mL, 10.0 mmol), $[Pd(PPh_3)_2Cl_2]$ (200 mg, 0.26 mmol) and CuI (6.70 mg, 0.04 mmol) were dissolved in anhydrous THF (40 mL) and anhydrous diisopropylamine (10 mL) under a nitrogen atmosphere. The reaction mixture was heated at 45 °C for 3 h. After cooling to r.t., the mixture was diluted with CH_2Cl_2 and washed with sat. aq. NH_4Cl. The organic phase was dried over Na_2SO_4, and the solvents removed under reduced pressure. Purification by column chromatography (SiO_2; pure pentane) afforded the product as a colorless oil (0.82 g, 3.04 mmol, 71%).

^{1}**H-NMR** (400 MHz, $CDCl_3$): δ 7.38 (s, 4H), 0.24 (s, 9H) ppm.

H-cc-Ph-cc-H

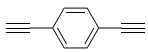

TMS-cc-Ph-cc-TMS (0.82 g, 3.04 mmol) and KF (0.58 g, 9.91 mmol) were stirred in a THF/MeOH mixture (40 mL, 1:1) at 60 °C for 4 h. Water was added and the product extracted into CH_2Cl_2. The combined organic phases were dried over Na_2SO_4, and the solvents removed under reduced pressure. Purification by column chromatography (SiO_2; pure pentane) afforded the product as an off-white solid (350 mg, 2.77 mmol, 91%).

^{1}**H-NMR** (400 MHz, $CDCl_3$): δ 7.44 (s, 4H), 3.17 (s, 2H) ppm.

H-cc-tmb-cc-H

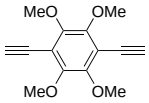

Mebynol-cc-tmb-cc-mebynol (100 mg, 0.28 mmol) and NaOH (37.5 mg, 0.94 mmol) were stirred in anhydrous toluene (5 mL) under a nitrogen atmosphere at 110 °C for 3 h. Water was added to the reaction and neutralized with sat. aq. NH_4Cl solution. The product was extracted into toluene, the combined organic phases dried over Na_2SO_4, and the solvents removed under reduced pressure. Purification by column chromatography (SiO_2; pentane:EtOAc 4:1) afforded the product as a light-blue solid (52 mg, 0.21 mmol, 77%).

^{1}**H-NMR** (400 MHz, $CDCl_3$): δ 3.92 (s, 12H), 3.56 (s, 2H) ppm.

Naph-1-OH,5-I

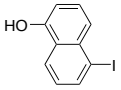

Naph-1-OH,5-I was synthesized by adapting a literature procedure.[98]
5-Aminonaphthalen-1-ol (3.0 g, 18.8 mmol) was dissolved in an aqueous HCl solution (10% , 100 mL), cooled to 0 °C and kept at that temperature over the course of the reaction. A solution of $NaNO_2$ (1.40 g, 20.3 mmol) in water (10 mL) was added quickly and stirred for 20 min. A solution of KI (5.66 g, 34.1 mmol) in water (10 mL) was added in one portion and the mixture continued to stirr for 3 h. The reaction mixture was poured into Et_2O/water (5:2, 700 mL) and filtered through a cotton plug. The phases were separated and the aqueous phase extracted with Et_2O. The combined organic phases were washed with brine, and dried over Na_2SO_4, and the solvents removed under reduced pressure. Purification by column chromatography (SiO_2; pentane:EtOAc 9:1) afforded the product as a brown solid (0.70 g, 2.59 mmol, 14%).

^{1}**H-NMR** (400 MHz, $CDCl_3$): δ 8.23 (dt, J = 8.4, 1.0 Hz, 1H), 8.10 (dd, J = 7.4, 1.1 Hz, 1H), 7.70 (dt, J = 8.6, 0.9 Hz, 1H), 7.40 (dd, J = 8.6, 7.5 Hz, 1H), 7.17 (dd, J = 8.4, 7.3 Hz, 1H), 6.87 (dd, J = 7.5, 0.9 Hz, 1H), 5.24 (s, 1H) ppm.

Naph-1-OTf,5-I

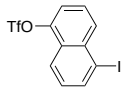

Naph-1-OH,5-I (0.50 g, 1.85 mmol) was dissolved in anhydrous CH_2Cl_2 (5 mL) and pyridine (0.30 mL, 3.70 mmol) under a nitrogen atmosphere. The mixture was cooled to 0 °C and trifluoromethanesulfonic anhydride (0.47 mL, 2.78 mmol) added dropwise. The reaction was warmed to r.t. overnight and diluted with EtOAc. The organic phase was washed with an aqueous HCl solution (1 M), water and brine, and dried over Na_2SO_4, and the solvents removed under reduced pressure. Purification by column chromatography (SiO_2; pentane:EtOAc 9:1) afforded the product as a yellow solid (0.74 g, 1.85 mmol, quant.).

^{1}**H-NMR** (400 MHz, $CDCl_3$): δ 8.24-8.15 (m, 2H), 8.10 (dt, J = 8.6,1.0 Hz, 1H), 7.60 (dd, J = 8.4,7.7 Hz, 1H), 7.55 (dd, J = 7.8,1.1 Hz, 1H), 7.34 (dd, J = 8.5,7.4 Hz, 1H) ppm.

TfO-Naph(1,5)-cc-ph-cc-Naph(1,5)-OTf

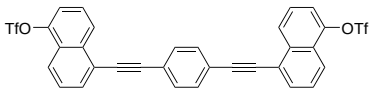

To **Naph-1-OTf,5-I** (372 mg, 925 µmol), **H-cc-ph-cc-H** (57.4 mg, 462 µmol), $[Pd(PPh_3)_2Cl_2]$ (24.4 mg, 34.8 µmol, 4 mol%) and CuI (6.00 mg, 3.15 µmol) under a nitrogen atmosphere, a THF/NEt_3 mixture (1:1, 10 mL) was added. The mixture was heated at reflux overnight. After cooling to r.t., the mixture was diluted with CH_2Cl_2 and washed with a sat. aq. NH_4Cl solution. The organic phase was dried over Na_2SO_4, and the solvents removed under reduced pressure. Purification by column chromatography (SiO_2; pentane:CH_2Cl_2 4:1) afforded the product as a yellow solid (253 mg, 375 µmol, 81%).

^{1}**H-NMR** (400 MHz, CD_2Cl_2): δ 8.54 (dt, J = 8.4, 1.0 Hz, 2H), 8.11 (dt, J = 8.6, 1.0 Hz, 2H), 7.93 (dd, J = 7.3, 1.1 Hz, 2H), 7.73 (s, 4H), 7.68 (ddd, J = 8.4, 7.5, 6.0 Hz, 4H), 7.58 (dd, J = 7.7, 1.1 Hz, 2H) ppm.
MS (ESI): m/z (%) = 672.95 (100, $[M]^+$), calcd for $C_{32}H_{16}F_6O_6S_2$ 673.02.

TfO-Naph(1,5)-cc-tmb-cc-Naph(1,5)-OTf

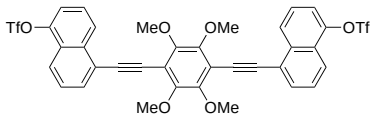

To **Naph-1-OTf,5-I** (258 mg, 643 µmol), **H-cc-tmb-cc-H** (72 mg, 292 µmol), $[Pd(PPh_3)_2Cl_2]$ (16 mg, 22.8 µmol, 4 mol%) and CuI (4.00 mg, 2.10 µmol) under a nitrogen atmosphere, a NEt_3/THF mixture (9 mL, 5:4) was added. The mixture was heated at reflux overnight. After cooling down to r.t. the mixture was diluted with CH_2Cl_2 and washed with a sat. aq. NH_4Cl solution. The organic phase was dried over Na_2SO_4, and the solvents removed under reduced pressure. Purification by column chromatography (SiO_2; pentane:CH_2Cl_2 1:1) afforded the product as a white solid (188 mg, 237 µmol, 81%).

^{1}**H-NMR** (400 MHz, CD_2Cl_2): δ 8.70 (dt, J = 8.5, 1.0 Hz, 2H), 8.12 (dd, J = 8.6, 1.1 Hz, 2H), 7.94 (dd, J = 7.2, 1.1 Hz, 2H), 7.70 (dd, J = 8.6, 7.3 Hz, 2H), 7.59 (dd, J = 7.8, 1.0 Hz, 4H), 4.09 (s, J = 7.7, 1.1 Hz, 12H) ppm.
^{13}**C-NMR** (101 MHz, CD_2Cl_2): δ 151.0, 146.4, 135.3, 132.1, 128.0, 127.6, 127.0, 126.9, 122.2, 122.1, 119.2, 114.8, 96.9, 88.4, 62.0 ppm.

PTZ-TD-Ph

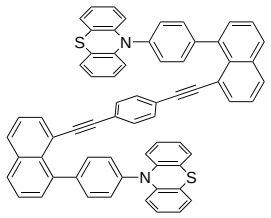

Naph-1-(Ph-PTZ),8-I (380 mg, 0.72 mmol), **H-cc-Ph-cc-H** (45 mg, 0.36 mmol), $[Pd(PPh_3)_2Cl_2]$ (35.0 mg, 52.7 µmol, 7 mol%) and CuI (7.00 mg, 36.8µ mol) were dissolved in anhydrous NEt_3 (20 mL) and anhydrous $CHCl_3$ (20 mL) under a nitrogen atmosphere. The reaction was stirred at 65 °C for 42 h. Water was added and the mixture washed with a sat. aq. NH_4Cl solution. The organic phase was dried over Na_2SO_4, and the solvents removed under reduced pressure. The crude product was purified by column chromatography (SiO_2; pentane:CH_2Cl_2 3:1 to CH_2Cl_2) and extensive washing

of the resulting solid with CH_2Cl_2, pre-cooled in a dry ice/acetone bath. The product was obtained as a light-brownish solid (43 mg, 46.5 µmol, 13%).

Single crystals were obtained by diffusion of pentane into a CH_2Cl_2 solution, containing **PTZ-TD-Ph** and one equivalent of $SbCl_5$.
^{1}**H-NMR** (400 MHz, CD_2Cl_2): δ 7.98 (dd, J = 8.2, 1.3 Hz, 2H), 7.94 (dd, J = 8.2, 1.4 Hz, 2H), 7.83 (dd, J = 7.2, 1.4 Hz, 2H), 7.65-7.52 (m, 8H), 7.46 (dd, J = 7.1, 1.4 Hz, 2H), 7.34-7.29 (m, 4H), 7.05 (dd, J = 7.6, 1.6 Hz, 4H), 6.94 (s, 4H), 6.80 (td, J = 7.5, 1.2 Hz, 4H), 6.66 (ddd, J = 8.1, 7.4, 1.6 Hz, 4H), 6.30 (dd, J = 8.2, 1.2 Hz, 4H) ppm.
EA (%): $C_{66}H_{40}N_2S_2 \cdot 0.75\ CH_2Cl_2$ calcd C 81.08, H 4.23, N 2.83; found C 81.06, H 4.35, N 3.03.
Crystal data for **(PTZ-TD-Ph)(SbCl$_6$)$_2$**: $C_{68}H_{44}Cl_{16}N_2S_2Sb_2$, M = 1763.99 g/mol, brown plate, 0.020 · 0.170 · 0.190 mm^3, monoclinic, a = 16.5777(12) Å, b = 9.8372(7) Å, c = 21.2783(14) Å, α = 90°, β = 93.548(3)°, γ = 90°, V = 3463.4(2) Å^3, space group P 21/n, Z=2, radiation (wavelength) Cu K_α (1.54178 Å), $2\Theta_{max}$ = 138.086, 40741 reflections measured, 6374 independent reflections. The final $R_1(F)$ = 0.0375 ($I > 2\sigma(I)$), 0.0384 (all data). The final $wR_2(F^2)$ = 0.0434 ($I > 2\sigma(I)$), 0.0470 (all data). Goodness of fit 1.0595.

PTZ-TD-tmb

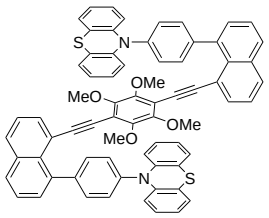

Naph-1-(Ph-PTZ),8-I (200 mg, 379 µmol), **H-cc-tmb-cc-H** (45 mg, 182 µmol), [Pd(PPh$_3$)$_2$Cl$_2$] (20.0 mg, 30.1 µmol, 8 mol%) and CuI (3.00 mg, 15.8 µmol) were dissolved in anhydrous NEt_3 (5 mL) and anhydrous DMSO (4 mL) under a nitrogen atmosphere. The reaction was stirred at 90 °C for 24 h. CH_2Cl_2 was added and the mixture subsequently washed with a sat. aq. NH_4Cl and Na_2CO_3 solution and water. The organic phase was dried over Na_2SO_4, and the solvents removed under reduced pressure. Purification by column chromatography (SiO_2; CH_2Cl_2:pentane 2:1) afforded the product as an off-white solid (116 mg, 111 µmol, 61%).

Single crystals were obtained by diffusion of pentane into a CH_2Cl_2 solution of **PTZ-TD-Ph**.

^{1}**H-NMR** (400 MHz, CD_2Cl_2): δ 8.02 (dd, J = 8.4, 1.3 Hz, 2H), 7.97 (dd, J = 8.3, 1.3 Hz, 2H), 7.87 (dd, J = 7.1, 1.4 Hz, 2H), 7.70-7.65 (m, 4H), 7.60 (ddd, J = 8.2, 7.1, 4.8 Hz, 4H), 7.50 (dd, J = 7.0, 1.4 Hz, 2H), 7.32-7.26 (m, 4H), 6.96 (dd, J = 7.6, 1.5 Hz, 4H), 6.73 (td, J = 7.5, 1.2 Hz, 4H), 6.54 (ddd, J = 8.2, 7.3, 1.6 Hz, 4H), 6.06 (dd, J = 8.3, 1.2 Hz, 4H), 3.57 (s, 12H) ppm.

EA (%): $C_{70}H_{48}N_2O_4S_2 \cdot 0.20\ H_2O$ calcd C 80.16, H 4.65, N 2.67; found C 79.96, H 4.77, N 2.92.

Crystal data for **(PTZ-TD-tmb)**: $C_70H_48N_2O_4S_2$, M = 1045.29 g/mol, colorless plate, 0.030 · 0.100 · 0.110 mm^3, monoclinic, a = 17.3484(10) Å, b = 19.6438(12) Å, c = 7.8622(5) Å, α = 90°, β = 96.591(3)°, γ = 90°, V = 2661.6(3) Å^3, space group P 1 21/c 1, Z=2, radiation (wavelength) Cu K_α (1.54178 Å), $2\Theta_{max}$ = 140.346, 18571 reflections measured, 4909 independent reflections. The final $R_1(F) = 0.0334$ ($I > 2\sigma(I)$), 0.0397 (all data). The final $wR_2(F^2) = 0.0659$ ($I > 2\sigma(I)$), 0.0684 (all data). Goodness of fit 0.9269.

PTZ-Ref-tmb

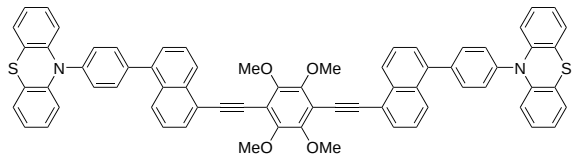

TfO-Naph(1,5)-cc-tmb-cc-Naph(1,5)-OTf (125 mg, 157 µmol), **PTZ-Ph-BE** (189 mg, 471 µmol), Cs_2CO_3 (511 mg, 1.57 mmol) and [Pd(dppf)Cl_2]· CH_2Cl_2 (51.0 mg, 62.1 µmol, 20 mol%) were suspended in anhydrous DMF (6 mL) under a nitrogen atmosphere and heated at 60 °C overnight. The reaction was cooled to r.t. and diluted with THF to dissolve the product. The organic phase was washed with H_2O, dried, and the solvents removed under reduced pressure. Purification by column chromatography (SiO_2; pentane:CH_2Cl_2 3:2) afforded the product as a yellow solid (112 mg, 107 µmol, 68%).

EA (%): $C_{70}H_{48}N_2O_4S_2$ calcd C 80.43, H 4.63, N 2.68; found C 80.16, H 4.90, N 2.93.

pent-CO-CBZ-H

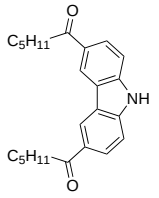

pent-CO-CBZ-H was synthesized according to literature conditions.[91]
Anhydrous CH_2Cl_2 (75 mL) was added to $AlCl_3$ (9.30 g, 69.7 mmol) under a nitrogen atmosphere. The mixture was cooled to 0 °C and hexanoyl chloride (9.00 mL, 69.7 mmol) slowly added, after which carbazole (5.00 g, 29.9 mmol) was added in portions. The reaction mixture was warmed to r.t. overnight and poured onto ice. The precipitate was filtered, washed with water and methanol, and dried under reduced pressure to obtain the product as a light violet solid (9.93 g, 27.3 mmol, 91%).

^{1}**H-NMR** (400 MHz, DMSO-d_6): δ 12.04 (s, 1H), 9.05 (d, J = 1.7 Hz, 2H), 8.07 (dd, J = 8.6, 1.7 Hz, 2H), 7.59 (dd, J = 8.6, 0.7 Hz, 2H), 3.15 (t, J = 7.3 Hz, 4H), 1.74-1.64 (m, 4H), 1.41-1.64 (m, 8H), 0.94-0.85 (m, 6H) ppm.

CBZ-H

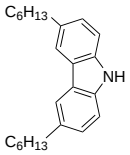

CBZ-H was synthesized according to literature conditions.[91]
$AlCl_3$ (6.53 g, 49 .0 mmol) was dissolved in anhydrous THF (200 mL) and cooled to 0 °C. $LiAlH_4$ (3.75 g, 98.0 mmol) was added in portions, after which a suspension of **pent-CO-CBZ-H** (8.95 g, 25.0 mmol) in anhydrous THF (200 mL) was slowly added. After warming to r.t. overnight the reaction was quenched by carefully adding aqueous HCl solution (5%), while cooling in an ice bath. The product was extracted into CH_2Cl_2, the combined organic phases dried over Na_2SO_4, and the solvents were removed under reduced pressure. Purification by column chromatography (SiO_2; pentane:CH_2Cl_2 5:1 to 2:1) afforded the product as an off-white solid (6.65 g, 19.8 mmol, 81%).

^{1}H-NMR (400 MHz, $CDCl_3$): δ 7.85 (d, J = 1.4 Hz, 2H), 7.31 (d, J = 8.2 Hz, 2H), 7.22 (dd, J = 8.2, 1.5 Hz, 2H), 2.77 (t, J = 7.8 Hz, 4H), 1.77-1.65 (m, 4H), 1.46-1.26 (m, 12H), 0.94-0.85 (m, 6H) ppm.

CBZ-Ph-Br

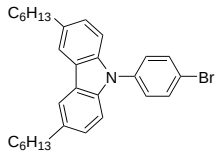

CBZ-Ph-Br was synthesized by modifying a literature procedure.[99]
CBZ-H (2.20 g, 6.56 mmol), 1-bromo-4-fluorobenzene (2.89 mL, 26.3 mmol) and Cs_2CO_3 (8.56 g, 26.3 mmol) were dissolved in DMF (26 mL) and heated at 160 °C overnight. After cooling to r.t., sat. aq. NH_4Cl solution was added and extracted with CH_2Cl_2. The combined organic phases were washed with sat. aq. NH_4Cl solution and water. After drying over Na_2SO_4, the solvents were removed under reduced pressure. Purification by column chromatography (SiO_2; pentane:CH_2Cl_2 10:1 to 5:1) afforded the product as a colorless oil (0.93 g, 1.90 mmol, 29%).

^{1}H-NMR (400 MHz, acetone-d_6): δ 8.02 (dd, J = 1.7, 0.8 Hz, 2H), 7.88-7.81 (m, 2H), 7.62-7.56 (m, 2H), 7.33 (dd, J = 8.3, 0.7 Hz, 2H), 7.27 (dd, J = 8.4, 1.7 Hz, 2H), 2.84-2.75 (m, 4H), 1.78-1.66 (m, 4H), 1.45-1.28 (m, 12H), 0.93-0.84 (m, 6H) ppm.
MS (ESI): m/z (%) = 489.15 (100, $[M]^+$), calcd for $C_{30}H_{36}BrN$ 489.20.

CBZ-Ph-BE

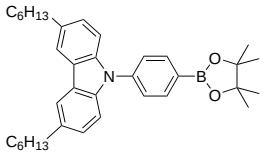

CBZ-Ph-BE was synthesized by applying method C with **CBZ-Ph-Br** (0.93 g, 1.90 mmol) as aryl halide.
Purification by column chromatography (SiO_2; pentane:CH_2Cl_2 3:1) afforded the product as a colorless glass (0.59 g, 1.10 mmol, 58%).

^{1}H-NMR (400 MHz, acetone-d_6): δ 8.06-8.00 (m, 4H), 7.68-7.63 (m, 2H), 7.39 (dd, J = 8.4, 0.7 Hz, 2H), 7.27 (dd, J = 8.4, 1.7 Hz, 2H), 2.83-2.77 (m, 4H), 1.77-1.67 (m, 4H), 1.45-1.28 (m, 24H), 0.93-0.85 (m, 6H) ppm.

Naph-1-(Ph-CBZ),8-I

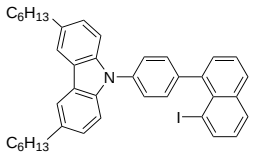

Naph-1-(Ph-CBZ),8-I was synthesized using method A, with **1,8-Naph-I$_2$** as aryl halide (598 mg, 1.58 mmol) and CBZ-Ph-BE as boronic acid (446 mg, 0.83 mmol).
Purification by column chromatography (SiO_2; pentane:CH_2Cl_2 7:1 to 5:1) afforded the product as a yellow glass (230 mg, 0.35 mmol, 42%).

^{1}H-NMR (400 MHz, acetone-d_6): δ 8.25 (dd, J = 7.3, 1.2 Hz, 1H), 8.05-7.99 (m, 3H), 7.99-7.94 (m, 1H), 7.57-7.52 (m, 4H), 7.47-7.43 (m, 2H), 7.39 (d, J = 8.4 Hz, 2H), 7.22 (dd, J = 8.4, 1.7 Hz, 2H), 7.17 (dd, J = 8.1, 7.3 Hz, 1H), 2.80-2.73 (m, 4H), 1.75-1.64 (m, 4H), 1.42-1.27 (m, 12H), 0.92-0.83 (m, 6H) ppm.
^{13}C-NMR (101 MHz, acetone-d_6): δ 143.4, 141.4, 140.8, 138.2, 136.6, 135.1, 133.6, 132.2, 131.8, 130.8, 130.3, 127.5, 126.9, 124.4, 120.4, 110.4, 92.4, 36.6, 33.1, 32.6, 29.8, 23.3, 14.5 ppm.

Br-dmb-Br

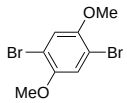

Br-dmb-Br was synthesized by adapting a literature procedure.[100]
1,4-Dimethoxybenzene (5.00 g, 36.2 mmol) was dissolved in acetic acid (10 mL) and cooled to 0 °C. Br_2 (3.70 mL, 72.4 mmol) dissolved in acetic acid (3.5 mL) was slowly added. The reaction was continued to stirr at r.t. for 3 h, and the precipitate filtered off. The solid was dissolved in CH_2Cl_2 and washed with sat. aqueous $Na_2S_2O_3$ solution. Drying over Na_2SO_4, followed by evaporation of solvents under reduced pressure,

afforded the product as a white solid (7.40 g, 25.0 mmol, 69%).
^{1}**H-NMR** (400 MHz, $CDCl_3$): δ 7.11 (s, 2H), 3.85 (s, 6H) ppm.

TMS-cc-dmb-cc-TMS

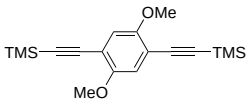

Br-dmb-Br (1.00 g, 3.38 mmol), trimethylsilylacetylene (1.12 mL, 8.11 mmol), $[Pd(PPh_3)_2Cl_2]$ (95.0 mg, 0.13 mmol) and CuI (5.50 mg, 0.03 mmol) were dissolved in anhydrous THF (40 mL) and anhydrous diisopropylamine (10 mL) under a nitrogen atmosphere. The reaction mixture was heated at 45 °C for 3 h. After cooling to r.t., the mixture was diluted with CH_2Cl_2 and washed with sat. aq. NH_4Cl. The organic phase was dried over Na_2SO_4, and the solvents removed under reduced pressure. Purification by column chromatography (SiO_2; pentane:CH_2Cl_2 3:1) afforded the product as a colorless oil (0.68 g, 2.05 mmol, 61%).

^{1}**H-NMR** (400 MHz, $CDCl_3$): δ 6.91 (s, 2H), 3.83 (s, 6H), 0.27 (s, 18H) ppm.

H-cc-dmb-cc-H

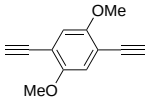

TMS-cc-dmb-cc-TMS (0.68 g, 2.05 mmol) and KF (0.39 g, 6.71 mmol) were stirred in a THF/MeOH mixture (40 mL, 1:1) at 55 °C for 2 h. Water was added, and the product extracted into CH_2Cl_2. The combined organic phases were dried over Na_2SO_4, and the solvents removed under reduced pressure. Purification by column chromatography (SiO_2; pentane:CH_2Cl_2 2:1 to 1:1) afforded the product as a white solid (185 mg, 0.99 mmol, 48%).

^{1}**H-NMR** (400 MHz, $CDCl_3$): δ 6.98 (s, 2H), 3.86 (s, 6H), 3.40 (s, 2H) ppm.

TfO-Naph(1,5)-cc-dmb-cc-Naph(1,5)-OTf

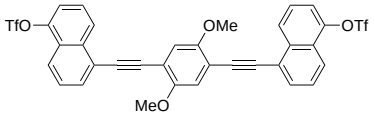

Naph-1-OTf,5-I (261 mg, 649 µmol), **H-cc-dmb-cc-H** (45.0 mg, 247 µmol), $[Pd(PPh_3)_2Cl_2]$ (17.0 mg, 24.2 µmol, 5 mol%) and CuI (4.00 mg, 2.10 µmol) were dissolved in a THF/NEt_3 mixture (10 mL, 1:1) under a nitrogen atmosphere. The mixture was heated at reflux overnight. After cooling to r.t. the mixture was diluted with CH_2Cl_2 and washed with sat. aq. NH_4Cl. The organic phase was dried over Na_2SO_4, and the solvents removed under reduced pressure. Purification by column chromatography (SiO_2; pentane:CH_2Cl_2 1:1) afforded the product as a yellow solid (126 mg, 172 µmol, 70%).

^{1}**H-NMR** (400 MHz, CD_2Cl_2): δ 8.67 (dt, J = 8.4, 1.0 Hz, 2H), 8.10 (dt, J = 8.8, 1.1 Hz, 2H), 7.92 (dd, J = 7.2, 1.1 Hz, 2H), 7.71-7.65 (m, 4H), 7.58 (dd, J = 7.7, 1.1 Hz, 2H), 7.22 (s, 2H), 4.02 (s, 6H) ppm.

CBZ-Ph-TMS

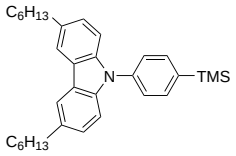

CBZ-H (2.50 g, 7.45 mmol), **Br-Ph-TMS** (1,70 g, 7.45 mmol), NaO*t*Bu (10.8 g, 112 mmol) and $[Pd(dba)_2]$ (125 mg, 0.22 mmol, 3 mol%) were suspended in anhydrous toluene (47 mL) under a nitrogen atmosphere. The mixture was deaerated for 15 min, after which $[HP(tBu)_3]BF_4$ (63.0 mg, 0.22 mmol) was added. The reaction was heated at 80 °C overnight. After cooling to r.t., water was added. The phases were separated and the aqueous phase extracted with toluene. The combined organic phases were dried over Na_2SO_4, followed by evaporation of the solvent under reduced pressure. Purification by column chromatography (SiO_2; pentane:CH_2Cl_2 1:1) afforded the product as a colorless oil (2.62 g, 5.41 mmol, 73%).

^{1}**H-NMR** (400 MHz, CD_2Cl_2): δ 8.04-7.99 (m, 2H), 7.88-7.81 (m, 2H), 7.65-7.58 (m,

2H), 7.35 (d, J = 8.4 Hz, 2H), 7.26 (dd, J = 8.5, 1.7 Hz, 2H), 2.82-2.76 (m, 4H), 1.72 (p, J = 7.6 Hz, 4H), 1.45-1.27 (m, 12H), 0.93-0.85 (m, 6H), 0.37 (s, 9H) ppm.

CBZ-TD-Ph

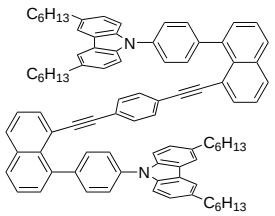

Naph-1-Ph-CBZ,8-I (140 mg, 211 µmol), **H-cc-Ph-cc-H** (12.2 mg, 96.7 µmol), CuI (0.10 mg, 0.53 µmol) and $[Pd(PPh_3)_2Cl_2]$ (11.6 mg, 16.5 µmol, 12 mol%) were suspended in anhydrous NEt_3 (8 mL) under a nitrogen atmosphere. The reaction mixture was heated at reflux overnight. After cooling to r.t., it was diluted with CH_2Cl_2 and washed with sat. aq. NH_4Cl solution. The organic phase was dried over Na_2SO_4, and the solvents removed under reduced pressure. Purification by column chromatography (SiO_2; pentane:CH_2Cl_2 5:1) afforded the product as a light-yellow solid (71 mg, 59.3 µmol, 61%).

^{1}**H-NMR** (400 MHz, CD_2Cl_2): δ 7.99 (dd, J = 8.2, 1.3 Hz, 2H), 7.95 (dd, J = 8.2, 1.3 Hz, 2H), 7.87 (d, J = 1.6 Hz, 4H), 7.81 (dd, J = 7.1, 1.3 Hz, 2H), 7.62-7.50 (m, 8H), 7.46 (dd, J = 7.0, 1.4 Hz, 2H), 7.26-7.21 (m, 4H), 7.00 (dd, J = 8.4, 1.7 Hz, 4H), 6.87 (d, J = 8.4, 4H), 6.77 (s, 4H), 2.73-2.66 (m, 8H), 1.67-1.56 (m, 8H), 1.30-1.16 (m, 24H), 0.85 (t, J = 6.8, 12H) ppm.
^{13}**C-NMR** (101 MHz, CD_2Cl_2): δ 141.9, 140.3, 139.5, 137.5, 135.3, 135.2, 135.0, 131.8, 131.7, 131.6, 130.8, 130.3(2), 129.2(8), 127.1, 126.1, 125.9, 125.7, 123.8, 123.5, 120.9, 119.6, 110.1, 100.6, 98.6, 92.6, 36.5, 32.9, 32.3, 29.7, 23.2, 14.5 ppm.
MS (MALDI): m/z (%) = 1197.031 (100, $[M]^+$), calcd for $C_{90}H_{88}N_2$ 1196.695.

CBZ-TD-dmb

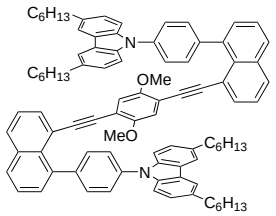

1-Ph-CBZ,8-iodonaphthalene (100 mg, 0.15 mmol), **H-cc-tmb-cc-H** (13.3 mg, 0.07 mmol), CuI (0.10 mg, 0.53 μmol) and $[Pd(PPh_3)_2Cl_2]$ (8.30 mg, 11.8 μmol, 17 mol%) were suspended in anhydrous diisopropylamine (4 mL) under a nitrogen atmosphere. The reaction mixture was heated at reflux overnight. After cooling to r.t., it was diluted with CH_2Cl_2 and washed with sat. aq. NH_4Cl solution. The organic phase was dried over Na_2SO_4, and the solvents removed under reduced pressure. Purification by column chromatography (SiO_2; pentane:CH_2Cl_2 2:1) afforded the product as a yellow solid (52 mg, 41 μmol, 58%).

^{1}**H-NMR** (400 MHz, CD_2Cl_2): δ 8.00 (dd, J = 8.2, 1.4 Hz, 2H), 7.96 (dd, J = 8.3, 1.4 Hz, 2H), 7.88-7.82 (m, 6H), 7.64-7.48 (m, 10H), 7.02 (dd, J = 8.5, 1.7 Hz, 4H), 6.91 (d, J = 8.4, 4H), 6.40 (s, 2H), 3.24 (s, 6H), 2.68 (t, J = 7.8 Hz, 8H), 1.67-1.57 (m, 8H), 1.31-1.18 (m, 24H), 0.90-0.81 (m, 12H) ppm.
MS (MALDI): m/z (%) = 1256.056 (100, $[M]^+$), calcd for $C_{92}H_{92}N_2O_2$ 1256.716.

CBZ-Ref-Ph

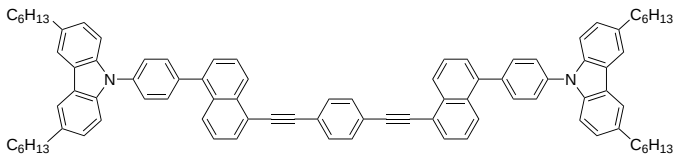

TfO-Naph(1,5)-cc-Ph-cc-Naph(1,5)-OTf (71.1 mg, 116 μmol), **CBZ-Ph-BE** (125 mg, 233 μmol), Cs_2CO_3 (363 mg, 1.11 mmol) and $[Pd(dppf)Cl_2] \cdot CH_2Cl_2$ (35.6 mg, 43.0 μmol, 19 mol%) were suspended in anhydrous DMF (10 mL) under a nitrogen atmosphere and heated at 60 °C overnight. The reaction was cooled to r.t. and diluted with CH_2Cl_2. The organic phase was washed with H_2O, dried over Na_2SO_4, and the solvents removed under reduced pressure. Purification by column chromatography (SiO_2; pentane:CH_2Cl_2 3:1) afforded the product as a yellow solid (82.0 mg, 68 μmol,

59%).

^{1}**H-NMR** (400 MHz, CD_2Cl_2): δ 8.59 (dt, J = 8.3, 1.1 Hz, 2H), 8.11 (dt, J = 8.6, 1.1 Hz, 2H), 7.97 (d, J = 1.6 Hz, 4H), 7.88 (dd, J = 7.1, 1.1 Hz, 2H), 7.79-7.71 (m, 14H), 7.64 (dd, J = 7.1, 1.3 Hz, 2H), 7.57-7.47 (m, 6H), 7.29 (dd, J = 8.5, 1.7 Hz, 4H), 2.86-2.80 (m, 8H), 1.81-1.71 (m, 8H), 1.49-1.31 (m, 24H), 0.97-0.89 (m, 12H) ppm.
^{13}**C-NMR** (101 MHz, CD_2Cl_2): δ 140.7, 140.0, 139.6, 138.1, 135.3, 134.2, 132.3, 132.0(9), 132.0(6), 131.3, 128.4, 127.2, 127.1, 127.0, 126.2, 124.1, 124.0, 121.6, 120.1, 110.1, 94.8, 90.3, 36.6, 32.9, 32.4, 29.7, 23.3, 14.5 ppm.
MS (MALDI): m/z (%) = 1196.999 (100, $[M]^+$), calcd for $C_{90}H_{88}N_2$ 1196.695.

CBZ-Ref-dmb

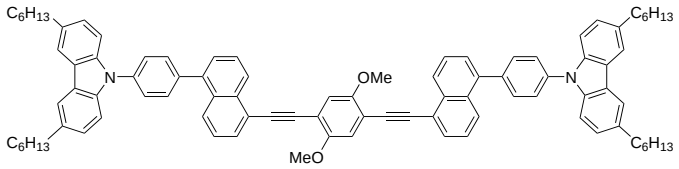

TfO-Naph(1,5)-cc-dmb-cc-Naph(1,5)-OTf (135 mg, 183 µmol), **CBZ-Ph-BE** (210 mg, 391 µmol), Cs_2CO_3 (610 mg, 1.87 mmol) and $[Pd(dppf)Cl_2]\cdot CH_2Cl_2$ (60.0 mg, 73 µmol, 20 mol%) were suspended in anhydrous DMF (10 mL) under a nitrogen atmosphere and heated at 60 °C overnight. The reaction was cooled to r.t. and diluted with CH_2Cl_2. The organic phase was washed with H_2O, dried over Na_2SO_4, and the solvents removed under reduced pressure. Purification by column chromatography (SiO_2; pentane:CH_2Cl_2 2:1) afforded the product as a yellow solid (179 mg, 142 µmol, 77%).

^{1}**H-NMR** (400 MHz, CD_2Cl_2): δ 8.71 (dt, J = 8.4, 1.1 Hz, 2H), 8.10 (dt, J = 8.7, 1.0 Hz, 2H), 7.96 (dd, J = 1.8, 0.8 Hz, 4H), 7.88 (dd, J = 7.1, 1.1 Hz, 2H), 7.79-7.71 (m, 10H), 7.65 (dd, J = 7.1, 1.3 Hz, 2H), 7.57-7.47 (m, 6H), 7.31-7.26 (m, 6H), 4.08 (s, 6H), 2.86-2.79 (m, 8H), 1.74 (p, J = 7.4 Hz, 8H), 1.47-1.31 (m, 24H), 0.95-0.88 (m, 12H) ppm.
MS (MALDI): m/z (%) = 1256.238 (100, $[M]^+$), calcd for $C_{92}H_{92}N_2O_2$ 1256.716.

Bibliography

[1] V. Balzani (Ed.), *Electron Transfer in Chemistry*. **2008**, 1–800.

[2] V. Balzani, G. Bergamini, P. Ceroni, *Angew. Chem. Int. Ed.* **2015**, *54*, 11320–11337.

[3] H. Zhou, R. Yan, D. Zhang, T. Fan, *Chem. Eur. J.* **2016**, *22*, 9870–9885.

[4] M. Grätzel, *Inorg. Chem.* **2005**, *44*, 6841–6851.

[5] J. M. R. Narayanam, C. R. J. Stephenson, *Chem. Soc. Rev.* **2011**, *40*, 102–113.

[6] C. K. Prier, D. A. Rankic, D. W. C. MacMillan, *Chem. Rev.* **2013**, *113*, 5322–5363.

[7] L. Sun, Y. A. Diaz-Fernandez, T. A. Gschneidtner, F. Westerlund, S. Lara-Avila, K. Moth-Poulsen, *Chem. Soc. Rev.* **2014**, *43*, 7378–7411.

[8] H. Zipse, *Angew. Chem. Int. Ed.* **1997**, *16*, 1697–1700.

[9] R. A. Marcus, N. Sutin, *Biochim. Biophys. Acta* **1985**, *811*, 265–322.

[10] M. N. Paddon-Row, *Adv. Phys. Org. Chem.* **2003**, *38*, 1–85.

[11] M. Sparpaglione, S. Mukamel, *J. Phys. Chem.* **1987**, *91*, 3938–3943.

[12] M. Natali, S. Campagna, F. Scandola, *Chem. Soc. Rev.* **2014**, *43*, 4005–4018.

[13] J.-M. Lopez-Castillo, A. Filali-Mouhim, I. L. Plante, J. Jay-Gerin, *J. Phys. Chem.* **1995**, *99*, 6864–6875.

[14] J. R. Winkler, H. B. Gray, *J. Am. Chem. Soc.* **2014**, *136*, 2930–2939.

[15] P. P. Edwards, H. B. Gray, M. T. J. Lodge, R. J. P. Williams, *Angew. Chem. Int. Ed.* **2008**, *47*, 6758–6765.

[16] M. D. Ward, *Chem. Soc. Rev.* **1997**, *26*, 365.

[17] N. R. Lokan, M. N. Paddon-Row, M. Koeberg, J. W. Verhoeven, *J. Am. Chem. Soc.* **2000**, *122*, 5075–5081.

[18] K. Kumar, Z. Lin, D. H. Waldeck, M. B. Zimmt, V. Pro, R. Island, V. Uni, V. Pennsyl, R. V. August, *J. Am. Chem. Soc.* **1996**, *118*, 243–244.

[19] H. Han, M. B. Zimmt, *J. Am. Chem. Soc.* **1998**, *120*, 8001–8002.

[20] A. M. Napper, I. Read, D. H. Waldeck, N. J. Head, A. M. Oliver, M. N. Paddon-Row, *J. Am. Chem. Soc.* **2000**, *122*, 5220–5221.

[21] A. M. Napper, N. J. Head, A. M. Oliver, M. J. Shephard, M. N. Paddon-Row, I. Read, D. H. Waldeck, *J. Am. Chem. Soc.* **2002**, *124*, 10171–10181.

[22] A. M. Napper, I. Read, R. Kaplan, M. B. Zimmt, D. H. Waldeck, *J. Phys. Chem. A* **2002**, *106*, 5288–5296.

[23] M. Koeberg, M. De Groot, J. W. Verhoeven, N. R. Lokan, M. J. Shephard, M. N. Paddon-Row, *J. Phys. Chem. A* **2001**, *105*, 3417–3424.

[24] M. Liu, N. Ito, M. Maroncelli, D. H. Waldeck, A. M. Oliver, M. N. Paddon-Row, *J. Am. Chem. Soc.* **2005**, *127*, 17867–17876.

[25] S. Chakrabarti, M. Liu, D. H. Waldeck, A. M. Oliver, M. N. Paddon-Row, *J. Phys. Chem. A* **2009**, *113*, 1040–1048.

[26] I. Read, A. Napper, R. Kaplan, M. B. Zimmt, D. H. Waldeck, *J. Am. Chem. Soc.* **1999**, *121*, 10976–10986.

[27] M. Liu, D. H. Waldeck, A. M. Oliver, N. J. Head, M. N. Paddon-Row, *J. Am. Chem. Soc.* **2004**, *126*, 10778–10786.

[28] Y. K. Kang, I. V. Rubtsov, P. M. Iovine, J. Chen, M. J. Therien, *J. Am. Chem. Soc.* **2002**, *124*, 8275–8279.

[29] D. I. Schuster, P. Cheng, P. D. Jarowski, D. M. Guldi, C. Luo, L. Echegoyen, S. Pyo, A. R. Holzwarth, S. E. Braslavsky, R. M. Williams, G. Klihm, *J. Am. Chem. Soc.* **2004**, *126*, 7257–7270.

[30] A. S. Sandanayaka, H. Sasabe, Y. Araki, Y. Furusho, O. Ito, T. Takata, *J. Phys. Chem. A* **2004**, *108*, 5145–5155.

[31] M. Ortiz, S. Cho, J. Niklas, S. Kim, O. G. Poluektov, W. Zhang, G. Rumbles, J. Park, *J. Am. Chem. Soc.* **2017**, *139*, 4286–4289.

[32] R. M. Young, S. M. Dyar, J. C. Barnes, M. Juríček, J. F. Stoddart, D. T. Co, M. R. Wasielewski, *J. Phys. Chem. A* **2013**, *117*, 12438–12448.

[33] M. J. Shephard, M. N. Paddon-Row, K. D. Jordan, *Chem. Phys.* **1993**, *176*, 289–304.

[34] J. Hankache, O. S. Wenger, *Chem. Commun.* **2011**, *47*, 10145.

[35] J. Chen, O. S. Wenger, *Chem. Sci.* **2015**, *6*, 3582–3592.

[36] M. Kuss-Petermann, O. S. Wenger, *J. Am. Chem. Soc.* **2016**, *138*, 1349–1358.

[37] C. R. Bock, J. A. Connor, A. R. Gutierrez, T. J. Meyer, D. G. Whitten, B. P. Sullivan, J. K. Nagle, *J. Am. Chem. Soc.* **1979**, *101*, 4815–4824.

[38] J. Pei, J. Ni, X.-H. Zhou, X.-Y. Cao, Y.-H. Lai, *J. Org. Chem.* **2002**, *67*, 4924–4936.

[39] C.-L. Chiang, C.-F. Shu, C.-T. Chen, *Org. Lett.* **2005**, *7*, 3717–3720.

[40] K. Sreenath, C. V. Suneesh, K. R. Gopidas, R. A. Flowers, *J. Phys. Chem. A* **2009**, *113*, 6477–6483.

[41] R. H. Goldsmith, L. E. Sinks, R. F. Kelley, L. J. Betzen, W. Liu, E. A. Weiss, M. A. Ratner, M. R. Wasielewski, *Proc. Natl. Acad. Sci. USA* **2005**, *102*, 3540–3545.

[42] D. W. Thompson, A. Ito, T. J. Meyer, *Pure Appl. Chem.* **2013**, *85*, 1257–1305.

[43] A. Juris, V. Balzani, P. Belser, A. von Zelewsky, *HeIv. Chim. Acta* **1981**, *64*, 2175–2182.

[44] P. Dongare, B. D. Myron, L. Wang, D. W. Thompson, T. J. Meyer, *Coord. Chem. Rev.* **2017**, *345*, 86–107.

[45] A. C. Benniston, A. Harriman, P. Li, J. P. Rostron, R. W. Harrington, W. Clegg, *Chem. Eur. J.* **2007**, *13*, 7838–7851.

[46] Y. Tsuji, R. Hoffmann, *Chem. Eur. J.* **2016**, *22*, 4878–4888.

[47] R. Lomoth, T. Häupl, O. Johansson, L. Hammarström, *Chem. Eur. J.* **2002**, *8*, 102–110.

[48] M. B. Robin, P. Day, *Adv. Inorg. Chem.* **1967**, *10*, 247–422.

[49] D. M. D'Alessandro, F. R. Keene, *Chem. Soc. Rev.* **2006**, *35*, 424–440.

[50] A. Heckmann, C. Lambert, *Angew. Chem. Int. Ed.* **2012**, *51*, 326–392.

[51] K. Lancaster, S. A. Odom, S. C. Jones, S. Thayumanavan, S. R. Marder, J. L. Brédas, V. Coropceanu, S. Barlow, *J. Am. Chem. Soc.* **2009**, *131*, 1717–1723.

[52] D. R. Kattnig, B. Mladenova, G. Grampp, C. Kaiser, A. Heckmann, C. Lambert, *J. Phys. Chem. C* **2009**, *113*, 2983–2995.

[53] K. Lancaster, *Intramolecular Electron Transfer in Mixed-Valence Triarylamines* **2009**, Ph.D. Thesis, Georgia Institute of Technology.

[54] Y. Hirao, M. Urabe, A. Ito, K. Tanaka, *Angew. Chem. Int. Ed.* **2007**, *46*, 3300–3303.

[55] P. Mücke, R. F. Winter, K. Kowalski, *J. Organomet. Chem.* **2013**, *735*, 10–14.

[56] R. F. Winter, *Organometallics* **2014**, *33*, 4517–4536.

[57] P. Day, N. S. Hush, R. J. H. Clark, *Philos. Trans. R. Soc. London, Ser. A* **2008**, *366*, 5–14.

[58] T. C. Stamatatos, G. Christou, *Philos. Trans. R. Soc. London, Ser. A* **2008**, *366*, 113–25.

[59] C. Lambert, C. Risko, V. Coropceanu, J. Schelter, S. Amthor, N. E. Gruhn, J. C. Durivage, J. L. Brédas, *J. Am. Chem. Soc.* **2005**, *127*, 8508–8516.

[60] J. Hankache, O. S. Wenger, *Chem. Rev.* **2011**, *111*, 5138–5178.

[61] D. Volz, M. Wallesch, C. Flechon, M. Danz, A. Verma, J. M. Navarro, D. M. Zink, S. Bräse, T. Baumann, *Green Chem.* **2015**, *17*, 1988–2011.

[62] M. Zhu, C. Yang, *Chem. Soc. Rev.* **2013**, *42*, 4963.

[63] C. B. Larsen, H. Van Der Salm, G. E. Shillito, N. T. Lucas, K. C. Gordon, *Inorg. Chem.* **2016**, *55*, 8446–8458.

[64] M. Kaupp, M. Renz, M. Parthey, M. Stolte, F. Würthner, C. Lambert, *Phys. Chem. Chem. Phys.* **2011**, *13*, 16973.

[65] S. Amthor, C. Lambert, S. Dümmler, I. Fischer, J. Schelter, *J. Phys. Chem. A* **2006**, *110*, 5204–5214.

[66] C. Lambert, S. Amthor, J. Schelter, *J. Phys. Chem. A* **2004**, *108*, 6474–6486.

[67] P. J. Low, M. A. J. Paterson, D. S. Yufit, J. A. K. Howard, J. C. Cherryman, D. R. Tackley, R. Brook, B. Brown, *J. Mater. Chem.* **2005**, *15*, 2304.

[68] B. R. Kaafarani, C. Risko, T. H. El-Assaad, A. O. El-Ballouli, S. R. Marder, S. Barlow, *J. Phys. Chem. B* **2016**, *120*, 3156–3166.

[69] S. F. Nelsen, A. E. Konradsson, J. P. Telo, *J. Am. Chem. Soc.* **2005**, *127*, 920–925.

[70] R. H. Voegeli, H. C. Kang, R. G. Finke, V. Boekelheide, *J. Am. Chem. Soc.* **1986**, *108*, 7010–7016.

[71] A. S. Jalilov, L. Han, S. F. Nelsen, I. A. Guzei, *J. Org. Chem.* **2013**, *78*, 11373–11381.

[72] S. Amthor, C. Lambert, *J. Phys. Chem. A* **2006**, *110*, 1177–1189.

[73] M. Kaupp, S. Gückel, M. Renz, S. Klawohn, K. Theilacker, M. Parthey, C. Lambert, *J. Comput. Chem.* **2015**, *1*, 93–102.

[74] H. C. Schmidt, M. Spulber, M. Neuburger, C. G. Palivan, M. Meuwly, O. S. Wenger, *J. Org. Chem.* **2016**, *81*, 595–602.

[75] D. L. Sun, S. V. Rosokha, S. V. Lindeman, J. K. Kochi, *J. Am. Chem. Soc.* **2003**, *125*, 15950–15963.

[76] D. Sun, S. V. Rosokha, J. K. Kochi, *J. Am. Chem. Soc.* **2004**, *126*, 1388–1401.

[77] G. Nöll, M. Avola, *J. Phys. Org. Chem.* **2006**, *19*, 238–241.

[78] S. F. Nelsen, A. E. Konradsson, M. N. Weaver, J. P. Telo, *J. Am. Chem. Soc.* **2003**, *125*, 12493–12501.

[79] M. Steeger, C. Lambert, *Chem. Eur. J.* **2012**, *18*, 11937–11948.

[80] S. Sarkhel, A. Rich, M. Egli, *J. Am. Chem. Soc.* **2003**, *125*, 8998–8999.

[81] A. Jain, V. Ramanathan, R. Sankararamakrishnan, *Protein Sci.* **2009**, *18*, 595–605.

[82] W. Kaim, A. Klein, M. Glockle, *Acc. Chem. Res.* **2000**, *33*, 755–763.

[83] A. Zweig, W. G. Hodgson, W. H. Jura, *J. Am. Chem. Soc.* **1964**, *86*, 4124–4129.

[84] L. G. Heinz, O. Yushchenko, M. Neuburger, E. Vauthey, O. S. Wenger, *J. Phys. Chem. A* **2015**, *119*, 5676–5684.

[85] E. Wagner, S. Filipek, M. K. Kalinowski, *Monatsh. Chem.* **1988**, *932*, 929–932.

[86] S. Barlow, C. Risko, V. Coropceanu, N. M. Tucker, S. C. Jones, Z. Levi, V. N. Khrustalev, M. Y. Antipin, T. L. Kinnibrugh, T. Timofeeva, S. R. Marder, J.-L. Brédas, *Chem. Commun.* **2005**, *377*, 764–766.

[87] V. Coropceanu, M. Malagoli, J. M. André, J. L. Brédas, *J. Am. Chem. Soc.* **2002**, *124*, 10519–10530.

[88] N. J. Bunce, *J. Chem. Educ.* **1987**, *64*, 907–914.

[89] P. J. Kersten, B. Kalyanaraman, K. E. Hammel, B. Reinhammar, T. K. Kirk, *Biochem. J* . **1990**, *268*, 475–480.

[90] S. K. Chiu, Y. C. Chung, G. S. Liou, Y. O. Su, *J. Chin. Chem. Soc.* **2012**, *59*, 331–337.

[91] X. Y. Wang, D. C. Yang, F. D. Zhuang, J. J. Liu, J. Y. Wang, J. Pei, *Chem. Eur. J.* **2015**, *21*, 8867–8873.

[92] S. Dapperheld, E. Steckhan, K.-H. Grosse Brinkhaus, T. Esch, *Chem. Ber.* **1991**, *124*, 2557–2567.

[93] E. A. Chandross, F. Sonntag, *J. Am. Chem. Soc.* **1966**, *88*, 1089–1096.

[94] M. G. Shin, S. O. Kim, H. T. Park, S. J. Park, H. S. Yu, Y. H. Kim, S. K. Kwon, *Dyes Pigm.* **2012**, *92*, 1075–1082.

[95] R. A. Kumar, C. U. Maheswari, S. Ghantasala, C. Jyothi, K. R. Reddy, *Adv. Synth. Catal.* **2011**, *353*, 401–410.

[96] R. N. Brookins, K. S. Schanze, J. R. Reynolds, *Macromolecules* **2007**, *40*, 3524–3526.

[97] S. H. Kim, R. D. Rieke, *Tetrahedron* **2010**, *66*, 3135–3146.

[98] J. A. O'Meara, C. Yoakim, P. R. Bonneau, M. Bös, M. G. Cordingley, R. Déziel, L. Doyon, J. Duan, M. Garneau, I. Guse, S. Landry, E. Malenfant, J. Naud, W. W. Ogilvie, B. Thavonekham, B. Simoneau, *J. Med. Chem.* **2005**, *48*, 5580–5588.

[99] L. Wang, E. Ji, N. Liu, B. Dai, *Synthesis* **2016**, *48*, 737–750.

[100] P. López-Alvarado, C. Avendaño, J. Carlos Menéndez, *Synth. Commun.* **2002**, *32*, 3233–3239.